Distribution Agreement

In presenting this thesis or dissertation as a partial fulfillment of the requirements for an advanced degree from Emory University, I hereby grant to Emory University and its agents the non-exclusive license to archive, make accessible, and display my thesis or dissertation in whole or in part in all forms of media, now or hereafter known, including display on the world wide web. I understand that I may select some access restrictions as part of the online submission of this thesis or dissertation. I retain all ownership rights to the copyright of this thesis or dissertation. I also retain the right to use in future works(such as articles or books) all or part of this thesis or dissertation.

_____ _____

Andrew Patrick Brown Date

Screening, hit expansion, and mechanistic studies for natural product analogs derived from traditional herbal medicine: curcumin and triptolide.

By

Andrew Patrick Brown

Doctor of Philosophy

Graduate Division of Biological and Biomedical Sciences

Program in Molecular and Systems Pharmacology

_____

Hyunsuk Shim, Ph.D.
Adviser

_____

James Snyder, Ph.D.
Adviser

_____

Jing Chen, Ph.D.
Committee Member

_____

Dennis Liotta, Ph.D.
Committee Member

Accepted

_____

Lisa A Tedesco, Ph.D.
Dean of the James T. Laney School of Graduate Studies

_____

Date

Abstract

Screening, hit expansion and mechanistic studies for natural product analogs derived from traditional herbal medicine: curcumin and triptolide.

By

Andrew Patrick Brown

The use of naturally-derived compounds in traditional medicine dates back thousands of years. Many of these compounds have served as predecessors for modern drug therapies. Despite this fact, obstacles such as variation in preparation and inconsistencies in chemical makeup have prevented mainstream acceptance of herbal medicine. Advances in medicinal chemistry have begun to allow for the purification and characterization of active ingredients in a number of traditional herbal preparations. Armed with this information, it has become possible to synthesize compounds inspired by the active ingredients in these preparations that possess better drug properties, such as a lower toxicity, better pharmacokinetics or increased potency. The work discussed herein details the characterization of analogs of two such compounds; curcumin, from the root of the curcuma longa plant, and triptolide, from the Chinese herb *Tripterygiumwilfordii Hook F* (TWHF).

The Chinese herb, *Tripterygiumwilfordii Hook F* (TWHF), has been used for centuries as a traditional medicine and is known to possess potent anti-inflammatory, immunosuppressive and anti-cancer properties. Previous investigations have shown that one of the discrete components of TWHF, triptolide, is a potent inhibitor of transcription promoted by NF-κB. Unfortunately, despite its interesting mechanism of action, triptolide is also quite toxic and exhibits poor water solubility. To circumvent these problems, a novel series of triptolide analogs was synthesized and a screen performed to determine the efficacy of the compounds' anti- NF-κB properties. In this work, several of the active analogs were then subjected to *in vitro* assays designed to examine cell toxicity, anti-IKKB kinase activity, and NF-κB translocation. In addition to the cell based assays, a number of assays were performed *in vivo* in order to determine the nature of the anti-inflammatory properties of these analogs, as well as their effects on the gene expression of downstream targets. The results demonstrate that the new triptolide

analogs are safe and potent anti-NF-κB compounds that may be useful as anti-inflammatory agents.

Curcumin is a biologically active component found in curry powder. The spice is made from the root of the curcuma longa plant and is used in Indian and Southeast Asian cuisine. A class of compounds related in structure to curcumin has been developed and shown to possess similar anti-inflammatory and anticancer properties. Here we examine aspects of these agents by exploring their kinase inhibition properties, their effects on cancer cells both *in vitro* and *in vivo*, the change of enzyme kinetics in reaction to ATP and molecular modeling of the potently inhibited enzymes. Overall, these curcumin analogs are shown to have measurable and varied effects in both cell and animal models, which are thought to derive from the pleiotropic nature of the kinase inhibitors that operate at multiple points along cell signaling cascades.

Screening, hit expansion and mechanistic studies for natural product analogs derived from traditional herbal medicine: curcumin and triptolide.

By

Andrew Patrick Brown

B.S., University of Wisconsin, 2005

Advisors:
Hyunsuk Shim, Ph.D.
James Snyder, Ph. D.

An abstract of

A dissertation submitted to the Faculty of the

James T. Laney School of Graduate Studies of Emory University

In partial fulfillment of the requirements for the degree of

Doctor of Philosophy in

Graduate Division of Biological and Biomedical Sciences

Program in Molecular and Systems Pharmacology

2012

Table of Contents

List of Figures

List of Abbreviations

absorption, distribution, metabolism, and excretion.....ADME

Acid dissociation constant..... pKa

Adenosine diphosphate.....ADP

Adenosine-5'-triphosphate.....ATP

Breakpoint cluster region protein.....BCR

Collagen-induced arthritis.....CIA

Cyclooxygenase-2.....COX-2

Dextran sulfate sodium.....DSS

Dimethyl sulfoxide.....DMSO

Disease Activity Index.....DAI

Eletorphoric mobility shift assay.....EMSA

Enzyme-linked immunosorbent assay.....ELISA

Ethylenediaminetetraacetic acid.....EDTA

Fetal bovine serum.....FBS

Fluorescence resonance energy transfer.....FRET

Gray.....Gy

Half maximal inhibitory concentration.....IC_{50}

Hematoxylin and eosin stain.....H&E

High Performance Liquid Cromatography.....HPLC

High throughput screening.....HTS

Horseradish peroxidase.....HRP

Hypoxia responsive element.....HRE

Hypoxia-inducible factor.....HIF

Inflammatory bowel disease.....IBD

Inhibitor dissociation constant.....K_i

Inhibitor of nuclear factor kappa-B.....IκB

Inhibitor of nuclear factor kappa-B kinase subunit beta.....IKKβ

Interferon.....IFN

Interleukin.....IL

Lipopolysaccharide.....LPS

Lithium aluminum hydride.....LAH

Mammalian target of rapamycin.....mTOR

Matrix metalloproteinase.....MMP

Maximum reaction rate.....V_{max}

Mechanism of action.....MOA

Messenger RNA.....mRNA

Michaelis constant.....K_m

Mitogen-activated protein.....MAP

Molecular mechanics - Generalized Born model augmented with the hydrophobic solvent accessible surface area.....MM-GBSA

NEMO binding domain.....NBD

NF-κB essential modifier.....NEMO

Nonsteroidal anti-inflammatory drug.....NSAID

Nuclear factor kappa-light-chain-enhancer of activated B cells.....NF-κB

Optimal Cutting Temperature compound.....OCT

Phorbol 12-myristate 13-acetate.....PMA

Phosphatidylinositol 3-kinases.....PI3K

Polyethylene glycol.....PEG

prostaglandin E2.....PGE2

Protein Data Bank.....PDB

Retardation Factor.....Rf

Reverse transcription polymerase chain reaction.....RT-PCR

Ribonuclease.....RNase

Ribonucleic acid.....RNA

Serine.....Ser

Signal transducer and activator of transcription 3.....Stat3

Structure-activity relationship.....SAR

Threonine.....Thr

Tissue inhibitors of metalloproteinases.....TIMP

Tripterygiumwilfordii Hook F.....TWHF

tumor necrosis factor-alpha.....TNF-α

Tyrosine.....Tyr

Virtual high throughput screening.....VHTS

Voltage-dependent anion-selective channel protein 1.....VDAC1

CHAPTER I: Introduction

1.1 Traditional herbal medicine.

Traditional medicinal practices date back for thousands of years and are evident in almost all societies in a variety of forms of herbalism or folk medicine. For example, the ancient Egyptians and Sumerians are known to have exploited a number of medicinal uses for plants. Ayurveda, which means "the knowledge for long life" and originated in India, and traditional Chinese medicine, were systems of medicine that developed over generations, before the era of modern medicine and both of which are characterized by expansive texts detailing preparations and treatments for many diseases. Traditional medicine is still important today, because most of the remedies come from locally available plants that can be harvested for little or no cost, they are often the only source of treatment for millions of people living in the undeveloped world. These treatments can be effective, but are often looked upon with skepticism by Western medicine.

In many cases, traditional medicines have served as predecessors for modern drug therapies. Traditional medical use of the opium poppy, for example predates written history. It was, in many ancient societies, the only source of analgesic medicine. In the early 1800s, detailed studies of the plant led to the isolation of morphine, which was followed decades later by codeine. In the early 1900s, the semi synthetic oxycodone was made from an alkaloid compound found in opium poppies. In addition, to serving as templates for effective drug therapies, the compounds isolated from these plants have helped spur research and expand human knowledge of pain pathways and opioid receptors. Another example is found with the Quechua Indians in Peru and Bolivia used the bark of the Cinchona tree to treat the shivers associated with malaria. The treatment was later brought to Europe by the Jesuits. The active component in the bark, quinine, is still used for the treatment of malaria today, though now it is

chemically synthesized instead of extracted from a plant. (Wachtel-Galor and Benzie 2011) These are only a few examples of natural, semi-synthetic, and synthetic drugs developed from plants found in traditional medicine.

1.2 Identifying biologically active compounds in traditional medicine and natural products.

As human exploration continues to reveal an astonishing diversity of plants, fungi, and bacteria found on our planet, we have recently begun to recognize the potential wealth of natural products that may be able to provide lead compounds for drug discovery. By looking at the plants and plant material used in various preparations in traditional medicine, there are still vast assortments of chemicals from which to mine lead compounds for therapeutic purposes. These compounds have unique biological activities and offer distinct advantages over randomly discovered natural products. For one, they have been derived from a natural system that has been "clinically" tested over hundreds if not thousands of years. In addition, the route of administration for many of these drugs is either enterally or topically, which is the preferred mode of administration for developed therapeutics. Also, they can be harvested from their plant of origin, so research can be conducted before having to tackle the problem of a challenging synthesis.

Despite these clear advantages, western medicine tends to look upon these remedies with skepticism. One problem is the preparations, which can be different from one provider to the other. Even the starting materials can cause dynamic changes in the safety or potency in these traditional medicines. Inconsistencies in the chemical makeup of plants used can be different from region to region, due to growing conditions. Even within the same region things like weather and soil can be vastly different. There is also a danger of counterfeit and poor quality herbal products. In addition, some of these preparations use multiple compounds which work

synergistically with each other. The specific compound or compounds that possessed the desired therapeutic effect are, therefore, relatively unknown.

With the advent of modern chemistry we are now able to isolate and identify the effective components in these traditional medicines. Doing so helps to establish a profile with regard to absorption, distribution, metabolism, and excretion (ADME) and toxicity, as well as determine the compound's mechanism of action (MOA).Though it is possible to bring a compound to the clinic without an exact mechanistic model, an incomplete understanding of a compound's MOA can make the development of a structure-activity relationship (SAR) to guide medicinal chemistry more difficult. Without a directed way to improve affinity, absorption, and influence selectivity with medicinal chemistry techniques,improving the effectiveness of a new compound class can be challenging. Also, as with most natural products, patentability is an issue. Thus, it is important to be able to create distinct drug entities from a naturally occurring structure.

With analytical and structural chemistry, researchers have been able to purify many compounds from plants used in traditional medicines. This process is generally referred to as "bioprospecting". Not only does this allow researchers to generate libraries of structurally diverse compounds, it also allows these newly discovered compounds to be chemically modified forming semi-synthetic compounds that may have slightly different properties from the parent compound. These libraries can then be screened using either focused or high throughput screening (HTS). High throughput screening uses robotics, to handle the addition and mixing of reagents, and specialized computers and software, to handle the collection and analysis of data. These are used with a bioassay for a specific pharmacological activity to rapidly test thousands to millions of compounds.

Another method that complements HTS is virtual high throughput screening (VHTS). The approach allows drug discovery programs to save huge costs in manpower and reagents to find compounds with similar substructures and pharmacophores (arrangements of atoms that interact with the receptor at certain key residues) that have a shared biological activity. Using *in silico* techniques, a pharmacophore can be developed for a specific enzyme from a known crystal structure, by mapping key residues at a binding pocket. In addition, a pharmacophore can be developed from a compound with a known activity. Once a favorable pharmacophore is developed, a virtual screen of a chemical library can be conducted. A specialized computer program will search thelibrary of structures to find ones that have molecular features that interact with critical key residues for effective receptor-ligand binding.One advantage of this technique is that researchers don't initially need physical access to a chemical library. By using these virtual screens from a known or potential structure activity relationship, researchers can often purchase smaller sub-libraries of compounds to test biologically. This increases the likelihood that effective hits can be found without the high cost of screening a huge chemical library. Furthermore, it is possible to discover a compound that is not only effective, but has good drug properties: lower toxicity, good pharmacokinetics, increased potency, and decreased cost of synthesis to pursue in the optimization process.

1.3 Triptolide, a biologically active compound in Lei Gong Teng

In classic texts, a tea made from roots of *Lei gong teng* was used to relieve pain and reduce swelling in patients who have swollen joints and difficulty moving. Previous investigations have shown that an alcohol extract from the plant possessed immunosuppressive activity. (Tao, Davis et al. 1991) This and other extracts were tested, along with one of the purified components, triptolide(**1.1**), and they were found to be as effective as steroidal anti-

inflammatory dexamethasone, in reducing LPS-stimulated induction of COX-2 mRNA and synthesis of PGE2. (Tao, Schulze-Koops et al. 1998)The herb itself is toxic however, as alluded to in its other common name, "*qi bu si"*, literally, "seven steps to death." Therefore, herbal extracts of TWHF have seen limited use in the clinic.

Figure I-1. Lei gong teng is the source of natural compound triptolide

The Chinese herb, *Tripterygiumwilfordii Hook F* (TWHF) (A), also known as Lei gong teng or "Thunder god vine" has been used for centuries as a traditional medicine. Triptolide (**1.1**) is a biologically active compound isolated from the root of the TWHF.

A

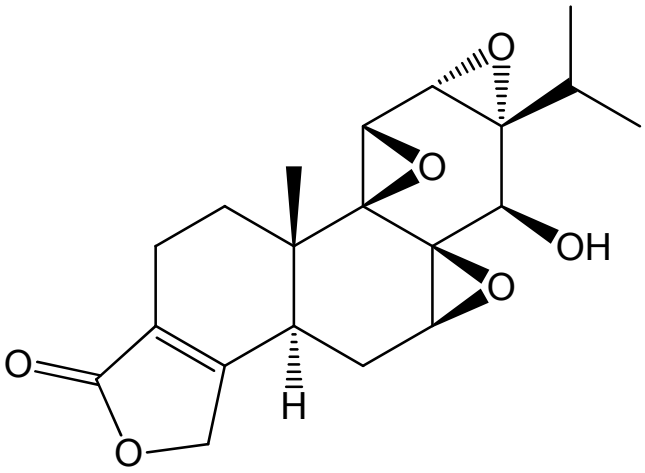

1.1

Triptolide (**1.1**) is a diterpenoidtriepoxide purified from TWHF (Qiu and Kao 2003), which has anti-inflammatory activities against various autoimmune diseases including rheumatoid arthritis (Lipsky and Tao 1997). These anti-inflammatory actions have been attributed to the inhibition of cyclooxygenase (COX)-2 and PGE2 production in rheumatoid fibroblasts and other cell types (Tao, Schulze-Koops et al. 1998).

In addition to inhibiting COX-2 and PGE2 production, triptolide (**1.1**)also has profound effects on immune cells and proinflammatory cytokines. A number of *in vitro* assays have demonstrated that it induces apoptosis in T cells (Yang, Liu et al. 1998), and inhibits lymphocyte proliferation, as well as preventing the synthesis and secretion of proinflammatory cytokines (Lee, Chang et al. 1999). It has been also reported that triptolide (**1.1**)interferes with the gene expression of proinflammatory cytokines in mouse macrophages (Lin, Sato et al. 2001). Finally, studies have shown that triptolide (**1.1**)inhibits dendritic cell-mediated chemo-attraction of neutrophils and T cells through inhibiting Stat3 phosphorylation and nuclear factor NF-κB activation (Liu, Chen et al. 2006).

In addition to its' anti-inflammatory effects in cell-based studies, triptolide (**1.1**)has been shown to effectively mitigate the incidence and severity of cartilage destruction in a rheumatoid arthritis mouse model. One such study showed that prophylactic treatment of triptolide (**1.1**)significantly reduced the arthritic symptoms in collagen-induced arthritis (CIA) rats (Gu, Brandwein et al. 1992). In this study, it was demonstrated that triptolide (**1.1**)effectively reduces cartilage destruction by Matrix metalloproteinase by up-regulation of tissue inhibitors of metalloproteinases (TIMP) production in the joints.In addition, triptolide (**1.1**)reduced the inflammatory response and down regulated the expression of proinflammatory cytokines and

COX-2. Importantly, these pathways are known to be regulated upstream by the transcription factor NF-κB (Siebenlist, Franzoso et al. 1994; Baeuerle and Baltimore 1996).

Together, these studies suggest a potential role for triptolide (**1.1**)as a profound regulator of this inflammatory pathway, however issues with toxicity and water solubility have, until recently, precluded meaningful investigation of this compound.

1.4 Curcumin, a biologically active compound from the tumeric spice.

Curcuma longa is a rhizomatous herbaceous perennial plant of the ginger family. The corresponding spice, turmeric, is extracted from the root of the plant to provide the universally distinctive flavor and yellow color in curry spices. In Ayurveda, tumeric has been used for roughly 4000 years to treat aches, pains, wounds, sprains, as well as disorders of the skin, liver, pulmonary and gastrointestinal systems. The primary reactive ingredient refined from turmeric is curcumin (**2.1**), a poorly soluble yellow powder.

Figure I-2. Curcuma longa is the source of the spice tumeric and the biologically active compound curcumin. The *Curcuma longa*plant (A) is harvested for its root, which is used to make the spice, turmeric (B). The main compound curcumin (**2.1**), is thought to be responsible for tumeric's medicinal properties.

A

B

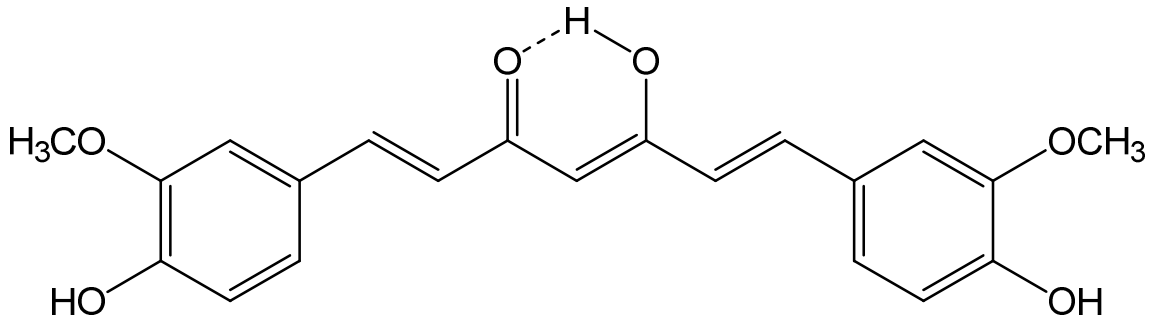

2.1

Curcumin (**2.1**) has been studied extensively as a therapeutic agent for its anti-inflammatory, anti-tumor and anti-angiogenesis properties. (Jurenka 2009; Perry, Demeule et al. 2010) It has been demonstrated that curcumin (**2.1**) inhibits cell proliferation and induces apoptosis in HT-29 colon cancer cells (Lee, Park et al. 2009). In small cell lung cancer, it can inhibit cell proliferation, cell cycle progression, migration, invasion and angiogenesis. (Yang, Liu et al. 2012) These anti-cancer effects have been associated primarily with an underlying mechanism of kinase inhibition. For example, mTOR, MAP kinases and AKT are all targets of curcumin (**2.1**) inhibition. (Zhou, Beevers et al. 2010) Many of curcumin's (**2.1**) anticancer effects have been linked to IKKβ mediated blockade of the NF-κB pathway. (Cohen, Veena et al. 2009)

Curcumin's (**2.1**) uses *in vivo*, however, are limited by its low oral bioavailability. One major problem with ingested curcumin (**2.1**) is that it undergoes rapid first-pass metabolism leading to poor systemic distribution. (Sharma, Steward et al. 2007) Various formulation and delivery strategies are under scrutiny to improve administration. (Ji, Huang et al. 2011) Nonetheless, the natural product is the subject of clinical trials for the treatment of advanced pancreatic cancer (Epelbaum, Schaffer et al. 2010), metastatic breast cancer (Bayet-Robert, Kwiatkowski et al. 2010) and inflammatory bowel disease. (Taylor and Leonard 2011)

1.5 Curcumin analogs.

In attempts to improve the solubility, bioavailability, and stability issues observed for curcumin (**2.1**), a panel of curcumin analogs was generated. The central keto-enol moiety of **2.1** was replaced by a mono-carbonyl group embedded in a heterocyclic six-membered ring conjugated with the flanking C=C bonds. The terminal oxygenated aromatic rings in **2.1** were exchanged for fluorophenyl and pyridine moieties among others. (Adams, Ferstl et al. 2004) The

curcumin (**2.1**) mimics express Michael acceptor properties and deliver stable conjugates when treated with glutathione. (Sun, Lu et al. 2009) Similar claims have been made for curcumin (**2.1**), however isolable conjugates are rarely obtained. (Awasthi, Pandya et al. 2000)

Figure I-3. Structurally similar series of compounds synthesized, based on the structure of curcumin. Both the central and terminal sectors of the molecule **2.1** were modified to give series **2.2**. During a screening by Adams et al., EF24 (**2.3**) became a lead compound in the series.

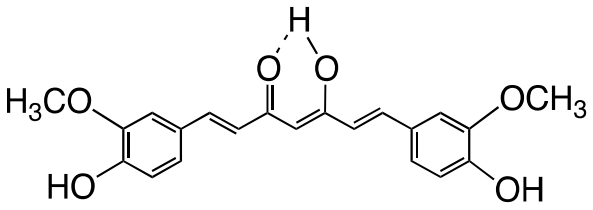

2.1

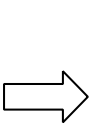

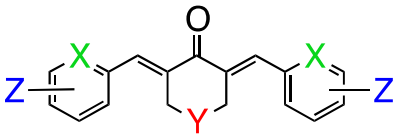

2.2

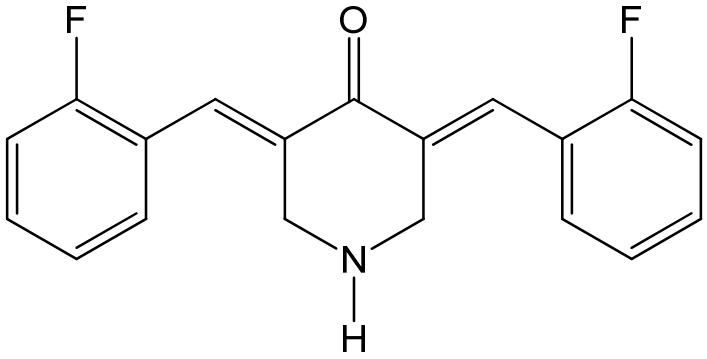

2.3

1.6 Initial screening of curcumin analogs.

Initially, a set of novel curcumin analogs embodied by **2.2** were subjected to the National Cancer Institute in vitro cell line screen. The compounds exhibited anti-cancer and anti-angiogenic activities in cell culture. Some revealed a high degree of cytotoxicity, and most inhibited tumor cell growth with potency greater than cisplatin, a well-established clinical chemotherapeutic agent. (Adams, Ferstl et al. 2004) One compound that performed particularly well in these screenings was EF24 (**2.3**). It was subsequently shown to induce apoptosis in two different cancer cell lines (Adams, Cai et al. 2005) and inhibit activation of the NF-κB pathway by blocking IKKβ kinase. This behavior has been posited to contribute to the compound's anti-inflammatory properties. (Kasinski, Du et al. 2008) EF31 (**2.4**) has also been shown to inhibit inflammation pathways by inhibiting NF-κB binding in mouse RAW264.7 macrophages. (Olivera, Moore et al. 2012)

1.7 NF-κB pathway

The transcription factor NF-κB is implicated in the regulation of many genes that encode for mediators of the immune, acute phase and inflammatory responses. NF-κB is composed of homo- and heterodimeric complexes of members of the Rel (NF-κB) family. There are five subunits of the NF-κB family in mammals: p50, p65 (RelA), c-Rel, p52 and RelB3. These proteins share a conserved 300 amino acid sequence in the N-terminal region, known as the Rel homology domain, that mediates DNA binding, protein dimerization and nuclear localization. This domain is also a target of the IκB inhibitors, which include IκBα, IκBβ, IκBγ, Bcl-3, p105 and p100.

Various dimer combinations of the NF-κB subunits have distinct DNA binding specificities and may serve to activate specific sets of genes such as adhesion molecules,

immunoreceptors, and cytokines. The DNA-binding protein complex recognizes a discrete nucleotide sequence (5´-GGGACTTTCC-3´) in the upstream region of a variety of cellular and viral response genes. The p50/p65 (NFκB1/RelA) heterodimers and the p50 homodimers are the most common dimers found in the NF-κB signaling pathway.

In the majority of cells, NF-κB exists in an inactive form in the cytoplasm, bound to the inhibitory Ⅰ B proteins. Treatment of cells with various inducers results in the phosphorylation, ubiquitination and subsequent degradation of IκB proteins. Proteolytic cleavage of p105 results in two antagonist proteins: p50, which has DNA-binding activity but no transactivation domain, and the inhibitory IκB protein. This results in the release of NF-κB dimers, which subsequently translocate to the nucleus, where they activate appropriate target genes. NF-κB can be activated by a number of stimuli, including components of bacterial cell walls, such as lipopolysaccharide, or inflammatory cytokines, such as TNF-α or IL-1β.

1.8 NF-κB, kinases, and cancer.

There are many examples of constitutive or over-activated kinases associated with cancer. Dependence on the corresponding over-activated signaling pathways create an opportunity for therapeutic intervention. IKKβ is a direct upstream regulator of NF-κB. (Schmid and Birbach 2008) Inhibition of IKKβ-driven NF-κB activation is an approach to cancer control with the capability to transform inflammation induced tumor growth to tumor regression, (Karin 2008) glioblastoma (Nogueira, Ruiz-Ontanon et al. 2011) and pancreatic cancer (Ochiai, Saito et al. 2008) representing two important therapeutic targets. In another example, transfection of either a constitutively active or an over-expressed form of AKT is capable ofblocking apoptosis in many cell types. (Datta, Brunet et al. 1999) Likewise, constitutive activation of the PI3K/AKT signaling pathway is associated with the transformation of a variety of human tumor

cells. Treatment of such tumor cells with agents that specifically inhibit the relevant kinase activity, however, completely suppresses cell proliferation. (Ozaki 2007) Development of new mono-therapeutics have employed this concept. A prime example is Imatinib, a drug that treats chronic myelogenous leukemia by blocking the constitutively activated BCR/ABL tyrosine kinase. (Wadleigh, DeAngelo et al. 2005)

1.9 NF-κB and autoimmune disease.

In patients with arthritis the activation of NF-κB leads to the expressions of many genes that contribute to an inflammatory phenotype, like TNFα from macrophages, MMP from synovial fibroblasts, and chemokines that recruit immune cells. (Simmonds and Foxwell 2008) NF-κB was recognized as one of the key targets to treating arthritis (Sipos, Pietschmann et al. 2008) and NF-κB inhibitors are expected to be a new class of arthritis medications. (D'Acquisto and Ianaro 2006)

1.10 Hypothesis

Dysfunction in the NF-κB pathway is pathological in many disease states including cancer and autoimmune disease. Two naturally occurring compounds triptolide (**1.1**)and curcumin (**2.1**)are good lead compounds that modulate NF-κB. We hypothesize that analogs of these two distinct compounds target a common pathway and they can be further refined to yield improved activity through molecular modeling and medicinal chemistry.

CHAPTER II: Triptolide

2.1 Introduction

The anti-inflammatory properties of the Chinese root Lei gong teng (or TripterygiumWilfordii Hook F; TWHF) have been recognized for centuries, however until recently, the biologically active compound underlying this phenomenon was unknown. Triptolide is a diterpenoidtriepoxide purified from TWHF that has been confirmed as the molecular component responsible for the therapeutic effects of the plant. While studies suggest that triptolide is profoundly effective at mitigating immune and inflammatory processes, such as those seen in cases severe arthritis, the compound itself is hampered by problems with water solubility and toxicity.

To address these problems, this study sought to synthesize and screen a series of triptolide analogs specifically with regard to their effects on NF-κB, a transcription factor that modulates a number of genes that are known components of inflammation pathways. As a part of this project, the analogs were subjected to *in vitro* assays designed to examine cell toxicity, anti-IKKβ kinase activity, and NF-κB translocation. In addition to the cell-based assays, several assays were performed *in vivo* in order to determine the nature of the anti-inflammatory properties of these analogs, as well as their effects on the gene expression of downstream targets.

2.2 Experimental Procedures

Synthesis of salicylaldehydes: To a magnetically stirred solution of 2,5-disubstituted or 2,3,5-trisubstituted phenols (20mmol) in toluene (10mL), triethylamine (8mmol) was added followed by the quick addition of $SnCl_4$ (2mmol from 1.0M solution in CH_2Cl_2). After stirring for half an hour at room temperature, paraformaldehyde (40mmol) was added, a reflux condenser was connected, and the slurry was heated to 95^{o}C for ~12 hours. The reaction mixture was cooled and poured into water (40mL) and acidified to pH 2 with 1 N HCl. The aqueous layer was

extracted with diethyl ether (3 x 60mL). The combined organics were washed with brine, dried with magnesium sulphate, filtered, and concentrated to give a yellow oil that was carried on to the next reaction without further purification. The Rf = 0.54 in hexanes/ethyl acetate 6:1.

Synthesis of salicylalcohols: The crude aldehyde (33mmol) was dissolved in THF (100mL), and the solution was cooled to -78^{o}C. Next, a solution of LAH (33mmol from a 1.0 M solution in THF) was added dropwise. After the addition of LAH was complete, the reaction mixture was allowed to stir at -78^{o}C for 30 minutes and was then allowed to warm to room temperature. The reaction was quenched by the addition of saturated ammonium chloride solution. The pH was adjusted to 4 by using concentrated HCl. The product was extracted using ethyl acetate (3 x 100mL). The combined organics were washed with brine (100mL), dried with magnesium sulphate, filtered, and concentrated to give an orange oil. The product was purified on silica (eluted with hexane:ethyl acetate 6:1) to give a white solid with an Rf = 0.28 in hexanes/ethyl acetate 6:1.

Formation of monoepoxide: To a stirred solution of the salicylalcohol (2mmol) in MeOH (12mL) and water (3mL), was added $NaIO_4$ (2.2mmol) in portions at 0^{o}C. During the course of the reaction a precipitate formed. Once the addition was complete stirring continued for about an hour. The precipitate was filtered off and washed with CH_2Cl_2 (25mL). Water (25mL) was added to the filtrate, and the product was extracted with CH_2Cl_2 (3 x 25mL). The combined organics were washed with brine, dried with magnesium sulphate, filtered, and concentrated. The product was purified on neutralized silica (eluted with hexane:ethyl acetate 8:1 1% triethylamine) to give a bright yellow oil. The Rf =0.39 in hexanes/ethyl acetate 6:1.

Formation of diepoxides: The monoepoxide (26mmol) was dissolved in MeCN (195mL) and 0.4mM $EDTA_{(aq)}$ (130mL). The solution was cooled to 0^{o}C and 1,1,1-trifluoroacetone (1mL)

was added. Next, sodium bicarbonate (202mmol) and oxone (130mmol) were mixed together and added in portions every 5-10 minutes. After addition was complete, the reaction was allowed to stir for another 5 hours at $0^{o}C$. Then the reaction mixture was poured into a sep funnel, water (500mL) was added, and the aqueous layer was extracted with CH_2Cl_2 (3 x 150mL). The combined organic layers were washed with brine (200mL), dried with magnesium sulphate, filtered, and concentrated. The product was purified on neutralized silica (eluted with hexane:ethyl acetate 8:1 1% triethylamine) resulting in two diastereomers. The spot with the higher Rf value corresponds to the trans diastereomer while the spot with lower Rf value corresponds to the cisdiastereomer.

Formation of triepoxides: The diepoxide (1mmol) was dissolved in MeOH (10mL) at room temperature and 1M NaOH (0.47mL) was added followed immediately by the addition of 30% H_2O_2 (1.5mmol). After one hour of stirring at room temperature, water was added (40mL). The aqueous layer was extracted with ethyl acetate. The combined organic layers were washed with brine, dried with magnesium sulfate, and then concentrated under vacuum. The product was obtained after purification on silica using 6:1 hexanes/ethyl acetate.

TransAM NF-κB binding assay. This assay is ELISA-based kit to detect and quantify transcription factor activation. TransAM NF-κB p65 (Cat# 40097, Active Motif, Carlsbad, CA) contains a 96-well plate to which oligonucleotide containing an NF-κB consensus binding site has been immobilized. The activated NF-κB contained in nuclear cell extracts specifically binds to this oligonucleotide. By using an antibody that is directed against the NF-κB p65 subunit, the NF-κB complex bound to the oligonucleotide is detected. Addition of a secondary antibody conjugated to HRP provides chemiluminescent readout that is quantified by luminescence. To overcome this, Active Motif offers a high-throughput assay to quantify NF-κB activation. The

TransAM Kit combines a fast and user-friendly ELISA format with a sensitive and specific assay for transcription factors. TransAM NF-κB Kits contain a 96-well plate on which has been immobilized oligonucleotide containing the NF-κB consensus site (5′-GGGACTTTCC-3′). The active form of NF-κB contained in nuclear extract the Jurkat cells that were stimulated by TPA and calcium ionophore, which was provided in the kit. The primary antibodies used to detect NF-κB recognize an epitope on p65 or p50 that is accessible only when NF-κB is activated and bound to its target DNA. An HRP-conjugated secondary antibody provides a sensitive chemiluminescent readout that is easily quantified by luminescence. As this assay is performed in a 96-well plate, a large number of samples can be handled simultaneously, allowing for high-throughput automation. This assay is specific for NF-κB activation and has been shown to be more sensitive than the gel retardation technique. We detect NF-κB activation with 2 μg of nuclear extract from Jurkat cells stimulated with TPA and calcium ionophore. The wild-type consensus oligonucleotide is provided as a competitor for NF-κB binding in order to monitor the specificity of the assay. Used at 20 pmol/well, the oligonucleotide will prevent NF-κB binding to the probe immobilized on the plate. Conversely, the mutated consensus oligonucleotide should have no effect on NF-κB binding. For TransAM HIF-1 assay (Cat# 47096), 2 μg of nuclear extract was used according to the manufacturers' instruction.

Semiquantitative RT-PCR of COX-2 mRNA. The mRNA levels of COX-2 from A172 cells were assessed by RT-PCR. On day 1 confluent 100 mm plate of A172 cells in DMEM (++) media were split 1:4 and then incubated at 37 degrees for 24 hours. After that the media was removed and replaced with media that contains 10nM PMA and then incubated at 37 degrees for 24 hours to allow for differentiation. Then the PMA media was aspirated and media was added to cells with either vehicle (0.1% DMSO) or test compound for 1 hr. LPS was added to a

concentration of 10mg/L to each plate except unstimulated control and the cells were incubated for 3 hours.

Total cellular RNA was obtained by Trizol RNA preparation protocol. First strand cDNA was synthesized from 2 μg total RNA in a 20 μL reaction volume using random decamers and M-MLV reverse transcriptase. The resultant cDNA was amplified by PCR following a standard PCR protocol. The COX-2 primers were sense: 5′GGGCAAAGACTGCGAAGAAG3′ and antisense: 5′CCCATGTGACGAAATGACTG3′, which result in a product of 275 bp. The β-actin primers were sense: 5′AGCGGGAAATCGTGCGTG3′ and antisense: 5′CAGGGTACATGGTGGTGCC3′, which result in a product of 305 bp. After an initial denaturation at 95 °C for 5 min, the following cycling profile was used: denaturation at 95 °C, annealing at 60 °C and extension at 72 °C for 30 s each. Amplification was performed 30 cycles for COX-2 and 20 cycles for β-actin. Reaction was ended with a final extension at 72 °C for 5 min. All PCR products were electrophoresed on 1% agarose gel and stained with ethidium bromide. The gels were visualized under ultraviolet illumination and photographed.

Semiquantitative RT-PCR of TNF-α and interferon-α mRNA Molt-4 cells were routinely maintained in 5% CO_2 at 37 degrees C in RPMI-1600 (Sigma, St. Louis, MO) supplemented with 10% fetal bovine serum (FBS; Sigma), 50 U/ml of penicillin, and 50 μg/ml of streptomycin (Invitrogen, Carlsbad, CA). They were treated with 1 ug/ml of LPS for 3 hrs after cells were treated with 1 ng/ml of PG490 (**1.1**), 1ng/ml or 10 ng/ml of GB67B (**1.5**)for 15min. Total RNA was isolated from these treated cells by using Trizol (Invitrogen). For RT-PCR, β-actin primers are from our previous post and TNF and IFNα2 primer sets were from SuperArray. 0.5 μg total RNA was transcribed in 20 μl reaction volume. 2 μl of cDNA from RT-reaction was in 20 μl of

PCR reaction. The thermal profile for PCR was 95°C for 10 min followed by 40 cycles of 95°C for 30 s, 55°C for 30 s, and 72°C for 30 s.

High Performance Liquid Chromatography Plasma samples were injected into a HPLC system comprised of a Beckman Gold 126 solvent module, a Gold 168 Detector, a Rheodyne 7725i manual sample injector and fitted with a Luna 5μ C18 column (4.6 mm x 250 mm, Phenomenex). The HPLC analysis employed a detection wavelength of 254 nm and a mobile phase consisting of a mixture of acetonitrile (ACN)-H_2O (35:65, v/v) under isocratic conditions.

λ-carrageenan paw edema model. Acute inflammation was induced by subdermal injection of 50 μl of λ-carrageenan (1% w/v in saline) or saline into the right or left hind paw of female C57BL/6J mice (Jackson Laboratories). Triptolide analogs were all administered intraperitoneal at 30 mg/kg 30 min following carrageenan challenge and continued daily. All triptolide analogs were dissolved in 10% DMSO and 90% 45% (2-Hydroxypropyl)-beta-cyclodextrin (CD). Control animals received corresponding i.p. injections of vehicle. The volume of the carrageenan injected hind paw was measured by a caliper and compared to the volume of untreated contralateral paw to obtain the edema volume. To get a baseline paw measurement, paw width is measured from the "palm" to the back of the paw on both the right and left hind paws. The volume of the contralateral paw was subtracted from the volume of the injected paw to obtain the edema volume. The animals were sacrificed 74 h after induction of inflammation, 2h after the last injection of triptolide analogs. Following the final paw measurements, the paws were photographed, then removed with scissors and placed into formaldehyde solution for paraffin embedding and histological analysis using H&E staining. Liver and brain were also removed and immediately frozen in liquid nitrogen, and kept at -80^{o}C.

RNase protection assays. RNase protection assays to simultaneously detect cytokine mRNAs (TNFalpha, IL-1 alpha, IL-1 beta, IFN-alpha, and IL-6) were performed using RNA extracts obtained from liver tissues with a riboquant custom probe set from PharMingen (San Diego, CA). The liver tissue samples were immediately homogenized with Trizol reagent (1 ml per 100 mg of tissues) using Eberbach Con-torque power unit (Ann Arbor, MI) to yield total RNA, and were centrifuged to remove cellular debris. RNA pellets for each liver section were obtained from three to five mice, and were resuspended in nuclease-free water for group/batch processing. ^{32}P-uridine triphosphate-labeled cRNA probes were hybridized overnight with 20 μg of total sample RNA at 56 ^{o}C, digested with RNase A/T1 mixtures, extracted with phenol/chloroform, ethanol precipitated and then separated on 5% polyacrylamide/8M urea gels. The gels were dried and then subjected to autoradiography to observe protected bands. Specific bands were identified based on their individual migration patterns in comparison with the undigested probes.

Disease Activity Index scoring. Disease activity index (Dai, Jin et al.) was determined by combining scores of a) weight loss b) stool consistency and c) bleeding (divided by 3). Each score was determined as follows, change in weight (0:<1%, 1: 1–5%, 2: 5–10%, 4:>15%), stool blood (0: negative, 2: positive) or gross bleeding (4), and stool consistency (0: normal, 2: loose stools, 4: diarrhea).(Dai, Jin et al.)

Colon pathology score. H&E-stained colon tissue sections were scored on a 0–4 scale, based on the following criteria for severity of histopathology: 0, No change from normal tissue; Grade 1, mild inflammation present in the mucosa, comprised mainly of mononuclear cells, with little epithelial damage; Grade 2, multifocal inflammation greater than a Grade1 score, including mononuclear and few polymorphonuclear cells (neutrophils), crypt glands pulled away from the basement membrane, mucin depletion from Goblet cells, and the epithelium occasionally pulled

away from the mucosa into the lumen; Grade 3, mutlifocalinflammation greater than a Grade 2 score, including mononuclear and neutrophils progressing into the submucosa, crypt abscesses present with increased mucin depletion, and presence of epithelial disruption, including some ulceration; Grade 4, crypts no longer present, severe mucosal inflammation mainly composed of neutrophils, and epithelium no longer present or completely detached. Anaverage of four fields of view per colon was determined foreach mouse. These scores were averaged per group and recordedas the histopathology score ± SE.

Real time PCR for GAPDH, TNF-α, IL1β, IL-6, MCP-2. Colonic tissue was used for isolation total RNA with Trizol reagent following manufactory instruction. cDNA was synthesized using SuperscriptTM First -Strand synthesis system (Invitrogen). Real-time PCR was performed using Bio-Rad iQTM SYBR Green supermix. The primers used in this study are: GAPDH, 5′-AAC TTTGGCATTGTGGAAGG and 3′-ACACATTGGGGGTAGGAACA; IL1β, 5′-AACCTGCTG GTGTGTGACGTTC and 3′-CAGCACGAGGCTTTTTTGTTGT; IL6, 5′-CGTGGAAATGAG AAAAGAGTTGTG and 3′-CCAGTTTGGTAGCATCCATCATTTCT; MCP-1, 5′-ACTGAA GCCAGCTCTCTCTTCCTC and 3′-TTCCTTCTTGGGGTCAGCACAGAC; IL-8, 5′-CTG GCCGTGGCTCTCTTGG and 3′-ATGCACTGACATCTAAGTTC; IL-10 5′-TACCTGGTA GAAGTGATGCC and 3′-CATCATGTATGCTTCTATTC; TNF-α, 5′-CCGATGGGTTGT ACCTTGTCT and 3′-TGTGGGTGAGGAGCACGTAGTCG. For GAPDH, TNF-α, IL1β, IL-6, MCP-2, Real time PCR reactions were performed at 50 °C 2min, 95 °C for 10min, and 45 cycles at 95°C for 30s and 60°C for 1min. For IL-8 and IL-10, those parameters were 95 °C for 10 min, and 45 cycles at 95°C for 30 s, 55°C for 30s and 72°C for 30s.

Z'Lyte Kinase Assay. See Chapter 3.2 Experimental procedures.

NF-κB Translocation Assay. HeLa cells were plated to a 96 well plate (4000 cells/well) with DMEM + 10% FBS, incubated for 24 hours. Cells were then treated with triptolide analog GB67B (**1.5**) (1uM) for 1hr. They were then stimulated with 5 ng/mL IL-1α. Cells were then fixed and labeled using Cellomics HitKit and visualized using fluorescence microscopy with overlays constructed with MetaMorph. Unstimulated control did not receive IL-1α and NF-κB is localized to the cytoplasm. In the stimulated control, NF-κB is localized to the nucleus and overlaps with Hoechst dye.

2.3 Results

2.3.1 The structure of the natural product triptolide inspires a series of analogs.

Despite its interesting mechanism of action, triptolide (**1.1**)is also quite toxic and has poor water solubility. To circumvent these problems, Greg Bluemling tried to develop analogs of triptolide (**1.1**)that exhibited improved potency, lower toxicity, and had a straightforward synthesis. It was hypothesized that the pharmacophore of triptolide (**1.1**)resided in its triepoxide moiety, so he chose to synthesize derivatives of the triepoxide array.

Figure II-1. Chemical synthesis of triptolide analogs

Greg Bluemling used salicylic alcohols derived from phenols to access the diepoxide and triepoxide system of the truncated triptolide analogs. Thus, starting from various phenols, he was able to produce a novel series of analogs by systematic and stepwise oxidation of early synthetic intermediates.

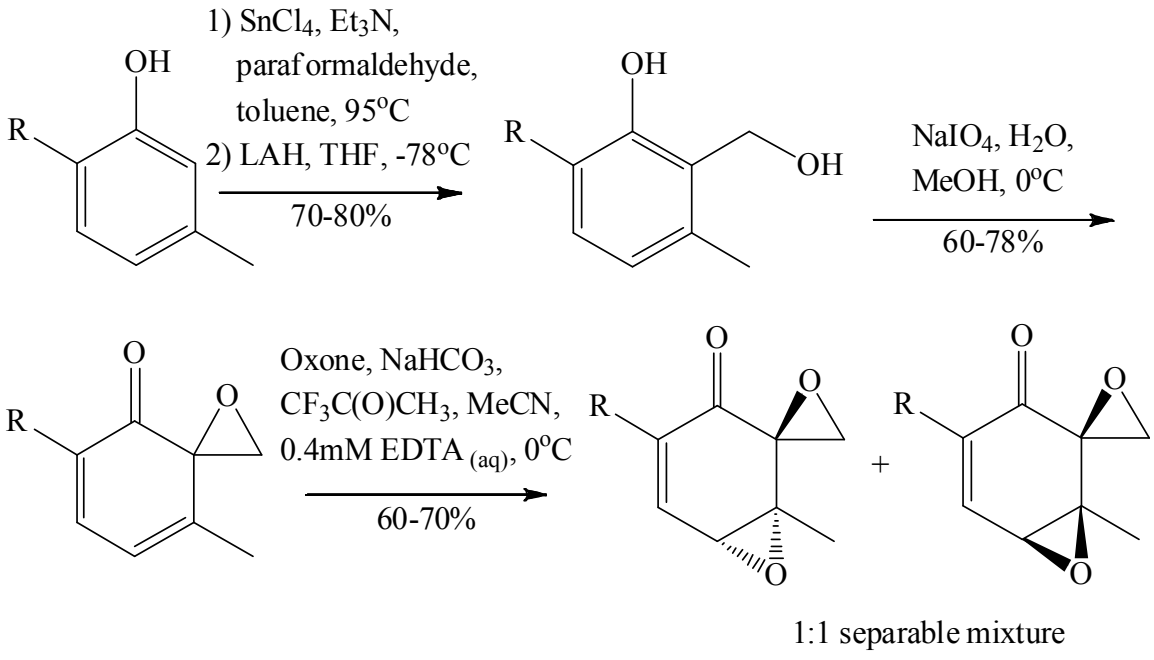
1) SnCl4, Et3N,
paraformaldehyde,
toluene, 95°C
2) LAH, THF, -78°C
70-80%
NaIO4, H2O,
MeOH, 0°C
60-78%
Oxone, NaHCO3,
CF3C(O)CH3, MeCN,
0.4mM EDTA (aq), 0°C
60-70%
1:1 separable mixture

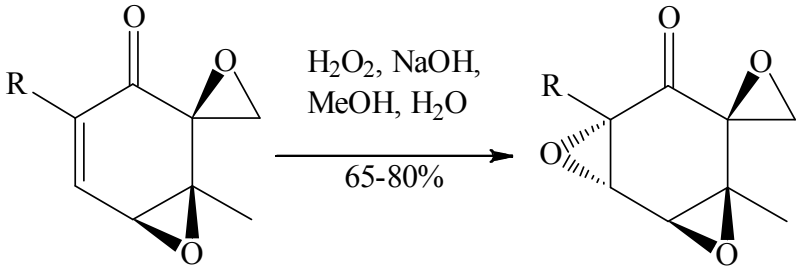
H2O2, NaOH,
MeOH, H2O
65-80%

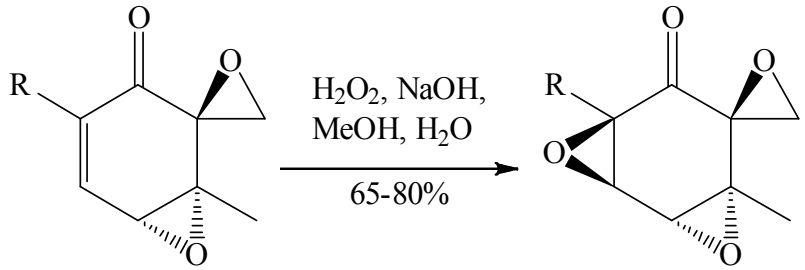
H2O2, NaOH,
MeOH, H2O
65-80%

Figure II-2. Structures of triptolide analogs

Using the synthesis methods outlined in Figure II-1, a variety of analogs were generated using various phenols some of which were commercially available and others that required their own synthesis.

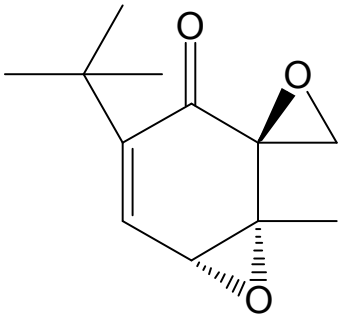

1.2

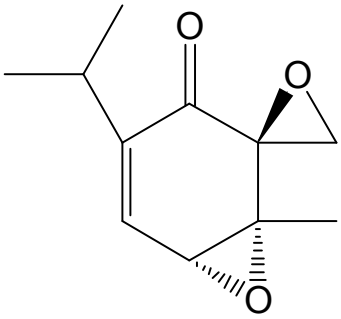

1.3

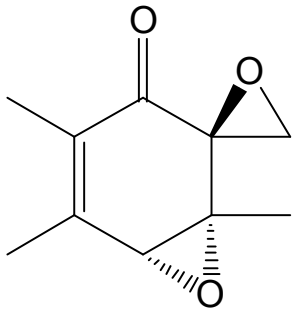

1.4

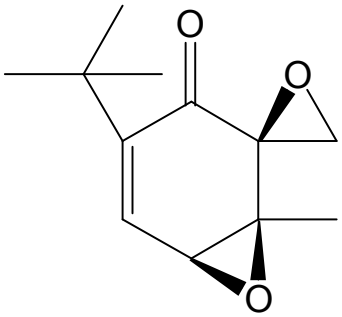

1.5

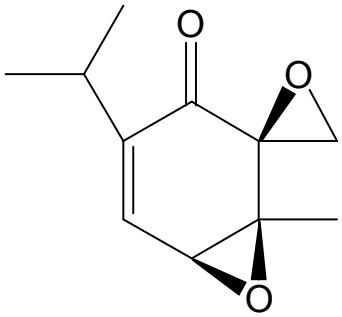

1.6

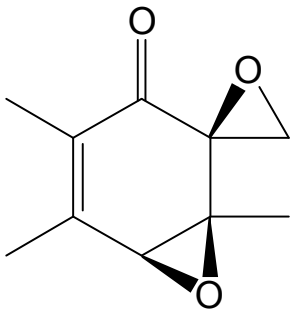

1.7

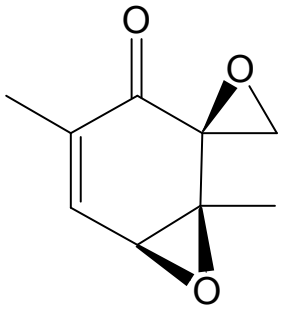

1.8

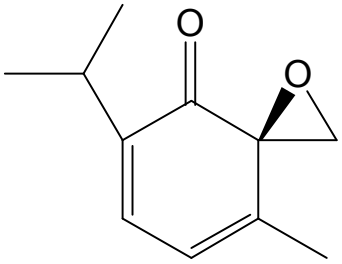

1.9

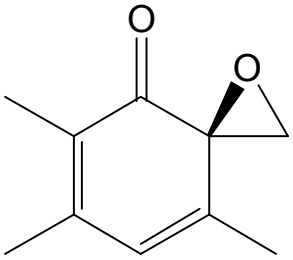

1.10

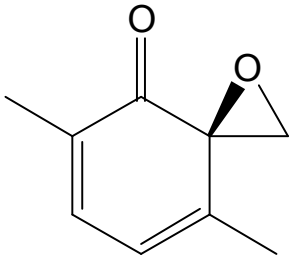

1.11

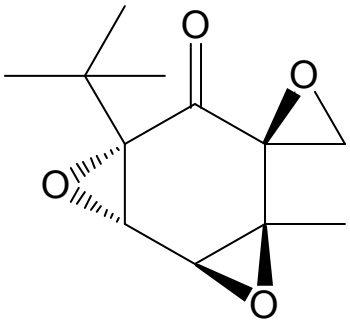

1.12

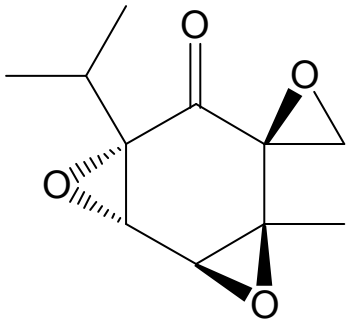

1.12

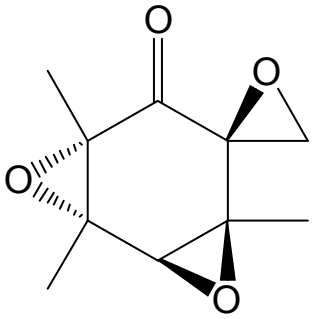

1.13

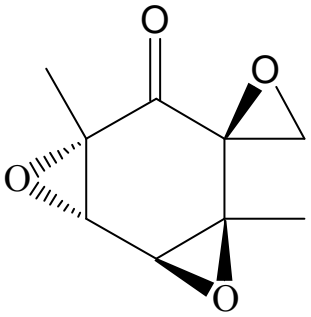

1.14

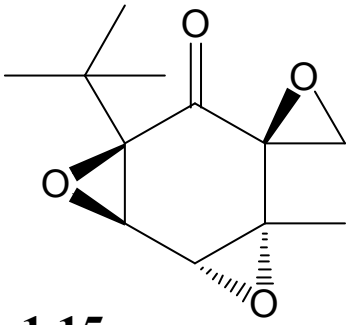

1.15

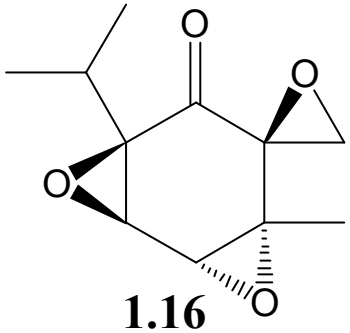

1.16

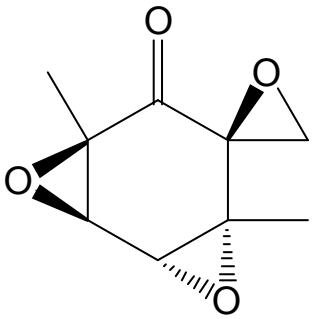

1.17

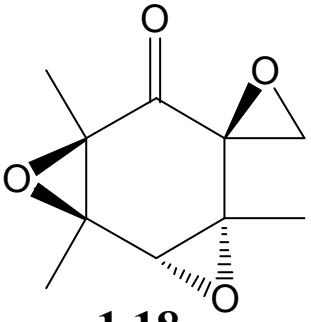

1.18

2.3.2 Screening of analogs for anti-NF-κB activity.

In order to determine which triptolide analogs were going to be effective anti-inflammatory agents we needed a primary screening method. To determine the efficacy, the TRANS-AM assay from Active Motif was selected as the primary screening tool. This assay measures p65 NF-κB binding to its DNA binding consensus sequence in a nuclear cell lysates, similar to the traditional gel shift assay in a high throughput format. The kit contains a 96-well plate to which oligonucleotide containing an NF-κB consensus-binding site has been immobilized. The activated NF-κB contained in nuclear cell extracts specifically binds to this oligonucleotide. By using an antibody that is directed against the NF-κB p65 subunit, the NF-κB complex bound to the oligonucleotide is detected. Addition of a secondary antibody conjugated to horseradish peroxidase (HRP) provides chemiluminescent readout that is easily quantified.

Figure II-3. Triptolide analogs exhibit better potency the triptolide itself.

By using TranAM NF-κB p65 assay kit, Sijia Wang screen a panel of triptolide analogs and determined their blocking efficiency for NF-κB DNA binding compared it to that of triptolide (**1.1**)(PG490) itself at 1 μM. Because the kit was provided with the concentrated nuclear extract, this does not actually represent true physiological conditions, in that normally there would be significantly less protein and genetic material.

We found that most of the novel triptolide analogs have much higher potency than triptolide (**1.1**)itself. Compounds GB97 (**1.15**) and GB67B(**1.5**) had over 90% inhibition at 1uM, and several more exhibited inhibition over 50%. This demonstrates higher blocking efficacy than triptolide (**1.1**). Many of the analogs were at least as good as triptolide(**1.1**), only 199C(**1.7**) and 187C (**1.14**) had significantly lower inhibition.

Compound	Designation	% Inhibition
1.15	GB97	98%
1.5	GB67B	90%
1.8	GB187D	77%
1.12	GB117B	67%
1.13	GB153	67%
1.6	GB65B	64%
1.12	GB99	55%
1.2	GB67A	42%
1.17	GB265B	37%
1.4	GB263	37%
1.16	GB117A	35%
1.1	GB197	34%
1.18	GB265A	31%
1.9	GB147	31%
1.1	Triptolide PG490	30%
1.3	GB65A	28%
1.11	GB165	26%
1.7	GB199C	10%
1.14	GB187C	0%

2.3.3 Further testing in cell based assays.

The screening demonstrated which compounds would be good candidates for further study by showing which compounds potently interfered with the binding interaction of NF-κB and its' DNA consensus sequence. In this manner, the field of compounds was reduced to the three best, GB97 (**1.15**), GB67B(**1.5**), and 187D (**1.8**). While the Trans-AM assay was a good assay for screening compounds, it is an artificial system and further testing of the compounds would be need to show that their effects are biologically relevant. We hypothesized that since triptolide(**1.1**) was known for NF-κB inhibition in cells, our analogs would affect genes unregulated by cells in response to a proinflammatory stimulus.

Figure II-4. Inhibition of COX-2 mRNA by triptolide analogs.

NF-κB regulates the transcription of many genes including COX-2. COX-2 mRNA levels are often used as an indicator of NF-κB activation. From the initial screen of the analogs, three of the most potent, GB67B (**1.5**),GB97 (**1.15**), 187D (**1.8**)were selected for further analysis and compared to triptolide (**1.1**) for a total of four drugs at four concentrations(1000nM, 100nM, 10nM, 1nM). Using the A172 astroglial cell line and LPS as a proinflammatory stimulus, COX-2 mRNA levels were analyzed using semi-quantitative reverse transcriptase PCR. All of these compounds showed a dose dependant decrease in COX-2 mRNA levels associated with increasing concentrations when compared to the untreated control (vehicle, +LPS) and the unstimulated control (vehicle, -LPS). Though there doesn't seem to be enough difference to make comparisons between the analogs.

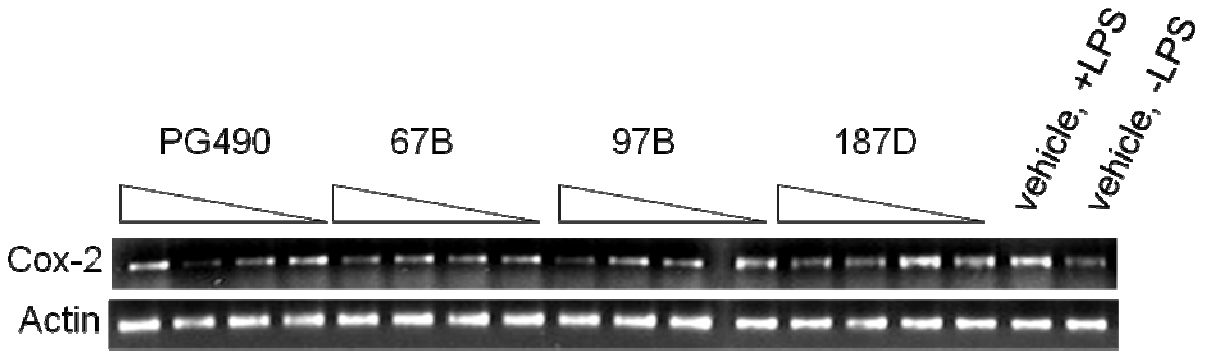
PG490
67B
97B
187D
vehicle, +LPS
vehicle, -LPS
Cox-2
Actin

Figure II-5. Inhibition of TNF-α and IFN-α mRNA by triptolide analogs.

Exposure of T-cell or B-cell lymphoblasts to LPS leads to activation of NF-κB, which leads to the initiation of transcription of genes that are relevant for the immune response (Muller, Ziegler-Heitbrock et al. 1993). The selected compounds were further tested for its blocking efficacy of LPS-induced cytokine upregulation (TNF-α and IFN-α) in MOLT-4 T lymphoblasts.

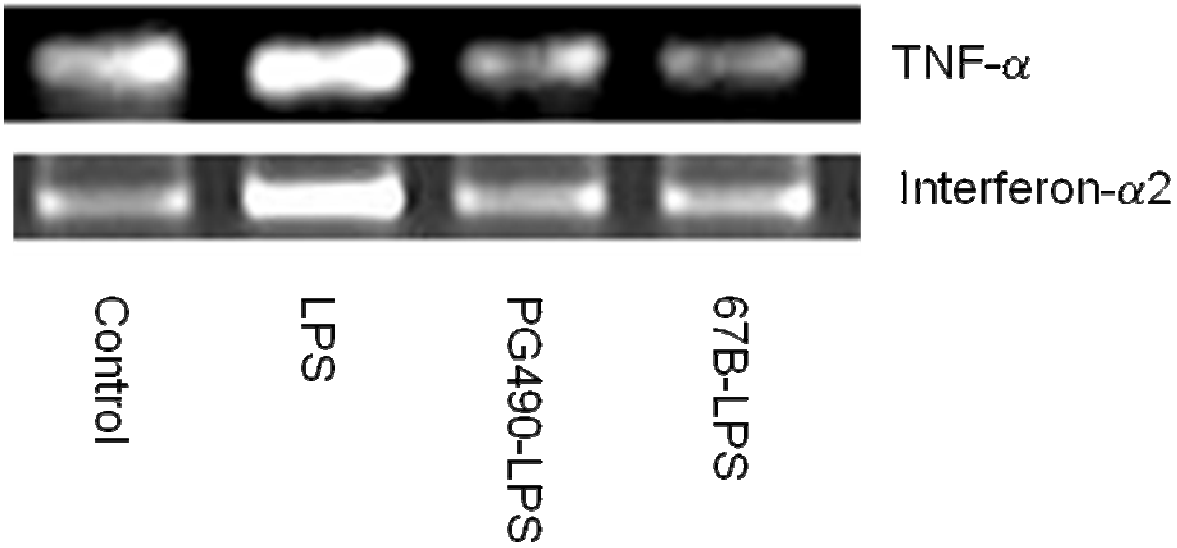
TNF-α
Interferon-α2
Control
LPS
PG490-LPS
67B-LPS

2.3.4 Inhibition of NF-κB target genes

This data builds on our initial findings with the in vitro assay. It shows that the analogs function in a cell based environment to interrupt NF-κB binding to DNA translates to changes in expression of genes that are upregulated by NF-κB. There was a nice dose response correlation with GB67B (**1.5**),GB97 (**1.15**), 187D (**1.8**), when looking at COX-2 mRNA. While there didn't appear to be a significant difference between GB67B(**1.5**) and triptolide (**1.1**)in the case of interferon α2, GB67B(**1.5**)clearly shows more inhibition of TNF-α than triptolide(**1.1**).

2.3.5 Pharmacokinetics

Having demonstrated the *in vitro* potency and efficacy of the triptolide analogs, we turned our attention to its serum stability and bioavailability profile in mice to establish a basis for advancement into *in vivo* models. In order, to determine if HPLC was a viable method for measuring drug levels in mice, an intravenous study was conducted first, and then followed up by an intraperitoneal injections and oral gavage.

Figure II-6. *In vivo* plasma stability study in mice

To determine the plasma half-life of GB67B(**1.5**), it was dissolved in a formulation of 10% (v/v) DMSO and 90% (v/v) 45% (2-Hydroxypropyl)-beta-cyclodextrin (CD) and administered intravenously to mice at 40 mg/kg. The retention time of GB67B(**1.5**) was determined to be 9.67 min at a flow rate of 1 ml/min (A). Plasma samples (~50 μl each) were collected at three time-points (5, 15, and 30 minutes) and processed to remove macromolecules and blood cells. GB67B(**1.5**)has a reasonable half-life of 45 minutes in mice when it is administered intravenously (B).

We also determined the plasma stability of the compound delivered intraperitoneally and by oral gavage. Mice were injected with 300 mg/kg i.p. or fed with 300 mg/kg using a feeding needle. The animals tolerated the high doses well without overt signs of toxicity. The high dose was required in order to achieve plasma concentrations that could be detected by our HPLC detection methods. At determined time points, ~50 μl of blood drawn by orbital bleed was processed as described above to determine the concentration of the compound in mouse plasma. As shown in (C) and (D), GB67B(**1.5**) levels were stable for 200 minutes following both intraperitoneal injection and oral gavage respectively. Of note, GB67B(**1.5**) was not toxic to mice up to the highest concentration tested (40 mg/kg, i.v., and 300 mg/kg i.p. and oral) whereas as a dose as low as 5 mg/kg intravenous injection of triptolide (**1.1**)itself, quickly resulted in the mice dying.

A

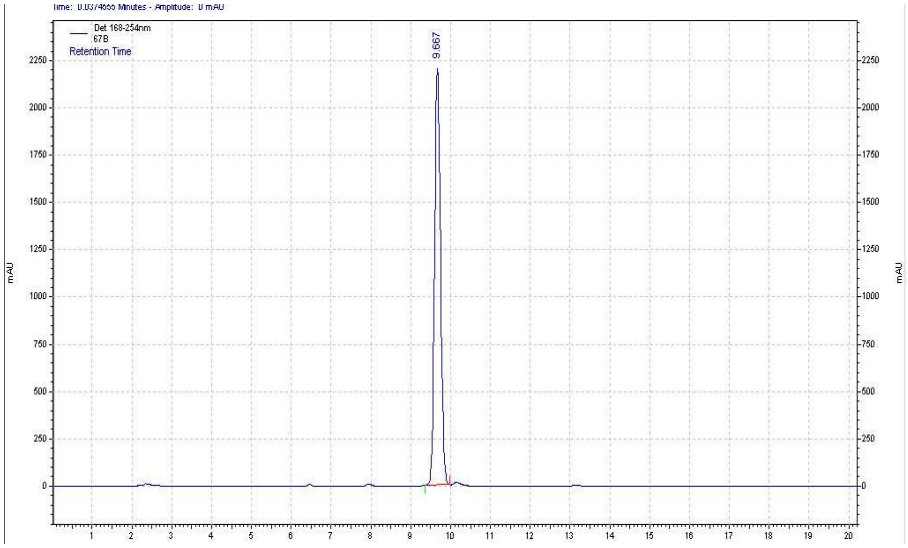
Det 168-254nm
67B
Retention Time
9.667
mAU

B

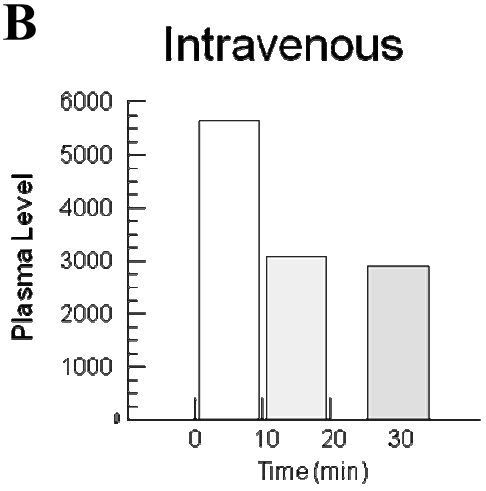
Intravenous
Plasma Level
6000
5000
4000
3000
2000
1000
0
10
20
30
Time (min)

C

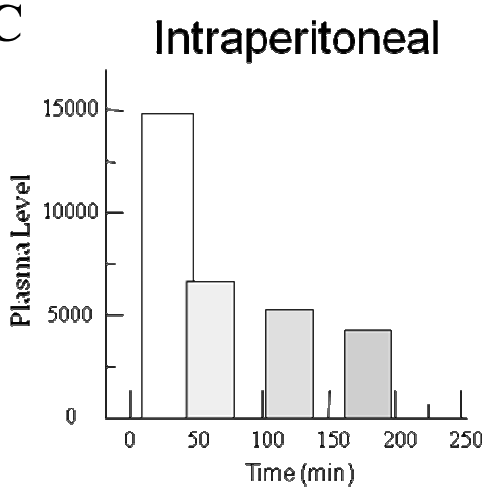
Intraperitoneal
Plasma Level
15000
10000
5000
0
50
100
150
200
250
Time (min)

D

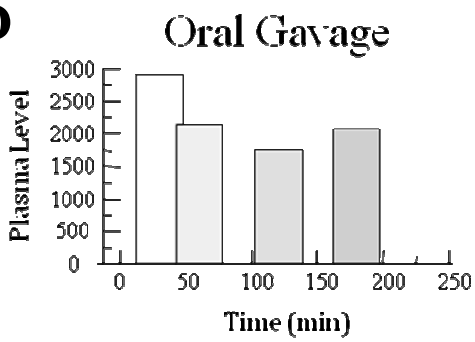
Oral Gavage
Plasma Level
3000
2500
2000
1500
1000
500
0
50
100
150
200
250
Time (min)

2.3.6 Toxicity

A critical problem of the parent compound triptolide (**1.1**) is its severe toxicity. One of our goals of the current drug development effort was to mitigate the toxicity of the triptolide analogs, while maintaining or improving the anti-inflammatory efficacy.

Figure II-7. Toxicity toward MDA-MB-231 cells.

We determined the cytotoxicity of the triptolide analogs in vitro using MDA-MB-231 cells treated with different concentrations of the antagonist and the effects on proliferation was determined. While 24-hour treatment of 10 μM PG490(**1.1**) reduced cell proliferation by 35%, GB97 (**1.15**) or GB67B(**1.5**) hardly affected cell proliferation. The toxicity of GB97 (**1.15**) or GB67B(**1.5**) was compatible to that of NEMO (NF-κB essential modifier or IKKγ)-binding domain peptide (NBD). NBD is a peptide-based selective inhibitor of NF-κB activation that blocks the interaction of NEMO with the IκB kinase complex (May, D'Acquisto et al. 2000). Our analogs did not affect MDA-MB-231 cell proliferation even at 10 μM concentration while triptolide (**1.1**) itself did. Thus, these new triptolide analogs are less cytotoxic than triptolide (**1.1**) in MDA-MB-231 cells.

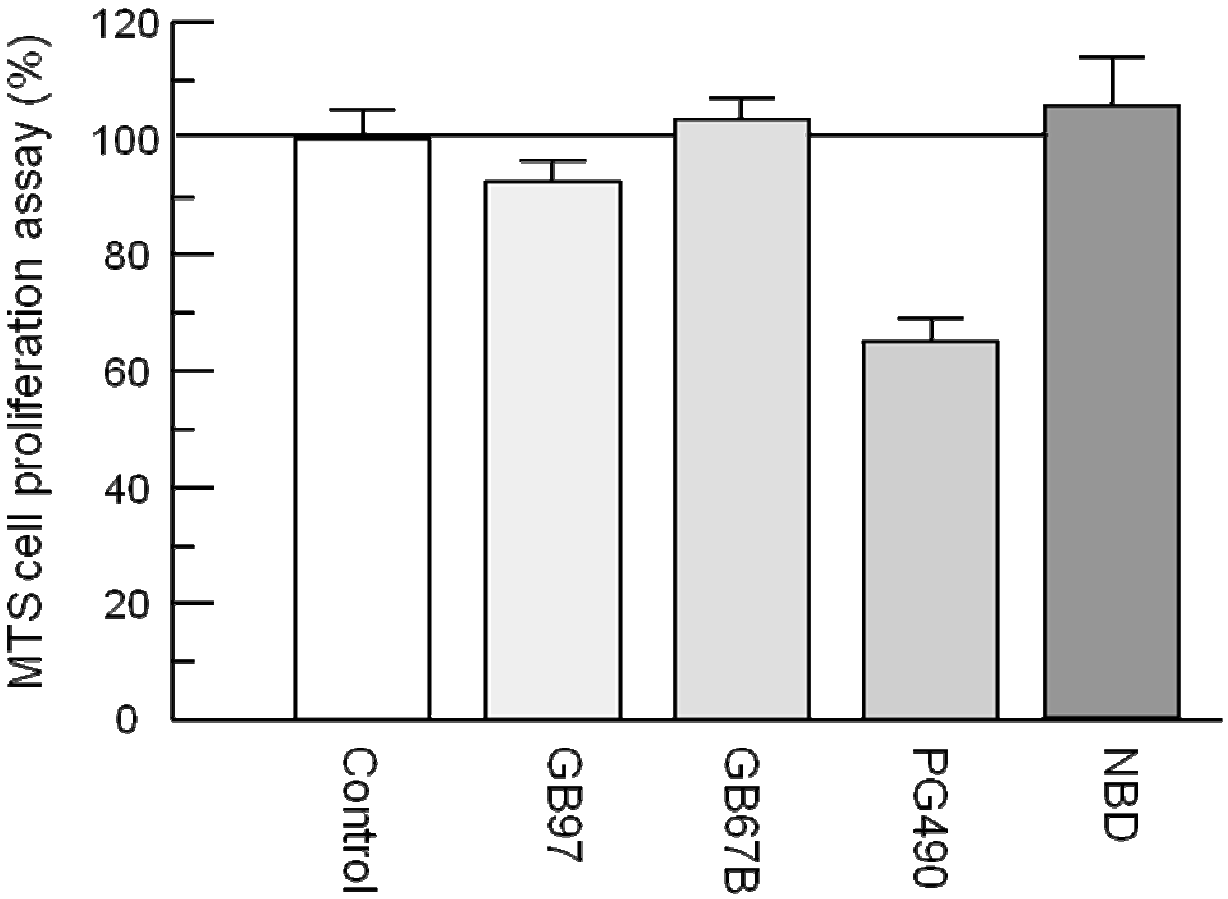
MTS cell proliferation assay (%)
120
100
80
60
40
20
0
Control
GB97
GB67B
PG490
NBD

Figure II-8. Five day toxicology study in mice.

Mice were dosed with 0 and 100 mg/kg of GB67B(**1.5**)i.p. once per day for 5 days. No signs or symptoms of toxicity were observed in any of the animals during the study, and no toxicity was observed upon termination from gross necropsy. The blood serum chemistry was analyzed by Charles River Diagnostics (Wilmington, MA) showed that treated mice did not exhibit any illness or organ dysfunction. To evaluate the possibility for systemic toxicity of the triptolide analogs, several organs were examined microscopically. In particular, no central necrosis was observed in the liver and no tubular necrosis in the kidney. H&E staining results demonstrate that there was no damage in these organs of the representative mice of each group.

Printed: Wednesday, June 6, 2007 at 13:07

Charles River Diagnostics
251 Ballardvale Street, Wilmington, MA 01887 USA
Tel: 800-338-9680 Fax: 978-658-7698

Sponsor: Emory University **Accession #: 2007-024617**

Diagnostic Summary Report

Division of Animal Resources
Whitehead Research Building G02
615 Michael Street
Atlanta, GA 30322 USA

Attn: Karen A. Lieber
Tel: 404-712-9902

Received: 01 Jun 2007
Approved: 06 Jun 2007, 13:05
Bill Method: Stdg PO# U000 8850
Test Specimen: serum Mouse
Product: L23 Study Mice (Serial: 21595)
Collected: May 31, 2007

Sample Set	Service (# Tested)	Profile	Assay	Tested	+	+/-	?
#1	Clinical Pathology (4)	All Results Negative					

* + = Positive, +/- = Equivocal, ? = Indeterminate

Service Approvals

Service	Approved By*	Date
Clinical Pathology	Janet M. Wunderlich	06 Jun 2007, 13:05

Printed: Wednesday, June 6, 2007 at 13:07

Charles River Diagnostics
251 Ballardvale Street, Wilmington, MA 01887 USA
Tel: 800-338-9680 Fax: 978-658-7698

Sponsor: Emory University **Accession #: 2007-024617**

Product: L23 Study Mice (Serial: 21595) **Test Specimen:** serum Mouse **Received:** 01 Jun 2007

Serology Clinical Pathology Results Report

Department Review: Approved by Janet M. Wunderlich, 06 Jun 2007, 13:05*

Chemistry Profile Complete

Sample #: / Code :	1 07-32xA	2 07-32xB	3 07-32xC	4 07-32xD
CHOL (mg/dl)	62	QNS	63	85
TRG (mg/dl)	58	QNS	94	97
GGT (u/l)	NT	NT	NT	NT
ALT (u/l)	75	125	60	60
AST (u/l)	138	294	203	226
ALK (u/l)	97	125	104	QNS
TBIL (mg/dl)	0.3	0.4	0.5	2.9
GLU (mg/dl)	QNS	QNS	QNS	QNS
PHOS (mg/dl)	6.1	11.5	6.5	5.2
TPR (g/dl)	4.9	5.8	5.7	6.1
CAL (mg/dl)	9.7	10.1	10.2	11.4
BUN (mg/dl)	33	34	34	23
CRE (mg/dl)	0.5	0.4	0.3	0.1
ALB (g/dl)	2.9	3.2	3.4	3.0
NA (meq/l)	QNS	QNS	QNS	QNS
K (meq/l)	QNS	QNS	QNS	QNS
CL (meq/l)	QNS	QNS	QNS	QNS

Remarks: NT= Specimen not tested
QNS= Quantity not sufficient

2.3.7 *In vivo* studies

Figure II-9. Carrageenan paw edema model.

Apparent edema response could be seen 24 h after the λ-carrageenan injection (compare to the contralateral paw that is injected with saline). Triptolide analogs were all administered i.p. at 30 mg/kg 30 min following carrageenan challenge and continued daily. The volume of the carrageenan injected hind paw was measured by a caliper and compared to the volume of untreated contralateral paw to obtain the edema volume. The animals were sacrificed 74 h after induction of inflammation, 2h after the last injection of triptolide analogs. Three of the best compounds were investigated and only GB67B(**1.5**) was found to reduce the edema paw volume.

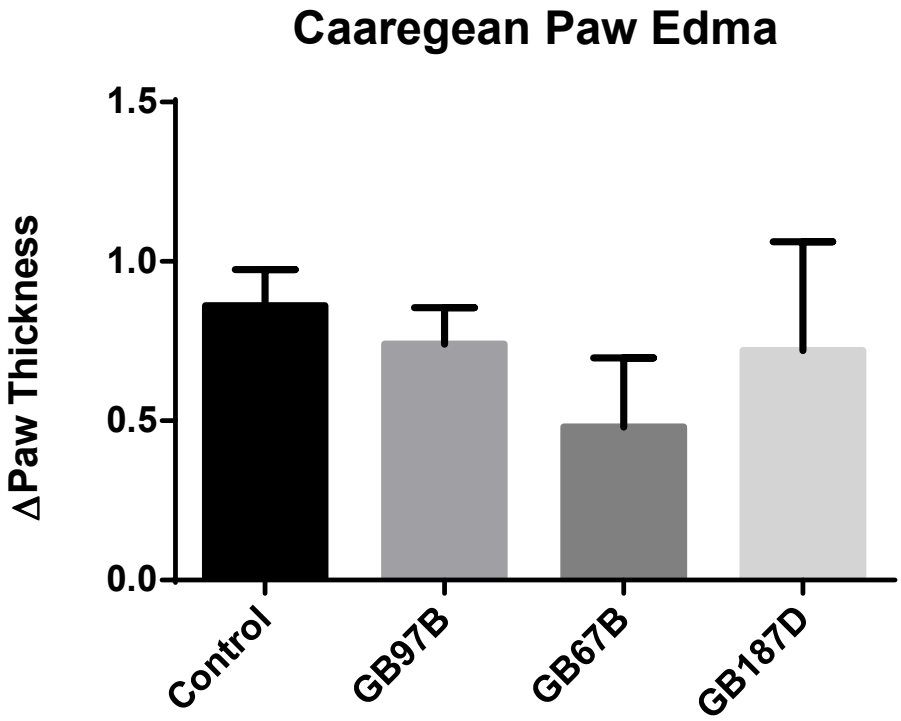
Caaregean Paw Edma
ΔPaw Thickness
1.5
1.0
0.5
0.0
Control
GB97B
GB67B
GB187D

Figure II-10. Mouse liver RNase protection assay.

The livers of mice from the various groups from paw edema model were processed by Trizol-based method to generate total RNAs. These total RNAs were used in conjunction with an RNase protection assay simultaneously detect the levels of inflammation-related cytokine levels.

Carrageenan injected to one of the paws dramatically increased inflammation-associated cytokine levels, such as TNF-α, IL-1α, IL-1β, Interferon-α, IL-6, interferon-γ in the liver that was measured by RNase protection assay lane 2. This upregulation of cytokine levels were blocked in various degrees by all three triptolide analogs, GB97 (**1.15**), GB67B(**1.5**), and 187D (**1.8**)shown in lanes 3, 4, and 5 respectively. Of note, although all three analogs were able to reduce carrageenan-induced cytokine upregulation, the treatment with GB67B(**1.5**), the most effective triptolide analog in this assay, was able to reduce paw inflammation in Figure II-9 while GB97 (**1.15**) and 187D (**1.8**) could not.

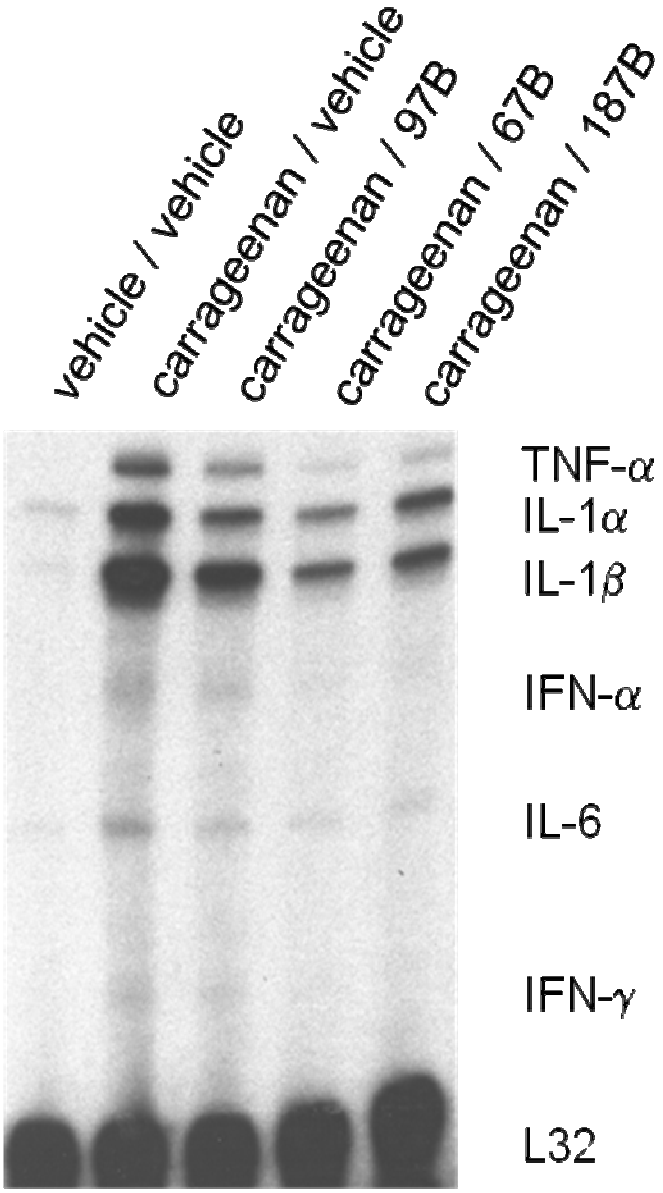
vehicle / vehicle
carrageenan / vehicle
carrageenan / 97B
carrageenan / 67B
carrageenan / 187B
TNF-α
IL-1α
IL-1β
IFN-α
IL-6
IFN-γ
L32

2.3.8 Dextran sulfate sodium (DSS) induced experimental colitis.

Crohn's disease and ulcerative colitis are examples of inflammatory bowel disease (IBD).Chris Yun studies this disease using an animal model for inflammatory bowel disease induced by dextran sulfate sodium (DSS.) (Murthy, Cooper et al. 1993; Berg, Davidson et al. 1996; Qualls, Kaplan et al. 2006)GB67B(**1.5**) was tested by in 6-8 week old female C57BL/6 mice, which were given 3% DSS in drinking water daily for five days. Then 10mg/kg GB67B(**1.5**) in 90% (v/v) 0.45% methyl cellulose and 10% PEG-200 was administred intraperitoneally starting at day 1 until mice were sacrificed at day 10. Mice in DSS group were treated with DSS and vehicle. Mice of control group were treated with vehicle alone.

Progression of colitis was monitored daily by body-weighing and examination for rectal bleeding, loose stools, and diarrhea. These parameters were monitored and evaluated using the DAI (Disease Activity Index.) Administration of GB67B(**1.5**) significantly reduced the average DAI score to 4.6±0.65, while the score of DSS group is 7.1±0.61.

Figure II-11. Histological evaluation of colonic tissue.

At day 10, mice were anesthetized with isoflurane and sacrificed by cervical dislocation. Distal colon was collected and snap frozen in liquid nitrogen and stored to at-80°C. Part of the distal colonic tissue specimens were fixed in 10% neutral buffered formalin, embedded in paraffin, cut into sections, and stained with H&E. Samples were analyzed by blinded researchers and evaluated using the colon pathology score detailed in the experimental procedures section. Histological evaluation revealed GB67B(**1.5**) improved mucosal integrity, epithelial damage, mucin depletion from Goblet cells and lymphocyte infiltration in distal colon in DSS-treated mice. The average histological score of GB67B(**1.5**) group is grade 1.63±0.74, while DSS group is 3.13±0.64. The data are the results from eight mice each group.

Colon Histology

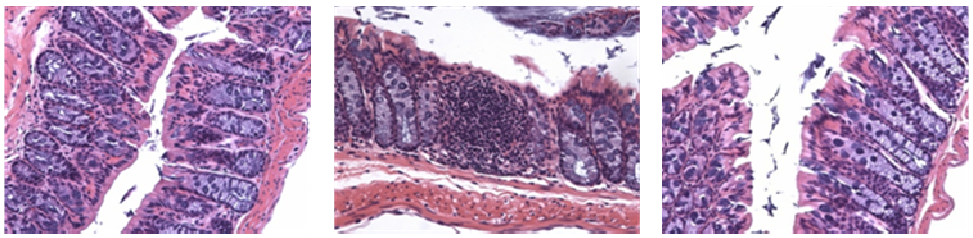

Control DSS DSS+GB67B

Figure II-12. Intestinal tissue mRNA levels.

Colonic tissue was used to isolate RNA test production of cytokines. Real time RT-PCR results shows GB67B(**1.5**) significantly reduced DSS-induced overproduction of proinflammatory cytokines, including TNF-α, IL-1β, IL-6, and MCP-2 in mouse intestinal tissue. There was no significant difference in levels of the anti-inflammatory cytokines IL-8, IL-10 between GB67B(**1.5**) and DSS group. These results would indicate that GB67B(**1.5**) may reduce DSS-induced inflammation by inhibiting only the proinflammatory cytokines.

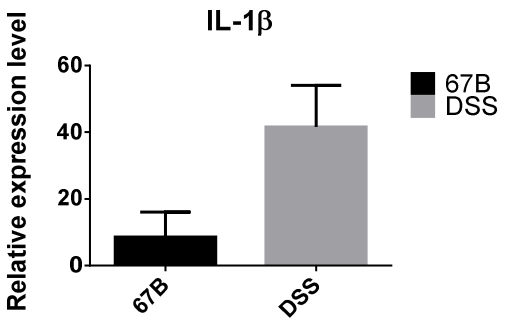
IL-1β
Relative expression level
60
40
20
0
67B
DSS
67B
DSS

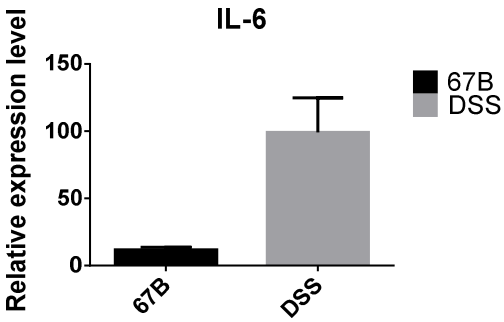
IL-6
Relative expression level
150
100
50
0
67B
DSS
67B
DSS

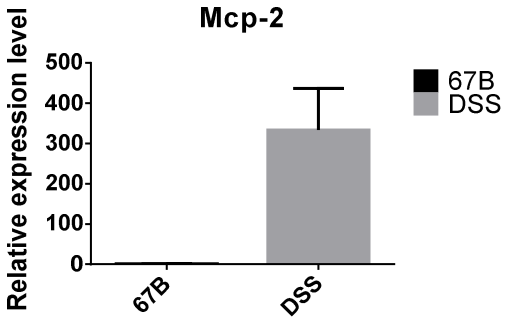
Mcp-2
Relative expression level
500
400
300
200
100
0
67B
DSS
67B
DSS

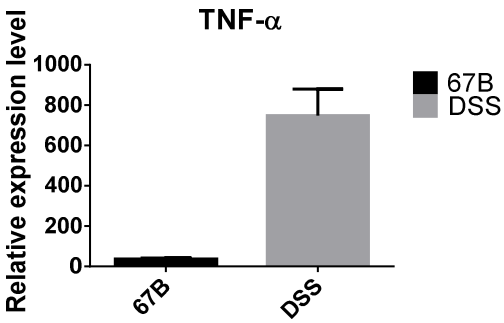
TNF-α
Relative expression level
1000
800
600
400
200
0
67B
DSS
67B
DSS

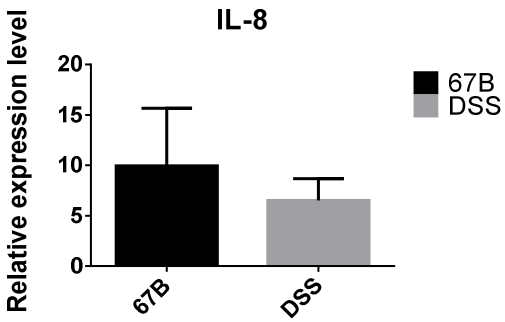
IL-8
Relative expression level
20
15
10
5
0
67B
DSS
67B
DSS

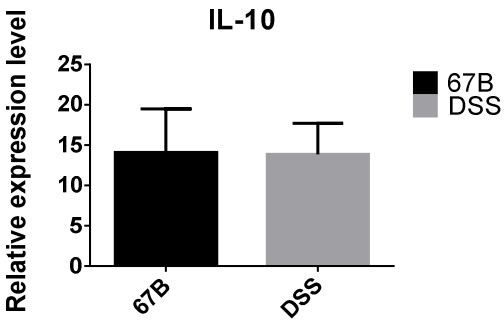
IL-10
Relative expression level
25
20
15
10
5
0
67B
DSS
67B
DSS

2.3.9 Triptolide mechanism of action.

Most anti-NF-κB inhibitors, e.g., curcumin(**2.1**), are anti-kinases that, in fact, block upstream kinases in NF-κB signaling, such as IKKβ. The purpose of the current drug screening is to develop specific anti-NF-κB inhibitor that directly interferes with NF-κB transactivation without affecting any upstream kinases.

Figure II-13. IKKβ kinase inhibition.

We tested the triptolide analogs against IKKβ serine/threonine kinase activity by using the FRET-based Z' Lyte kinase assay kit. The FRET-based assays showed no inhibition of the kinase involved in Iκβ phosphorylation (IKKβ.) To validate the assay a known kinase inhibitor, Staurosporine, was ran alongside the triptolide analogs and its experimental IC_{50} was compared with its' known IC_{50} value.

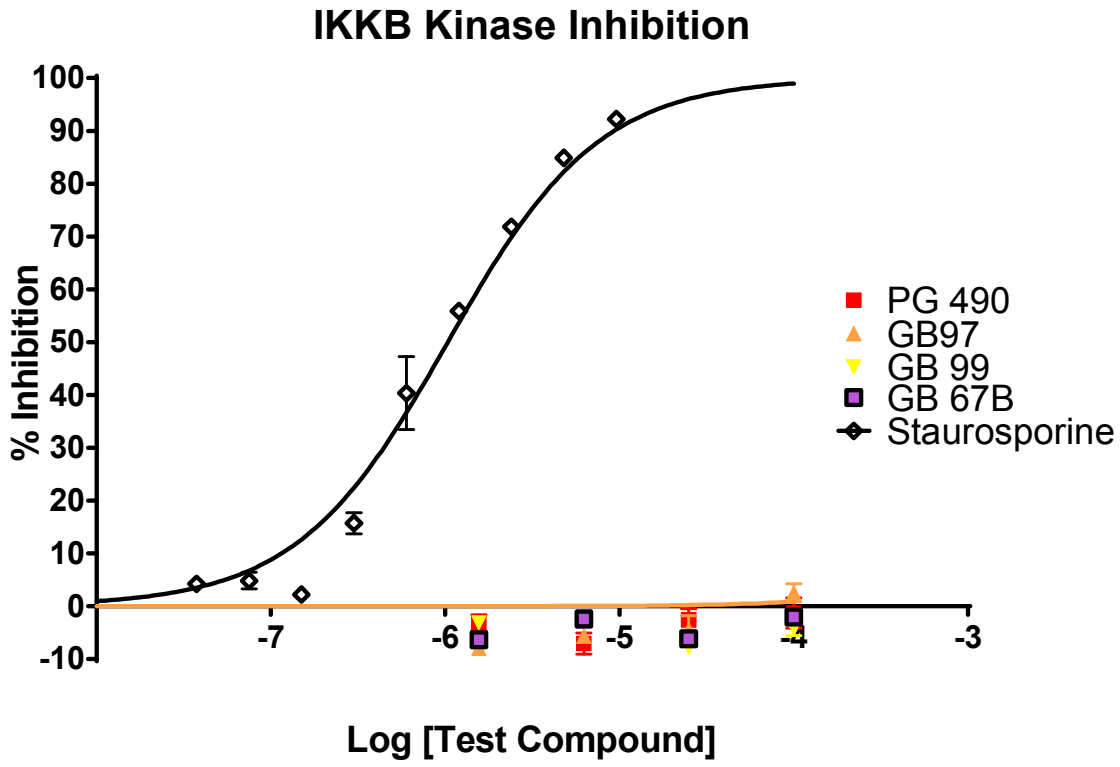
IKKB Kinase Inhibition
% Inhibition
100
90
80
70
60
50
40
30
20
10
0
-10
-7
-6
-5
-4
-3
Log [Test Compound]
PG 490
GB97
GB 99
GB 67B
Staurosporine

Figure II-14. NF-κB Translocation

Our hypothesis is that the triptolide analogs directly block NF-κB transactivation and not IKKβ kinase, one expects that they would not interfere with NF-κB translocation. Using the Cellomics HitKit for NF-κB activation, an immunofluorescence assay, we tested the effects of the triptolide analog GB67B (**1.5**) on nuclear translocation of NF-κB. The NF-κB is localized to the cytoplasm (green fluorescence) in the unstimulated control, which did not receive the proinflammatory stimulus IL-1α. If the cells did receive the proinflammatory stimulus then the NF-κB is localized to the nucleus and overlaps with Hoechst dye (blue fluorescence). The results of this assay showed that IL-1α-induced NF-κB translocation was not inhibited by these compounds. NBD, a protein based on the sequence of NEMO and a known inhibitor of NF-κB translocation, was used as a positive control. Therefore, our new triptolide analogs do not have anti-IKKβ kinase activity, nor do they interfere with NF-κB translocation induced by IL-1α.

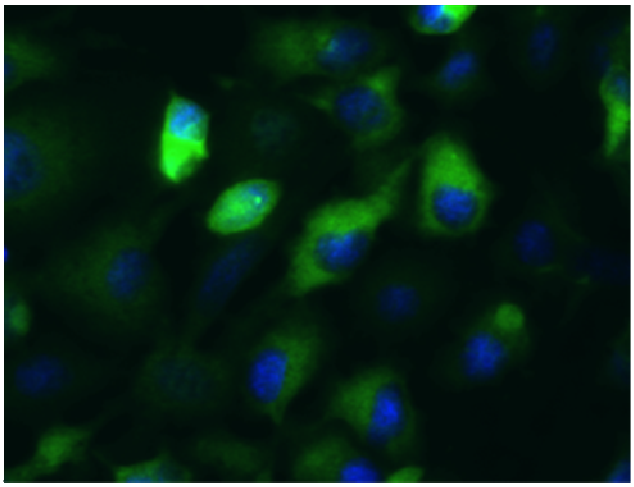

NBD + IL-1α

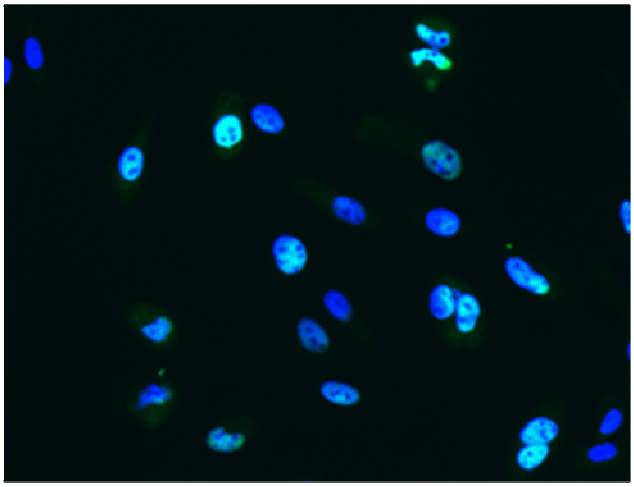

GB67B + IL-1α

Figure II-15. Protein DNA binding specificity

One mechanism that triptolide (**1.1**)could interfere with NF-κB binding would be if it had a non-specific DNA binding capacity. The purpose of the current drug screening is to develop an inhibitor that will only interfere with NF-κB transactivation activity without nonspecific DNA alkylating properties. If the triptolide analogs were to have alkylating properties, they would interfere with transactivation of other transcription factors. Thus, we sought to test these compounds for non-specific DNA binding by using the TranAM HIF-1 assay; a probe similar to our primary screening assay except that NF-κB is replaced with HIF-1 protein. Following this hypoxic stabilization, HIF-1α translocates to the nucleus where it heterodimerizes with HIF-1β to bind to the DNA sequence 5'-RCGTG-3' (hypoxia responsive element; HRE), located in the promoter of target genes. Neither GB67B(**1.5**) nor GB97 (**1.15**) inhibited HIF-1α binding to HRE while triptolide (**1.1**) inhibited 15% of HIF-1α activity. This interference is equivalent to 50% of anti-NF-κB activity shown in **Figure II-2**. Our triptolide analogs do not interfere with HIF-1 binding to HREs, which suggests that they are likely specific to the κB binding sequence. Triptolide(**1.1**)however, seems to possess more non-specific DNA binding properties.

Compound	Designation	% Inhibition
1.1	Triptolide PG490	15.3%
1.12	GB99	9.2%
1.5	GB67B	2.3%
1.15	GB97	1.9%

CHAPTER III: Curcumin

3.1 Introduction

Curcumin is the active ingredient in the spice turmeric, which has been used for centuries to treat disorders affecting the skin, liver, pulmonary and gastrointestinal systems. It has been studied extensively as a therapeutic agent, and has been shown to possess a range of anti-inflammatory, anti-tumor and anti-angiogenesis properties. While a number of studies have shown its efficacy in this regard, the therapeutic uses of curcumin are limited by its low oral bioavailability. It is not surprising that the development of analogous compounds with increased bioavailability have been pursued.

Earlier screenings of chemically synthesized curcumin analogs are promising, showing these compounds are highly effective in inhibiting tumor cell growth and mediating inflammatory pathways. (Adams, Cai et al. 2005) This study sought to further characterize these aspects of their profile by determining their kinase inhibition profile, examining their effects on cancer cells both *in vitro* and *in vivo*, defining ATP-mediated changes in enzyme kinetics, and developing molecular models of the potently inhibited enzymes.

3.2 Experimental Procedures

Figure III-1. Z' Lyte *In vitro* kinase assay (Invitrogen).

In a 10 µl kinase reaction, the IKKβ transfers the gamma-phosphate of ATP to a single Serine/ Threonine residue in a specific synthetic peptide substrate (2 µM). The peptide is labeled with the two fluorophores coumarin and fluorescein, one at each end of the peptide to make up a FRET pair. In the Development Reaction, 5 µl of a site-specific protease recognizes and cleaves any non-phosphorylated peptides. Cleavage disrupts FRET between the coumarin and the fluorescein on the peptide. Phosphorylation of the peptide suppresses cleavage by the protease. Uncleaved, phosphorylated peptides maintain the FRET pair. Five µl of stop reagent is added to halt the development reaction before the plate is read by an Envision 2102 plate reader from Perkin Elmer. During detection, a ratiometric read-out of the donor emission over the acceptor emission quantitates reaction progress. The ratio is low if the peptide is phosphorylated, and high if the peptide is non-phosphorylated. Percent phosphorylation was calculated using controls, and each compound concentration was run in triplicate. Results were graphed using GraphPad Prism, and IC_{50} values were calculated by using non-linear regression.

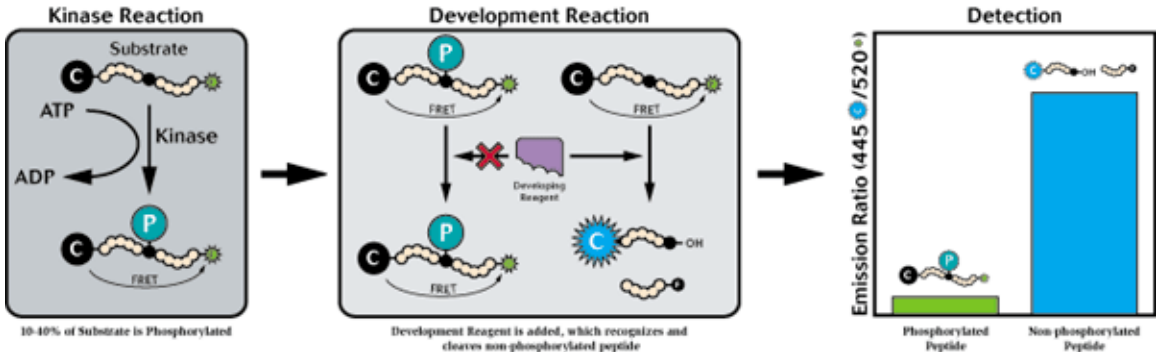
Kinase Reaction
Substrate
ATP
Kinase
ADP
FRET
10-40% of Substrate is Phosphorylated
Development Reaction
FRET
Developing Reagent
OH
Development Reagent is added, which recognizes and cleaves non-phosphorylated peptide
Detection
Emission Ratio (445/520)
Phosphorylated Peptide
Non phosphorylated Peptide

Figure III-2. Z' Lyte kinase cascade assay

Some of the assays require a cascade reaction in which inactivated kinase is activated by an upstream kinase. Two cascades were important for our studies: the RAF1-MEK1-ERK2 cascade and the MAPK14(p38α)-MAPKAPK2 cascade. A direct assay was used for MAPK14(p38α) when generating its nine point IC_{50} curve.

RAF1 (cRAF) Kinase Cascade

The final 10 µL Kinase Reaction consists of 0.001 – 0.005 ng RAF1 (cRAF), 10 ng inactive MAP2K1 (MEK1), and 100 ng inactive MAPK1 (ERK2).

MAP2K1 (MEK1) Kinase Cascade

The final 10 µL Kinase Reaction consists of 1.0 - 4.0 ng MAP2K1 (MEK1) and 105 ng inactive MAPK1 (ERK2).

MAPK14 (p38α) Kinase Cascade

The final 10 µL Kinase Reaction consists of 0.01 - 0.02 ng MAPK14 (p38α) and 5 ng inactive MAPKAPK2.

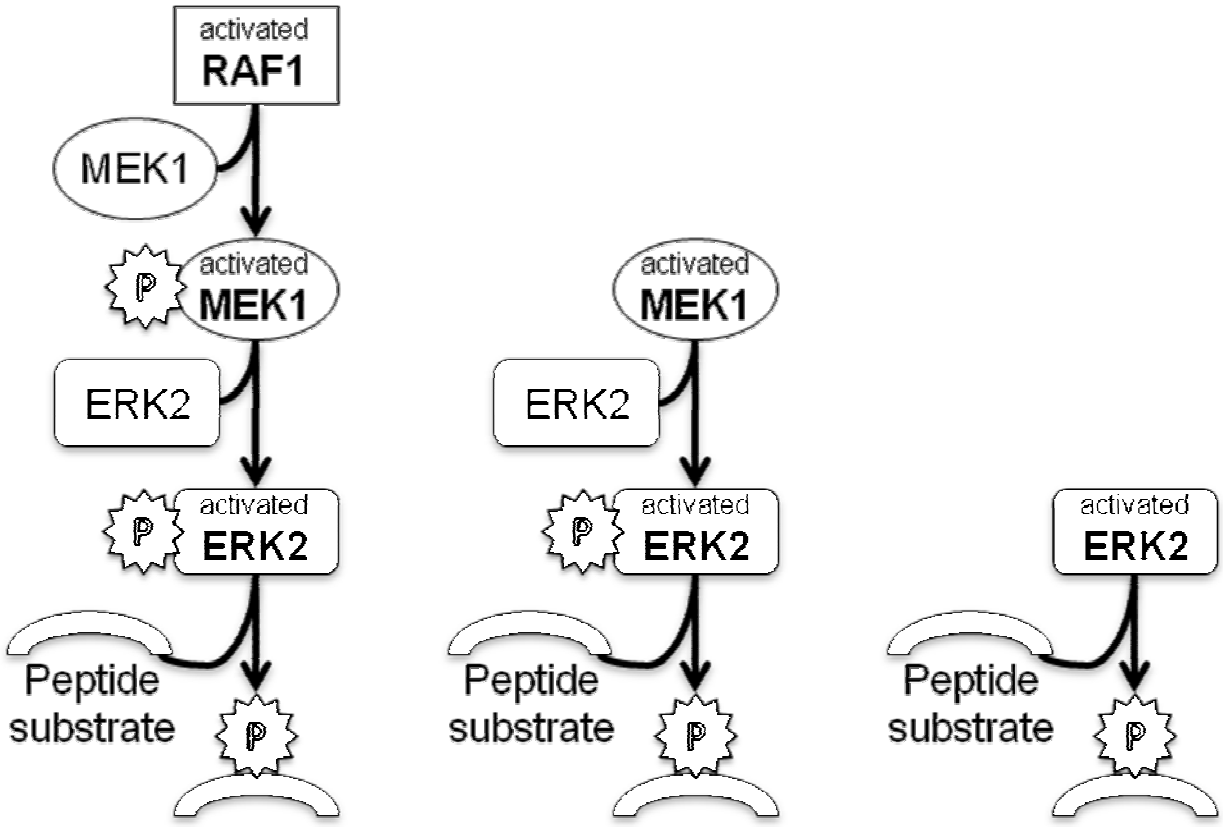
activated
RAF1
MEK1
P
activated
MEK1
ERK2
P
activated
ERK2
Peptide
substrate
P
activated
MEK1
ERK2
P
activated
ERK2
Peptide
substrate
P
activated
ERK2
Peptide
substrate
P

Kinase profile screen. Compound EF31 (**2.4**) was tested against a panel of kinases at a 5 μM concentration. Each data point was measured in duplicate using Z' Lyte substrates with two control wells. One control well contains a protease control to determine if the compound interferes with the development reaction. The second well encloses a fluorescence control to ascertain if the compound interferes with the fluorescence reading of the FRET pair.

Adapta Assay. After addition of inhibitor and all other kinase reaction components, the reaction was incubated for one hour. During this period, the kinase reaction produces phosphorylated peptide and ADP. A detection solution of Europium-labeled anti-ADP antibodies, a labeled ADP tracer and an EDTA to stop-kinase reaction were added. ADP formed by the kinase reaction will displace the ADP tracer from the antibody, resulting in a TR-FRET signal decrease. When an inhibitor is used, the amount of ADP formed by the kinase reaction is reduced, and the resulting intact antibody-tracer interaction results in a high TR-FRET signal. By comparing this to a control, the amount of inhibition can be calculated.

Gene Mining. The top ten kinases ≥85% blocked by 5 uM of EF31 (**2.4**) listed in Figure III-4 (C) were subjected to signaling pathway analysis using the Ingenuity Pathway Analysis software. (Systems 2012)

ADP Quest. Kinase assays for the enzyme kinetics were accomplished with ADP Quest assays. Using purified recombinant AKT-2 from Invitrogen (PV3184) and the Crosstide substrate from Millipore (Cat # 12-331), kinase reactions were run from 10-90 minutes using fresh samples of varying ATP concentrations. When the Crosstide substrate molecule is phosphorylated, an ADP molecule is generated. The ADP Quest procedure measures total ADP by an enzyme coupled reaction that causes a fluorescent signal. The latter is compared with a known control.

Michaelis-Menten analysis of enzyme kinetics. Analysis of reaction velocities was performed by first determining reaction rates using the ADP quest assay. The reaction rates were measured by following ADP produced over time. The reaction velocities were graphed on a Lineweaver-Burk plot and two Michaelis-Menten plots with appropriate constraints for the type of model represented.

Molecular modeling (docking). The structures of compounds EF24 (**2.3**), EF31 (**2.4**), UBS109(**2.12**) and **7** were drawn in 2D by Chemdraw, and then submitted to Ligprep in Maestro 9.0 to obtain 3D structures. The protein complexes (pdb code 3E88 for AKT-2 and 1YWN for VEGFR2) were processed by the protein preparation wizard in Maestro followed by removal of the ligands. The receptor grid was generated at the ATP binding sites. Ligand-docking was accomplished with : SP precision (Maestro 9.0) for flexible docking of the ligands. (Schrödinger 2009; Schrödinger 2009) The top 20 poses at each site were subsequently submitted to Prime MM-GBSA (Graves, Shivakumar et al. 2008) (all atoms of the receptor are frozen) for rescoring.

Linear Regression. For each ligand, the MM-GBSA rescored top pose was selected, and the calculated MM-GBSA ΔG value was used as an estimate of binding energy (ΔE). The relative binding energies (ΔE) and activities (IC_{50}) were fitted by the equation $\Delta E = -RT\ln(IC_{50})$.

NF-κB Translocation Assay. HeLa cells were plated to a 96 well plate (5000 cells/well) with DMEM + 10% FBS, incubated for 18-24 hours. Cells were then treated with curcumin analogs EF24 (**2.3**) and EF31 (**2.4**) for 1hr. They were then stimulated with 5 ng/mL IL-1^{α} for 15 minutes. Cells were then fixed and labeled using Cellomics HitKit and visualized using fluorescence microscopy with overlays constructed with MetaMorph. NF-κB staining is done with primary antibody to p65 with a secondary antibody attached to flourophore and is

represented by green fluorescence. Nuclear staining by Hoechst dye and is represented by blue fluorescence.

Cell Titer 96 AQ Cell Proliferation Assay. The Cell Titer assay (Promega, Madison, WI) was used to determine the cytotoxicity of the curcumin analogs *in vitro*. MDA-MB-231and U2OS cell lines were plated at 3000 cells/well in media at a volume of 100 uL in clear 96 well plates and incubated at 37 degrees overnight. On the following day, cells were treated with 10 uL of media containing 10X solutions of the analogs were added to the appropriate wells at concentrations of 50 uM, 10 uM, 1 uM, and 0.1 uM with a final concentration of 0.1 % DMSO. Also control wells (media only and cells) were set up with just DMSO. Cells were incubated at 37 degrees overnight. Next, 20 µl of CellTiter 96AQ reagent was added into each well and incubated for additional two hours. Readings were taken at 490 nm on a spectrophotometer absorbance was normalized to a % of control wells and plotted using Prism5.

λ-carrageenan paw edema model. See "λ-carrageenan paw edema model" in Chapter 2.2 Experimental procedures.

Breast cancer xenograft model. MDA-MB-231 cells were split 1:4 on 150mm plates in RPMI media + 10% FBS and incubated for 72 hours. Cells were scrapped off the plate and resuspended in 90% HBSS and 10 % Matrigel at a designated concentration. Then 200 ul of this solution was subcutaneously injected into the right and left flank of nude mice. At the conclusion of the experiment mice were euthanized and the tumors removed. They were then weighed and the dimensions measured with calipers. After that, the tumors were flash frozen in OCT using liquid nitrogen tumors for possible further histological examination.

3.3 Results

3.3.1 Curcumin analog's inhibitory effects on various kinases.

Figure III-3. Curcumin analogs.

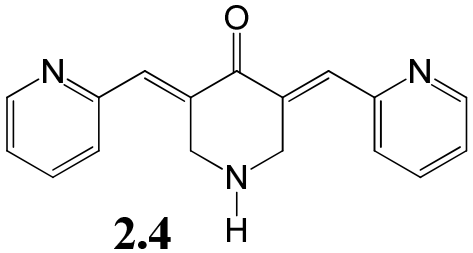

2.4

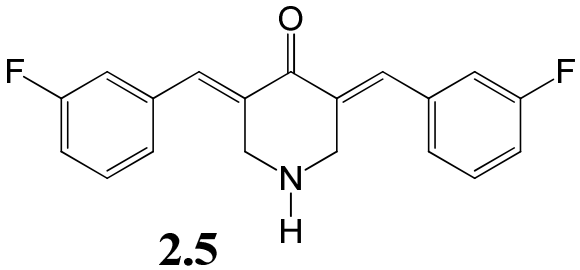

2.5

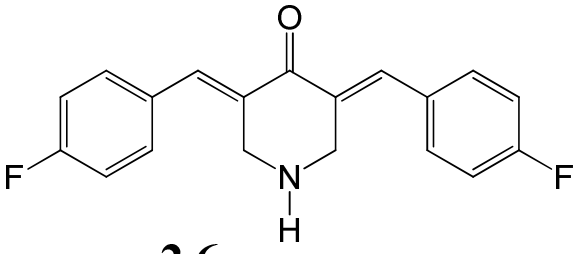

2.6

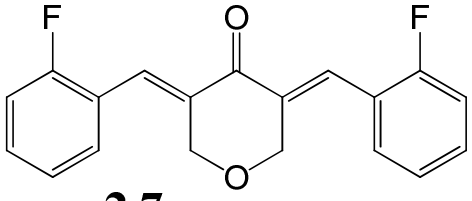

2.7

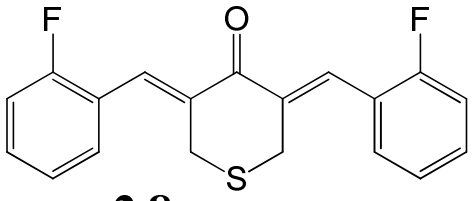

2.8

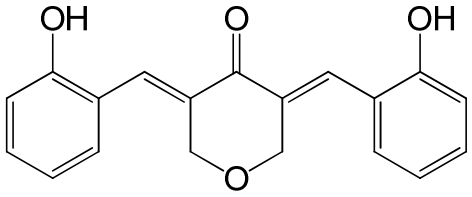

2.9

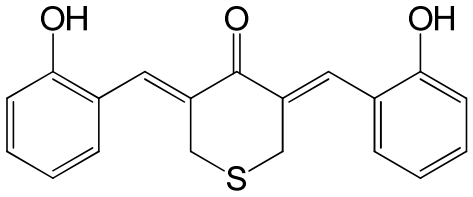

2.10

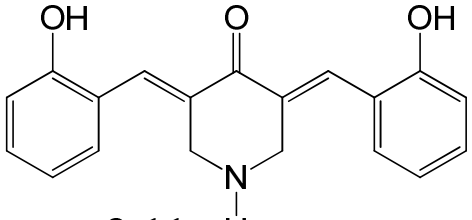

2.11

Figure III-4. Preliminary kinase screen.

A preliminary focused screen employing compounds **2.3-2.11** at four concentrations (100 uM, 25uM, 6.25 uM, and 1.56 uM) and a small panel of diverse kinases (Abl1, AKT-1, AKT-2, IKKβ, Src, RAF1, MEK1, IGFR) showed the curcumin analogs to have no measureable inhibition of receptor tyrosine kinase IGFR (data not shown), a weak effect on the cytoplasmic tyrosine kinase Abl1 and Src, moderate inhibition of Ser/Thr kinases (IKKβ, RAF1 and MEK1) and a significantly increased blocking action on AKT-1 and AKT-2.

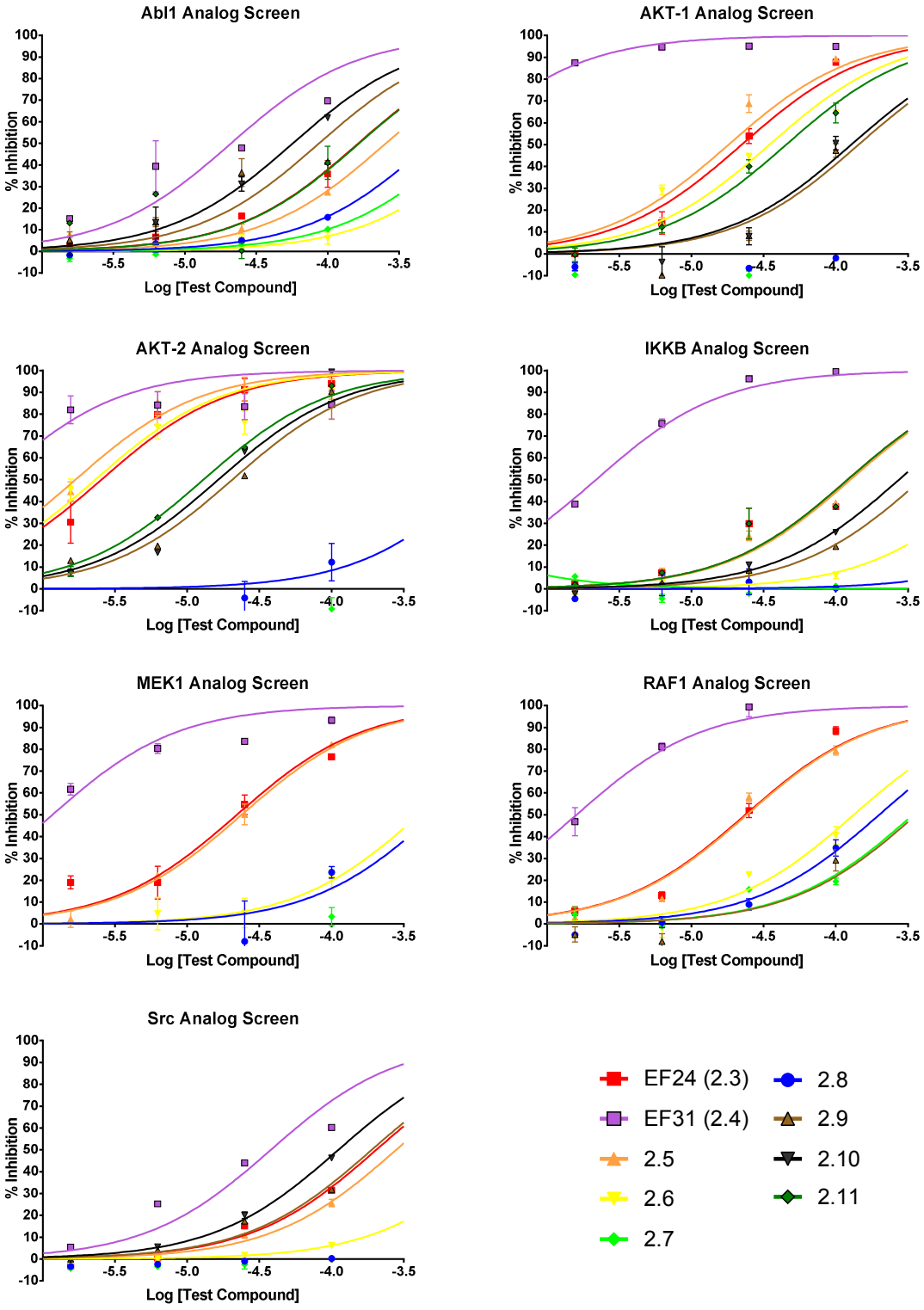
Abl1 Analog Screen
AKT-1 Analog Screen
AKT-2 Analog Screen
IKKB Analog Screen
MEK1 Analog Screen
RAF1 Analog Screen
Src Analog Screen
% Inhibition
Log [Test Compound]
EF24 (2.3)
EF31 (2.4)
2.5
2.6
2.7
2.8
2.9
2.10
2.11

3.3.2 EF31 (2.4) is a pleiotrophic kinase inhibitor.

We hypothesized that the current series of curcumin analogs are most likely pleiotropic and, as reported for curcumin (**2.1**), inhibit a number of different kinases. To examine trends in the types of kinases inhibited, and to gain broader knowledge concerning the range of kinases sensitive to curcumin analogs, we subjected the more potent EF31 (**2.4**) to screening by a panel of fifty kinases. Of those kinases tested in the profile screen, ten (20% of the kinases tested) were blocked by EF31 (**2.4**)at > 85% at 5 μM and designated as hits. AKT-1 and IKKβ, two kinases previously known to be inhibited by EF24 (**2.3**) and EF31 (**2.4**) from our initial screen, were added to the kinase screen to furnish positive controls (Figure III-4). Compound EF31 (**2.4**) exhibited 40-80% inhibition at 5 μM against twelve kinases, which were consequently categorized as "low activity". The other 28 phosphorylating enzymes (56% of kinases tested) were inhibited by EF31 (**2.4**) at ≤ 40% at 5 μM and are likely to be only modestly influential for the effects of the drug**.** In summary, EF31 (**2.4**) appears to be pleiotropic by blocking a range of kinases across a range of concentrations. In the discussion that follows, it is suggested that cell-based signaling pathways are significantly attenuated by this diversity of actions.

With regard to the selectivity of EF31 (**2.4**) for specific types of kinases, there is a definite trend. Of the 10 screening "hits", eight were Ser/Thr kinases (25% of Ser/Thr kinases tested), one was a dual function kinase (NEK1, 33% of the dual function kinases tested) and one was a Tyr kinase (KDR, 7% of all Tyr kinases tested). Thus, selectivity for Ser/Thr kinases emerges from this screen. Although the percentage of dual function kinases is higher, it results from the small sample size of this kinase class. Examination of the cross section of kinases with "low activity" reveals a somewhat different balance indicating a potential background role for Tyr kinases: five Ser/Thr kinases (10 % of all kinases, 15% of Ser/Thr kinases), six Tyr kinases

(12% of all kinases, 40% of Tyr kinases), and one dual function kinase (2% of all kinases, 33% of dual function kinases).

Figure III-5. Screening of a 50-kinase panel by curcumin analog EF31 (2.4). (A) Compound EF31 (**2.4**) was screened against the panel in duplicate at 5 μM with ATP concentrations at K_{mapp} for each individual kinase. Due to experimental error, values above 100% and below 0% are regarded as maximal or no inhibition respectively. (B) The types of kinases among the 50 in both number and % of total. (C) Activity ranges: hits (> 80% inhibition), modest activity (40-80% inhibition) and low activity (less than 40% inhibition.)

A

Kinase Tested	% Inhibition	Std Dev	Kinase Tested	% Inhibition	Std Dev
AKT1 (PKB alpha)	107	2.1	PHKG2	37	0.7
IKBKB (IKK beta)	107	1.4	PIK3CG (p110 gamma)*	34	0.7
MAPK14 (p38 alpha)**	104	2.1	MAPK1 (ERK2)	34	2.1
NEK1	102	0.0	CDK9/cyclin T1*	26	9.2
RPS6KB1 (p70S6K)	101	0.7	NTRK1 (TRKA)	25	2.1
AMPK A1/B1/G1	95	1.4	CDK1/cyclin B	24	0.0
PRKCB1 (PKC beta I)	91	0.7	MARK2	22	0.0
CHEK1 (CHK1)	90	2.1	RET	21	0.7
KDR (VEGFR2)	89	0.7	PAK4	18	3.5
MAPKAPK2	85	3.5	GSK3B (GSK3 beta)	17	0.0
			MAPK8 (JNK1)	16	1.4
AURKA (Aurora A)	77	2.1	IKBKE (IKK epsilon)	15	3.5
RPS6KA3 (RSK2)	77	1.4	INSR	15	2.1
MET (cMet)	75	4.2	JAK3	15	1.4
MAP4K4 (HGK)	72	2.1	LCK	13	2.1
FLT3	69	0.7	CSNK1G2 (CK1 gamma 2	12	0.7
FGFR1	66	10.6	PRKACA (PKA)	11	0.0
ROCK1	58	0.7	PIM1	10	8.5
PDK1 Direct	54	1.4	CSNK2A1 (CK2 alpha 1)	5	0.7
TEK (Tie2)	51	3.5	IRAK4	5	0.0
DYRK3	48	2.1	CDK7/cyclin H/MNAT1*	3	9.2
SYK	45	0.0	KIT	2	0.7
BTK	44	0.7	ACVR1B (ALK4)	1	2.8
			CDK2/cyclin A	1	2.8
			FRAP1 (mTOR)	-5	0.7
			EGFR (ErbB1)	-9	1.4
			PLK1	-9	0.7
			ERBB2 (HER2)	-13	1.4

B

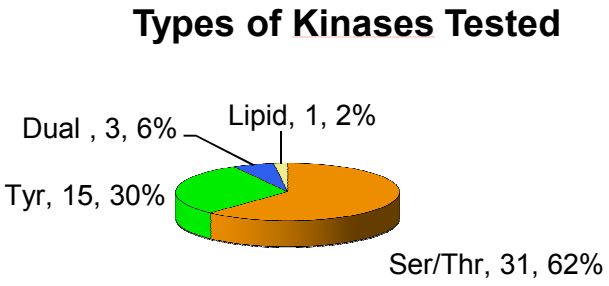
Types of Kinases Tested
Dual , 3, 6%
Lipid, 1, 2%
Tyr, 15, 30%
Ser/Thr, 31, 62%

C


Kinase Inhibition Results
Hits, 10, 20%
Misses, 28, 56%
Low Activity, 12, 24%

Figure III-6. IC_{50} curves: selection and testing of kinases and analogs.

In the kinase profile screen, any kinase eliciting $\geq$ 85% inhibition at 5 μM, was evaluated further using a more focused panel of five compounds. Previously proven inhibitors EF24 (**2.3**) and EF31 (**2.4**)were tested along with three new compounds, UBS109(**2.12**), **2.13** the mono-C=C reduction product of UBS109(**2.12**), and a sulfur analog SEF31 (**2.14**) (A). The analogs were tested at nine different concentrations using serial dilutions. Assays for RAF1 and MEK used the kinase cascade method discussed and diagramed in Experimental Procedures Figure III-2. Unlike the kinase profile screen, MAPK14 uses a direct assay. Accordingly, curves were fitted (B) and IC_{50} values calculated in uM, and displayed in (C).

A

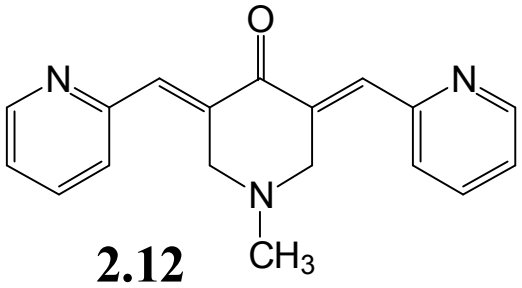

2.12

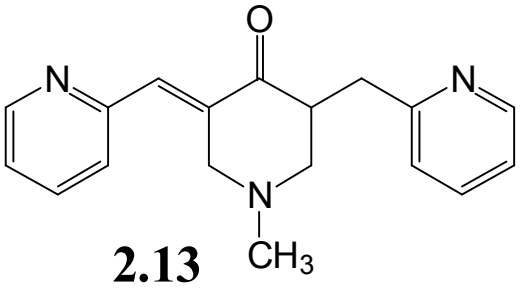

2.13

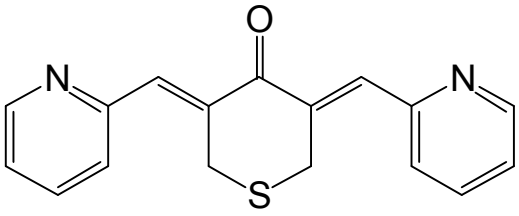

2.14

B

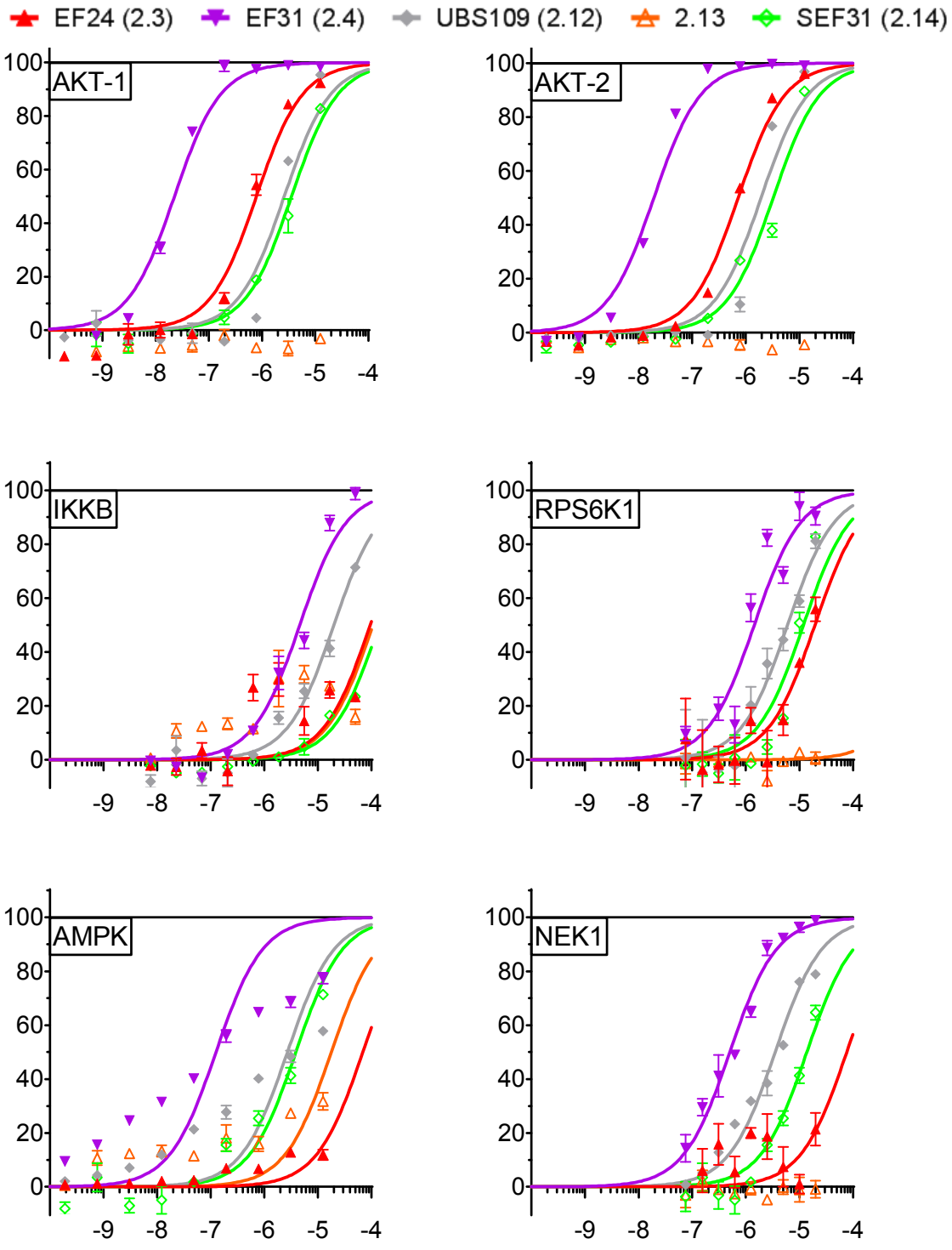
EF24 (2.3)
EF31 (2.4)
UBS109 (2.12)
2.13
SEF31 (2.14)
AKT-1
AKT-2
IKKB
RPS6K1
AMPK
NEK1
100
80
60
40
20
0
-9
-8
-7
-6
-5
-4

B

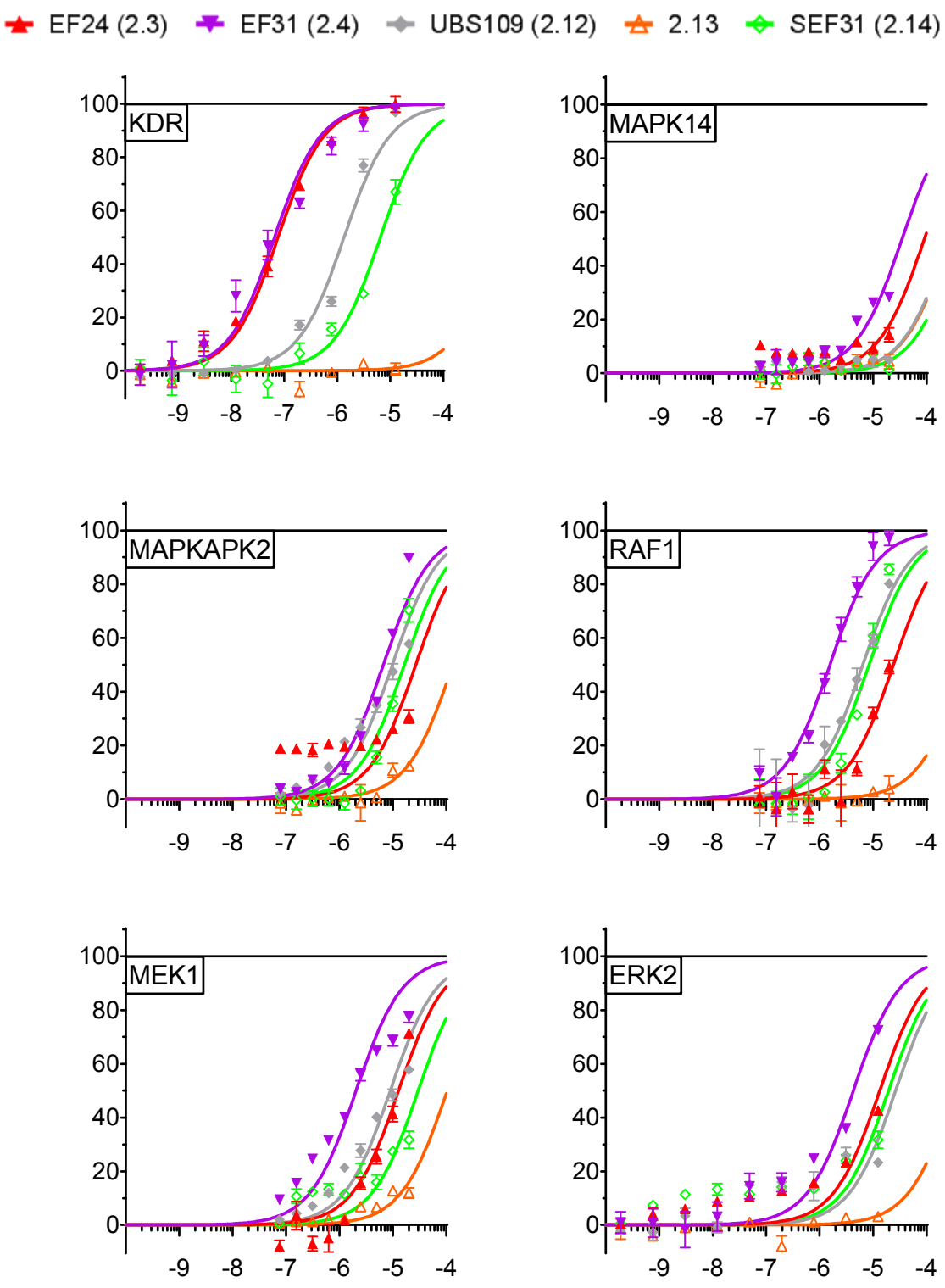
EF24 (2.3)
EF31 (2.4)
UBS109 (2.12)
2.13
SEF31 (2.14)
KDR
MAPK14
MAPKAPK2
RAF1
MEK1
ERK2
100
80
60
40
20
0
-9
-8
-7
-6
-5
-4

C

Kinase	Compound				
	EF24 **2.3**	EF31 **2.4**	UBS109 **2.12**	**2.13**	SEF31 **2.14**
AKT1 (PKB alpha)	0.78	0.023	2.6	>100	3.6
AKT-2	0.72	0.019	1.9	>100	3.3
IKBKB (IKKβ)	95	4.6	20	>100	>100
RPS6K1	20	1.4	6	>100	12
AMPK (A1/B1/G1)	>100	2.1	9	30	13
NEK1	77	0.5	3.5	83	14
KDR (VEGFR2)	0.77	0.66	1.3	>100	6.5
MAPK14 (p38α)	92	35	>100	>100	>100
MAPKAPK2	27	6.7	9.8	>100	16
RAF1 *	24	1.6	6.5	>100	8.5
MEK1 *	13	2	9	>100	28
ERK2	13	4.3	27	>100	20

3.3.3 Rationale for analogs selected in focused screen.

The inclusion of UBS109(**2.12**) was based on the outcome of a successful oral efficacy study in mice bearing a human tumor xenograft, while addition of the reduced analog **6** resulted from its noteworthy but reduced cellular cytotoxicity relative to UBS109(**2.12**)**.** (Yamaguchi, Moore et al. 2012)The sulfur-containing compound SEF31 (**2.14**) was selected because the sulfur atom in the central ring of **2.2** (Y = S) occasions significantly different physical properties (ring size and molecular polarity) by comparison with the nitrogen moieties in EF24 (**2.3**), EF31 (**2.4**), **2.12**, and **2.13**(i.e. **2.2**, Y = NH and NMe). This permits evaluation of the importance of proton donor and acceptor interactions at the bindingsites of the target kinases as well as the influence of protonation. These points are taken up in section 3.3.5 the molecular modeling section below.

3.3.4 Pleiotrophic kinase inhibition.

Interestingly, the kinases studied here represent a wide variety of cellular activities: regulation of protein synthesis and cell proliferation (RPS6KB1), energy sensing and sensitization of cancer cells to cisplatin treatment (AMPK), DNA damage repair and maintenance of mitochondrial membrane potential (NEK1), mediation of cellular responses to VEGF (KDR/VEGFR2), environmental stress relief and assistance of production of certain cytokines (MAPK14/p38α), cooperation with the latter kinase to expedite nuclear export, gene expression and cell proliferation (MAPKAPK2), development, cell proliferation and apoptosis regulation (RAF1, MEK1, ERK2). Two kinases blocked by EF31 (**2.4**) at $\geq$ 85%/5 uM, but not examined by dose-response, are CHEK1 and PRKCβ1. The former mediates cell cycle arrest in response to DNA irregularities, while the latter, activated by diacylglycerol, phosphorylates a

range of cellular proteins and serves as the receptor for phorbol esters, a class of tumor promoters.

These other analogs furnish a different profile (Figure III-5) suggesting an opportunity for reduced toxicity coupled to variable pan-kinase outcomes.Not surprisingly, most of these cellular functions are involved in the promotion of cancer and inflammation. Without yet understanding the details linking the wide diversity of biological responses, modest pleiotropic blockade of this set of kinases appears at the heart of the ability of the curcumin analogs to arrest both cancer, angiogenesis and inflammation under in vitro(Adams, Cai et al. 2005) and in vivo(Zhu, Moore et al. 2012) conditions. A pertinent example is the behavior of NEK1, the only dual function kinase that is significantly inhibited by EF31 (**2.4**) in the kinase screen (Figure III-5). Among other functions, it contributes to maintenance of the mitochondrial membrane potential (MMP). Inhibition of NEK1 causes a decrease in phosphorylation of voltage-dependent anion-selective channel protein 1 (VDAC1), which leads to an uncoupling of the MMP.(Chen, Craigen et al. 2009) Later stages in this event are identical to the manner in which EF24 (**2.3**) induces apoptosis in two cancer cell lines.(Adams, Cai et al. 2005)

3.3.5 RAF1-MEK1-ERK2 kinase cascade.

The dose-response assays performed for certain inhibited kinases involve activation of a given kinase, phosphorylation of a peptide substrate and disruption of a FRET signal upon cleavage of the peptide to provide the assay readout (see Experimental Procedures and Figures III-1 and III-2.)

Figure III-7. Blockade of Signal Transduction Pathways.

For example, when measuring inhibition of RAF1, the procedure takes advantage of the cellular mitogen activated protein (MAP) kinase cascade involving sequential phosphorylation and activation of inactive MEK1 and ERK2 followed by ERK2 phosphorylation of the substrate (Figure III-2). By examining individual kinases, it is clear that curcumin analogs EF24 (**2.3**), EF31 (**2.4**), UBS109(**2.12**) and SEF31 (**2.14**) block all three MAPK kinases to within a factor of three (Figure III-5 C). This leads to a dampening of the entire pathway and eliminates dependence on any one specific kinase. It is presently unknown whether assay constitution precisely mirrors these actions in a living cell.

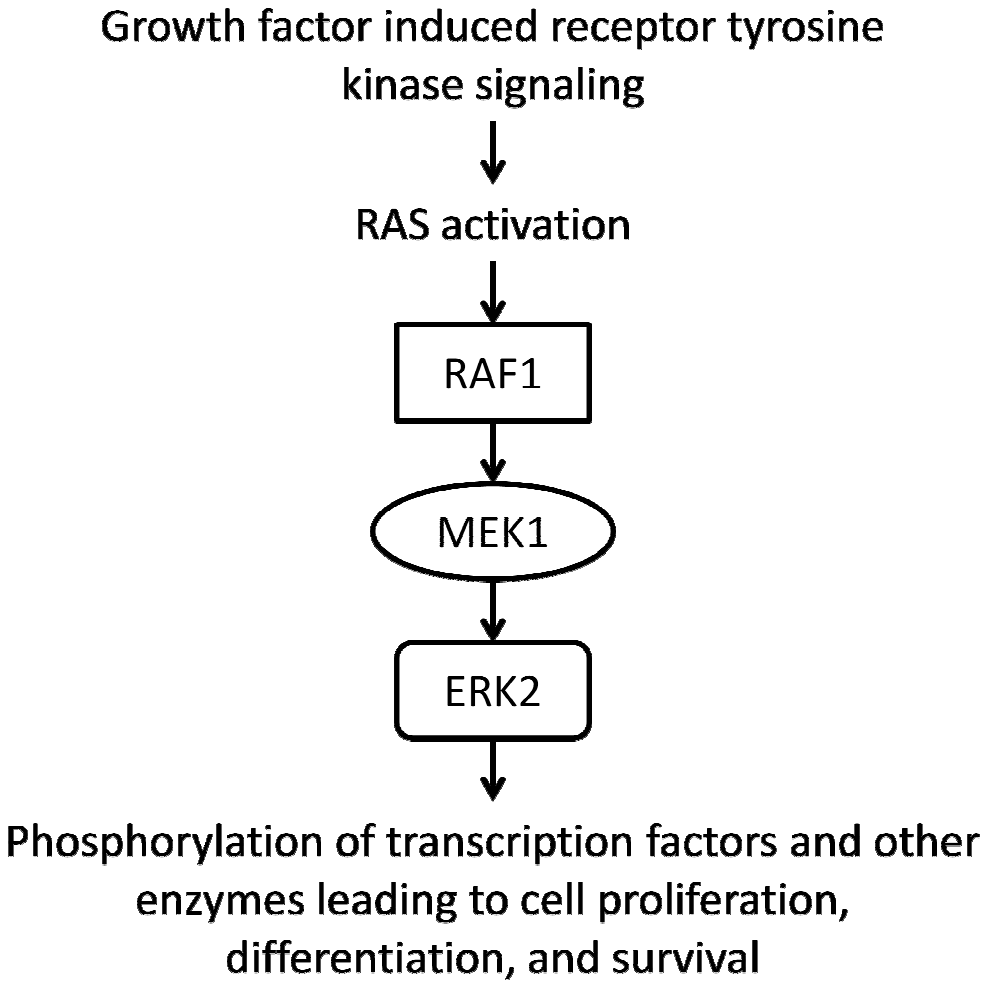
Growth factor induced receptor tyrosine kinase signaling
RAS activation
RAF1
MEK1
ERK2
Phosphorylation of transcription factors and other enzymes leading to cell proliferation, differentiation, and survival

3.3.6 MAPK14 (p38α)-MAPKAPK2 kinase cascade.

Another important MAP kinase cascade concerns MAPKAPK2 and its dependence on MAPK14 (p38α). Labeling p38α as a hit in the kinase screen is somewhat misleading, since both kinases are pathway-linked in that screen (Figure III-5)**.** Further examination of p38α inhibition, however, using a direct kinase assay, shows its blockade to be significantly reduced (Figure III-6 B and C). Thus, the inhibition of MAPKAPK2 downstream of p38α in the kinase cascade, contributes to determination of p38α as a hit in the kinase screen.

3.3.7 Pan kinase inhibition and interrelated signaling pathways.

These previous examples highlight drug action against multiple steps in a localized kinase interaction network by a family of readily accessible curcumin analogs. They simultaneously demonstrate the pleiotropic nature of the analogs both within a select segment of a pathway and among kinases in a more diffuse network (Figures III-5 and III-7). In a similar manner, the parent compound curcumin, inhibits cell signaling cascades at multiple nodes. Since these cascades are involved in cell proliferation and apoptosis, curcumin affects the overall process of carcinogenesis (Sa and Das 2008) as do substances **2.3**, **2.4**, **2.12**, **2.13**, and **2.14**. We have commented on both individual kinase functions and the potential coupling of kinases in subsections of signaling pathways.

Figure III-8. Inhibition of multiple signal transduction pathways.

Kinases highlighted in blue have been studied in this work. This captures the network of relationships among the twelve most readily blocked kinases portrayed in Figures III-5 and III-6. Given the tightly connected associations, simultaneous inhibition of these enzymes will exert pairwise-protein influence as well as a major network perturbation. As suggested by the multiple actions of the weaker curcumin parent, EF31 (**2.4**) is clearly a pleiotropic kinase blocker with 10-20 fold greater kinase suppression. (Kasinski, Du et al. 2008) At the same time, on average, the molecule exhibits only modest potency across the range of enzymes (sub-μM to 7 μM), the exception being EF31 (**2.4**) against AKT.

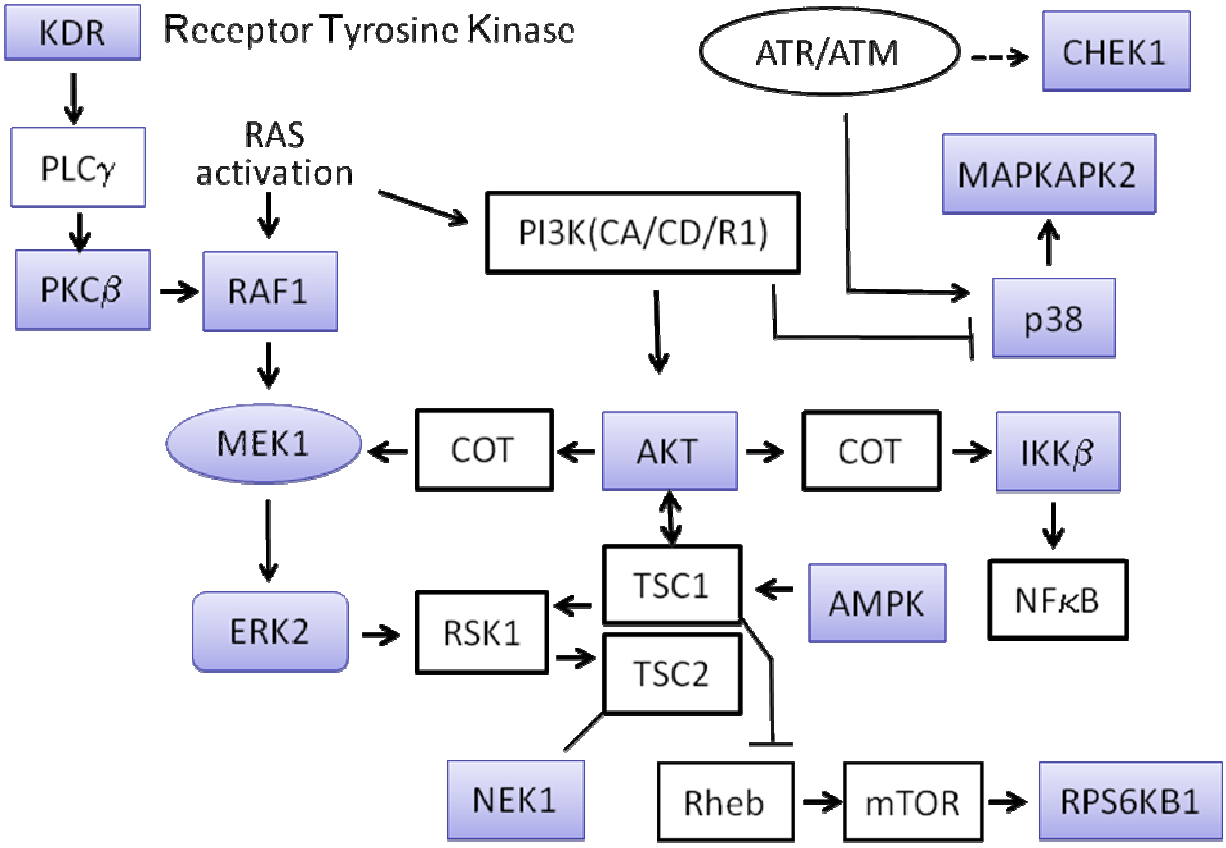
KDR
Receptor Tyrosine Kinase
ATR/ATM
CHEK1
PLCγ
RAS
activation
MAPKAPK2
PI3K(CA/CD/R1)
PKCβ
RAF1
p38
MEK1
COT
AKT
COT
IKKβ
TSC1
AMPK
NFκB
ERK2
RSK1
TSC2
NEK1
Rheb
mTOR
RPS6KB1

3.3.8 Enzyme kinetics of curcumin analog inhibition.

The curcumin mimics can exert their effects as kinase inhibitors by several possible mechanisms: reversible or irreversible, competition with ATP or the peptide substrate, or allosteric modulation. Since a great many such inhibitors function by competing with ATP and occupying the ATP binding pocket, we sought to explore this possibility by analyzing reaction rates at different ATP and inhibitor concentrations. AKT-2 and analog EF31 (**2.4**) were selected to probe this question as the most potent combination among kinases and blockers (Figure III-9).

Figure III-9. Enzyme kinetics of AKT-2 kinase inhibition.

The corresponding Lineweaver-Burk plot (A) reveals a clustering of lines on the Y axis indicative of a competitive inhibition model. To achieve a more quantitative evaluation, we plotted the data on a Michaelis-Menten graph. By selecting specific models that force shared parameters in the global analysis (K_m, V_{max}, K_i), a compromise solution applied to each model spreads the data across all the curves providing a framework that allows mechanistic distinctions to be made; namely, competitive or mixed models.[1]

Interestingly, when performing a global analysis that fits the reaction rates to a Michaelis-Menten graph, a critical constraint is $K_i>0$, but the optimized value is shared by all inhibitor concentrations. In a competitive model, in addition to the shared $K_i>0$ constraint, all reaction curves must also maintain a common optimized $V_{max}>0$.

Execution of the global analysis under the constraints of a competitive model as illustrated by the corresponding Michaelis-Menten graph significantly worsens the fit of the curves to the data (B). By contrast, casting the data in the context of a mixed mechanism provides a superior fit for the data (C). Comparison of these two models favors the mixed inhibition model with a p value >0.01. This suggests that competitive reversible inhibition is not the only mechanistic path traveled by EF31 (**2.4**) in its inhibition of AKT-2. The observation is consistent with a recent study reporting a mixed mechanism for the blockade of IKKB by analog EF24 (**2.3**). (Kasinski, Du et al. 2008)

[1] Footnote: Global analysis is a non-linear regression treatment for multiple curves corresponding to different inhibitor concentrations. The K_m, V_{max} and K_i parameters for each curve are adjusted for the best global fit of the data, but constrained to the same value for each curve. Thus, for example, the resulting V_{max} in a competitive model is forced to be shared across all curves (GraphicPad, Inc., *GraphicPad Prism 5*, La Jolla, CA, 2010)

A

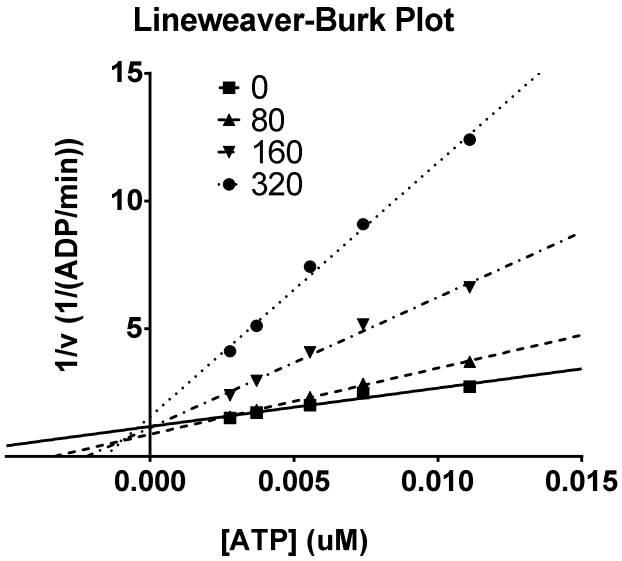
Lineweaver-Burk Plot
15
10
5
1/v (1/(ADP/min))
0
80
160
320
0.000
0.005
0.010
0.015
[ATP] (uM)

B

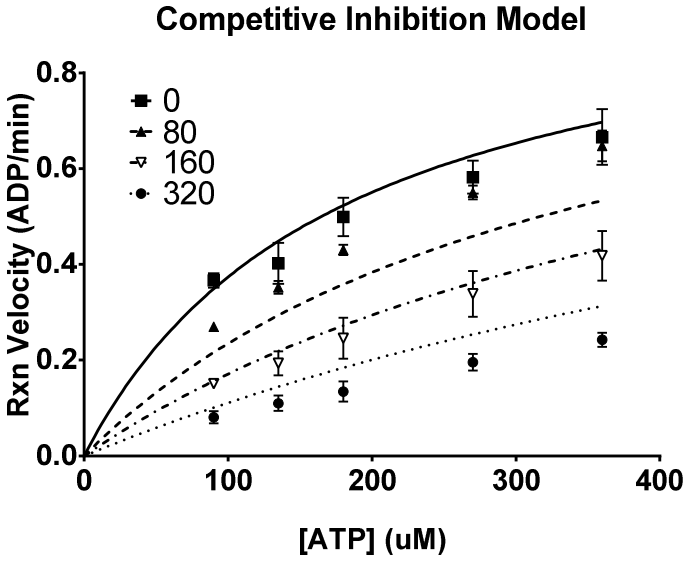
Competitive Inhibition Model
0.8
0.6
0.4
0.2
0.0
Rxn Velocity (ADP/min)
0
80
160
320
0
100
200
300
400
[ATP] (uM)

C

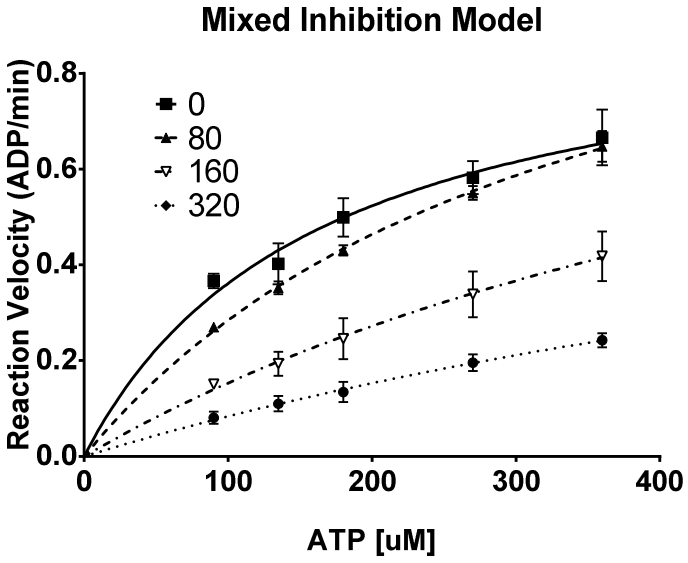
Mixed Inhibition Model
0.8
0.6
0.4
0.2
0.0
Reaction Velocity (ADP/min)
0
80
160
320
0
100
200
300
400
ATP [uM]

3.3.9 Mixed model inhibition.

To measure the quantitative extent of parallel mechanisms and the impact of substrate concentration (ATP) on kinase inhibition, the parameter αmust be examined in the global analysis.[2] Its value determines the degree to which the binding of inhibitor alters the affinity of the enzyme for its substrate and is always greater than zero. When α is very small (but greater than zero), binding of the inhibitor enhances substrate binding to the enzyme, and the mixed model becomes nearly identical to an uncompetitive model. When α =1, the inhibitor does not alter binding of substrate to the enzyme, and the mixed-model is identical to noncompetitive inhibition. With increasing α, the inhibitor increasingly prevents binding of the substrate, and ultimately the mixed-model becomes identical to competitive inhibition.

Using global analysis of the Michaelis-Menten graph, we calculate an α of 31 for the inhibitory action of EF31 (**2.4**) on AKT-2. This value >1 demonstrates that, while compound EF31 (**2.4**)has multiple mechanisms of inhibition, competition with ATP dominates action against this kinase. The mixed inhibition model has been reported for EF24 (**2.3**) and IKKB by Kasinski et al.(Kasinski, Du et al. 2008), although α was not calculated.

3.3.10 Possible mixed model inhibition mechanism of action.

We hypothesize that the other mode of inhibition may correspond to covalent binding of inhibitor to enzyme as a result of Michael addition of a free cysteine to the electrophilic enone moiety of EF31 (**2.4**). This is consistent with our earlier demonstration that two glutathione molecules are able to combine with a single molecule of EF31 (**2.4**) rapidly and quantitatively in

[2] Footnote: The parameter α derived from the global analysis of the data in GraphPad Prism differs from the similarly-named variables α and α' in the classic Michaelis-Menten equations. (GraphicPad, Inc., *GraphicPad Prism 5*, La Jolla, CA, 2010)

aqueous media. (Sun, Lu et al. 2009)This mechanistic option is discussed below from the viewpoint of the explicit interaction between ligand and kinase (Figure III-13).

3.3.11 Rationalizing the IC_{50} data by molecular modeling.

From Figure III-6 B, the action of compound EF31 (**2.4**) on AKT-1 and AKT-2 demonstrates the most potent IC_{50} values as reflections of binding. Accordingly, the sequences around the ATP pockets of AKT-1 and AKT-2 were compared by BLAST to show that the kinase domains of the two proteins possess 82% identity and 93% similarity.

Figure III-10. Homology of AKT-1 and AKT-2. Shown below are sequence alignments of AKT-1 (lower row) and AKT-2 (upper row with residue numbers). The residues around the ATP pocket (squared in black) are identical. The nearly identical IC_{50} values of AKT-1 and AKT-2 is therefore not surprising in a predominately ATP competitive inhibition.


156 KLLGKGTFGKVILVREKATGRYYAMKI 182
KLLGKGTFGKVILVKEKATGRYYAMKI
227 FVMEYANGGELFFHLSRERVFTEERAR 253
FVMEYANGGELFFHLSRERVFSEDRAR
276 IKLENLMLDKDGHIKITDFGLCKEGIS 303
LKLENLMLDKDGHIKITDFGLCKEGIK
432 SEVDTRYFDDEFTAQSITITPPDRYDS 458
SETDTRYFDEEFTAQMITITPPDQDDS

Figure III-11. Proposed analog binding in ATP binding pocket of AKT-2.

With the help of Qi Shi an attempt was made to rationalize the IC_{50} valuesof the various ligands by assuming they block the kinases primarily by occupying the ATP binding pocket in accord with the dominant mechanism derived from the kinetic measurements. Since AKT-1 and AKT-2 are very similar both biologically and structurally, AKT-2 was selected for the modeling work. The crystal structure of the AKT-2 kinase domain (PDB code: 3E88) was used as the receptor and processed by Maestro Protein Preparation Wizard. The ligands EF24 (**2.3**), EF31 (**2.4**), UBS109(**2.12**) and SEF31 (**2.14**) were docked by Glide into the ATP binding site. The top 20 poses for each conformer were re-ranked by MM-GBSA scoring.(A)illustrates the top pose re-ranked by MM-GBSA for EF31 (**2.4**) in AKT-2. A hydrogen bond is observed between one of the pyridine nitrogen atoms and Thr292 on the receptor. Residues Glu236 and Glu279 are in close proximity to another nitrogen atom on the ligand, which indicates favorable electrostatic interactions. Another possible contribution to a favorable coulombic association is the proximity of the ligand carbonyl group and residue Lys181. For EF24 (**2.3**), the top MM-GBSA pose is similar to that of EF31 (**2.4**)except the replacement of *ortho*-N on the pyridine rings with C-F on EF24 (**2.3**). As **(C)** demonstrates, a hydrogen bond can also be formed between the fluorine atom and Thr292, but the angle is less favorable by comparison with EF31 (**2.4**). In addition, the sum of Van der Waals radii for fluorine and oxygen exceeds the distance between the fluorine on EF24 (**2.3**) and the oxygen on Thr292, indicating an unfavorable steric clash. The weaker H-bond interaction and unfavorable steric clashes between EF24 (**2.3**) and AKT-2 most likely contribute to the relatively higher IC_{50} values of this ligand relative to EF31 (**2.4**).

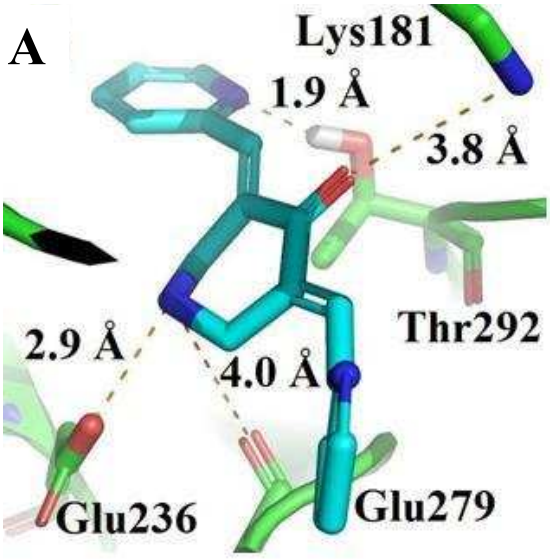
A
Lys181
1.9 Å
3.8 Å
Thr292
2.9 Å
4.0 Å
Glu236
Glu279

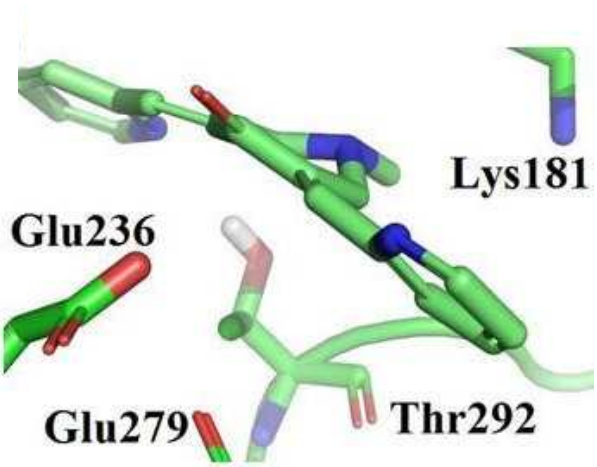
B
Lys181
Glu236
Glu279
Thr292

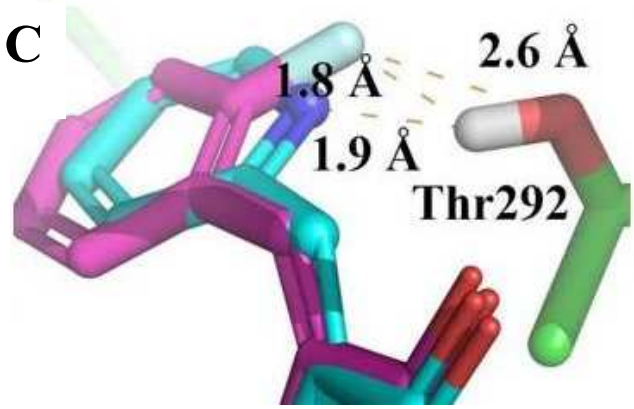
C
1.8 Å
2.6 Å
1.9 Å
Thr292

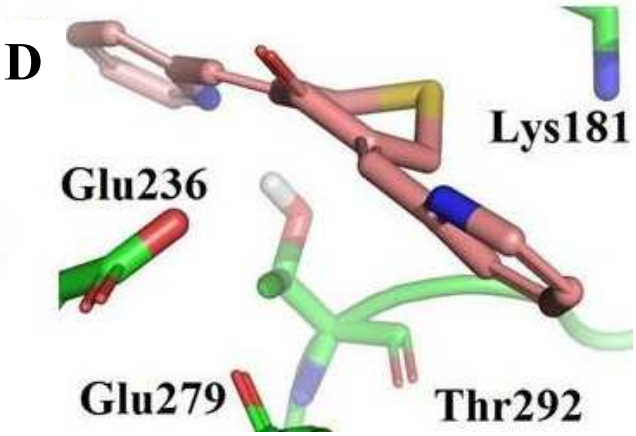
D
Lys181
Glu236
Glu279
Thr292

Figure III-12. IC_{50} data rationalized by conformational changes due to protonation of compound UBS109 (2.12).

Analogs UBS109(**2.12**) and SEF31(**2.14**) demonstrate different poses from EF31(**2.4**) as illustrated in Figure III-11(A) and (B). Because of the bulky N-methyl group and sulfur atom, the former structures are forced to new locations in the pocket where the ligands lose favorable H-bond and electrostatic interactions. Since UBS109(**2.12**) exhibits a pKa value of 6.2 (Performed by Analiza Inc., Cleveland, OH) identical with that for the histidine side chain, the ligand is likely to be protonated at the AKT-2 binding site. The top MM-GBSA poses for UBS109(**2.12**) with N-Me groups in axial and equatorial conformations are illustrated. The higher energy axial conformer adopts a pose similar to unmethylated EF31(**2.4**) and shows favorable electrostatic interactions with the two nearby glutamic acids Glu236 and Glu279. The energy difference between the protonated axial and the equatorial conformers is 5.0 kcal/mol. The binding energy for the axial conformer is predicted to be more stable than the equatorial one, resulting in a net stability of 1.7 kcal/mol for the bound axial form. Thus, the N-Me group of UBS109(**2.12**) would seem to be able to adopt the axial conformation upon binding to AKT-2 when protonated. However, the predicted MM-GBSA binding free energy for EF31 (**2.4**) is 3.0 kcal/mol greater than UBS109(**2.12**). Accordingly, the reduced activity of N-methylated UBS109(**2.12**) relative to EF24(**2.3**) and EF31(**2.4**) can be understood. Overall, a qualitative explanation of the various IC_{50} values for AKT-2 inhibition can be rationalized by the docking results. However, an attempt to develop a quantitative linear regression for MM-GBSA binding free energies and experimental (IC_{50}) values provided no correlation.

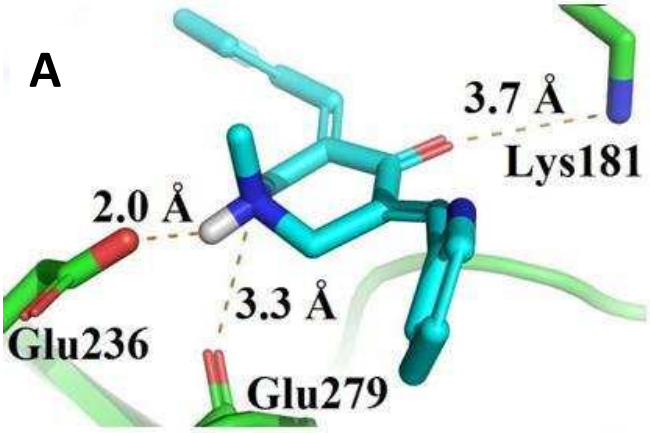
A
3.7 Å
Lys181
2.0 Å
3.3 Å
Glu236
Glu279

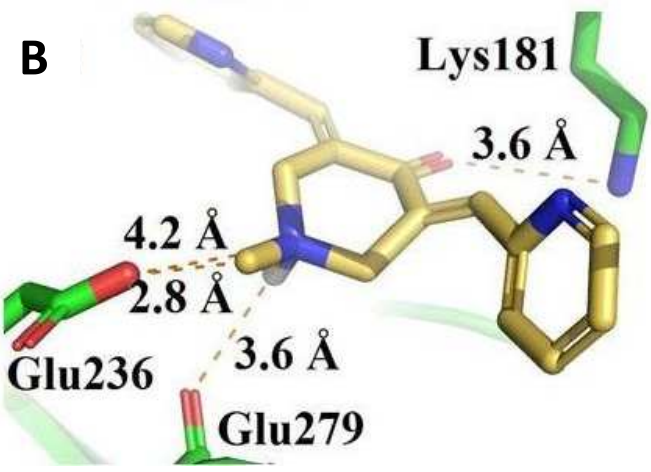
B
Lys181
3.6 Å
4.2 Å
2.8 Å
3.6 Å
Glu236
Glu279

Figure III-13. Hypothesis for mixed model inhibition

Since all the curcumin analogs carry an α,β-unsaturated ketone Michael acceptor, covalent bonds may be formed between cysteines on the AKT kinases and the analogs. In this way the mixed-inhibition observed above and previously reported(Kasinski, Du et al. 2008) can be understood. (A)shows that a cysteine (Cys310 for AKT-1 and Cys311 for AKT-2) is located near the substrate binding site. Consistent with the design of the bioassay, the formation of a covalent bond between ligand and cysteine will most likely interrupt substrate binding, making the target peptide reagent susceptible to cleavage and causing subsequent separation of the FRET pairs. Under these circumstances, an apparent high IC_{50} value will be observed. Unfortunately, such an event can hinder quantification of the non-covalent binding affinity of the ATP competitive inhibitor unless this mechanism is vanishingly small.

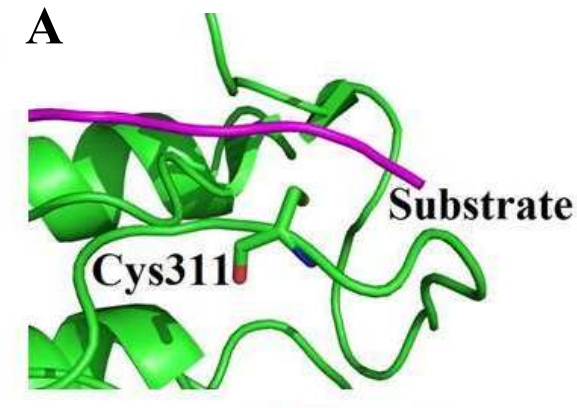
A
Substrate
Cys311

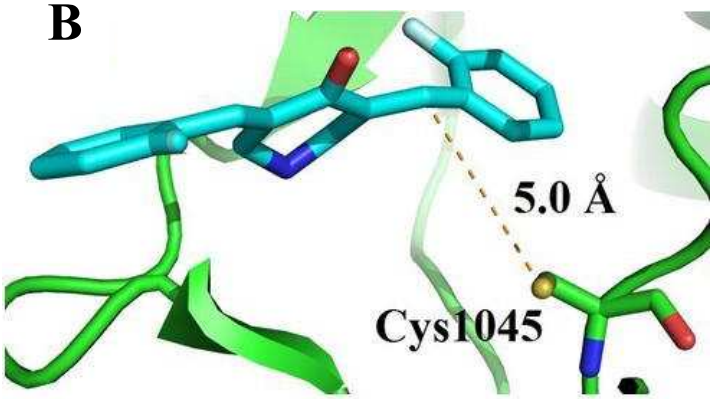
B
5.0 Å
Cys1045

3.3.12 Additional notes on kinase inhibition mechanisms.

It is worth noting that in cell-based assays, N-methyl UBS109(**2.12**) usually exhibits greater potency compared to fluorinated EF24 (**2.3**). In the present context, however, the IC_{50} values of UBS109(**2.12**) are generally higher (Figure III-6). One reasonable speculation is that other proteins inhibited to a greater extent by UBS109(**2.12**) in the cellular environment make an additional contribution to cell cytotoxicity. Therefore, antagonizing AKT-1 and AKT-2 alone might well elicit a less effective anti-tumor effect. Once again, the pleiotropic property of the current analogs is suggested to be a valuable advantage in a cancer setting.

It is noteworthy that the IC_{50} values for the four active ligands on KDR/VEGFR2 are much more similar than those measured for the AKT kinases. While an attempt to devise a linear correlation between the energy-refined docking results and the experimental IC_{50} values was unsuccessful, examination of the KDR binding site reveals two cysteines inside the ATP pocket. One of these, Cys1045, adopts an orientation that favors covalent Michael addition to the α,β-unsaturated ketone moiety (Figure III-13 B). It is conceivable that covalent binding dominates the binding affinities in this case and, thereby, rationalizes the similar IC_{50} values for KDR inhibition.

Figure III-14. AM series curcumin analogs.

In addition to those curcumin analogs explored thus far, nine more curcumin analogs were synthesized by Alessandra Mancini (post-doctoral fellow in Dr. Liotta's laboratory) and provided to us to test for anti-IKKβ activity using the Z'Lyte in vitro kinase assay.

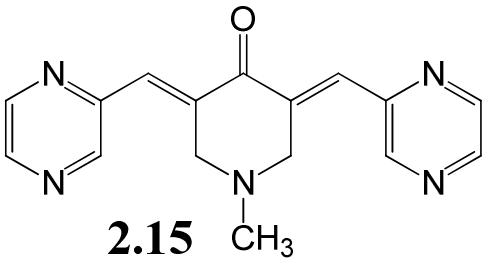

2.15

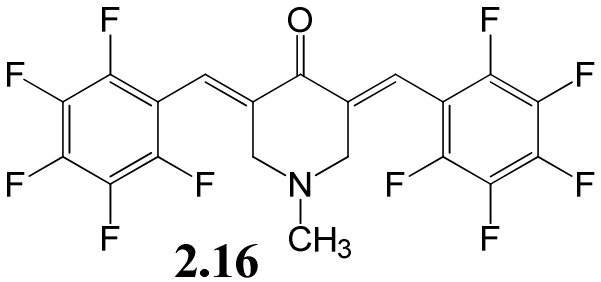

2.16

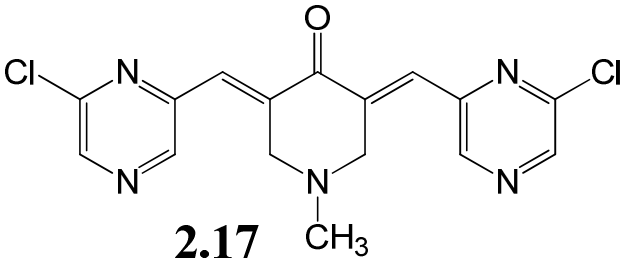

2.17

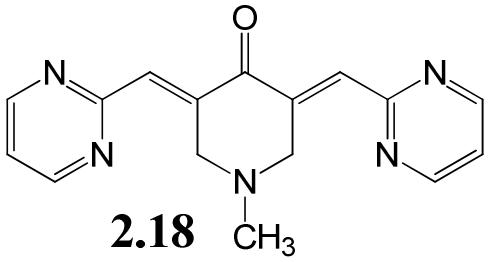

2.18

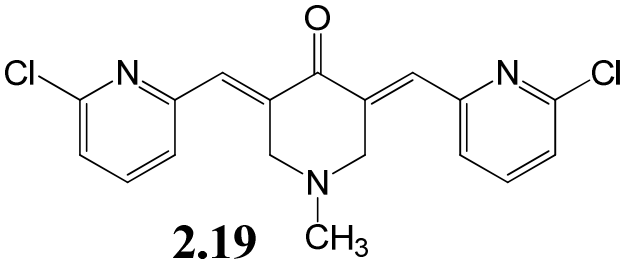

2.19

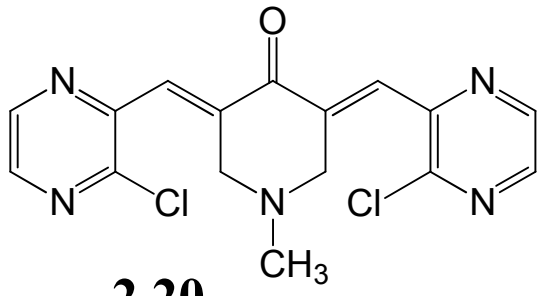

2.20

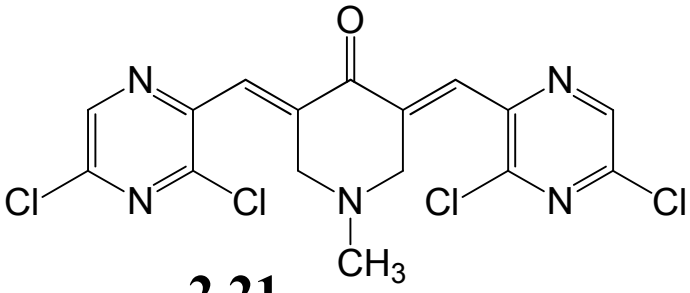

2.21

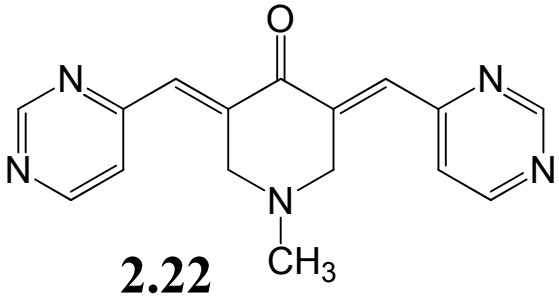

2.22

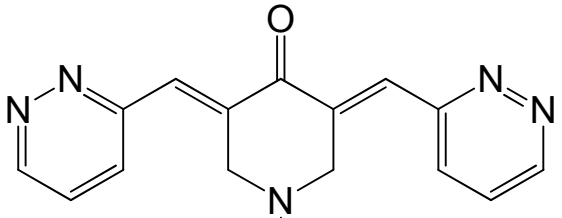

2.23

Figure III-15. IKKβ inhibition by AM series analogs.

AM-8 exhibited the highest potency in anti-IKKβ activity with IC50 of 0.86 μM, which is five-fold better than EF31 (**2.4**) in Table 1. The rank order is **2.22**>**2.23**=**2.18**>**2.20**>**2.15**>**2.19**>**2.21**>**2.17**>>**2.16**. Including more fluorines or chlorides around the benzene/pyrimidine/pyridazine/pyrazine rings seems to decrease anti-IKKβ activity. Anti- IKKβ activity was the best with pyrimidine and less effective with pyridazine, pyridine, and pyrazine ring replacement sequentially. It is interesting to compare **2.22** and **2.18** in respect to the location change of nitrogens in the pyrimidine rings.

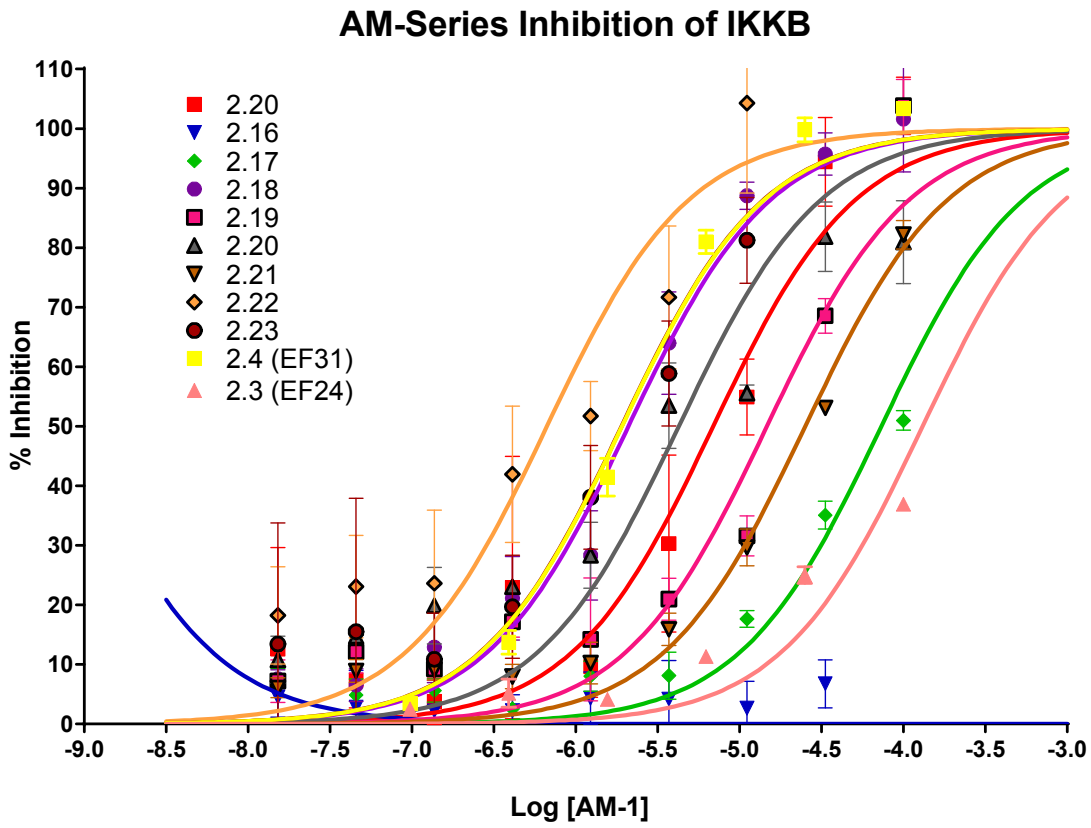
AM-Series Inhibition of IKKB
% Inhibition
Log [AM-1]
2.20
2.16
2.17
2.18
2.19
2.20
2.21
2.22
2.23
2.4 (EF31)
2.3 (EF24)
110
100
90
80
70
60
50
40
30
20
10
0
-9.0
-8.5
-8.0
-7.5
-7.0
-6.5
-6.0
-5.5
-5.0
-4.5
-4.0
-3.5
-3.0

Figure III-16. Inhibition of NF-κB Translocation by curcumin analogs.

IKKβ is a kinase in the NF-κB pathway which controls phosphorylation of IKB and subsequent translocation of NF-κB to the nucleus. We hypothesized that since the curcumin analogs inhibit IKKβ, they would in turn block NF-κB translocation. Using a cell-based assay, we wanted to show that treatment with curcumin analogs inhibit NF-κB translocation. In our assay, HeLa cells were then treated with curcumin analogs compound EF24 (**2.3**) and compound EF31 (**2.4**) for one hour. After that, they were then stimulated with 5 ng/mL IL-1α, a proinflammatory cytokine, for 15 minutes. In the unstimulated control, which did not receive IL-1α, there is NF-κB is localized to the cytoplasm (top left). In the stimulated control, NF-κB is localized to the nucleus which is designated as the blue fluorescent areas stained with Hoecht dye (top right). NF-κB translocation inhibition occurs at 10 μM compound EF24 (**2.3**) and 0.1 μM compound EF31 (**2.4**). This result correlates with their anti-IKKβ kinase activity in the upstream signaling of NF-κB.

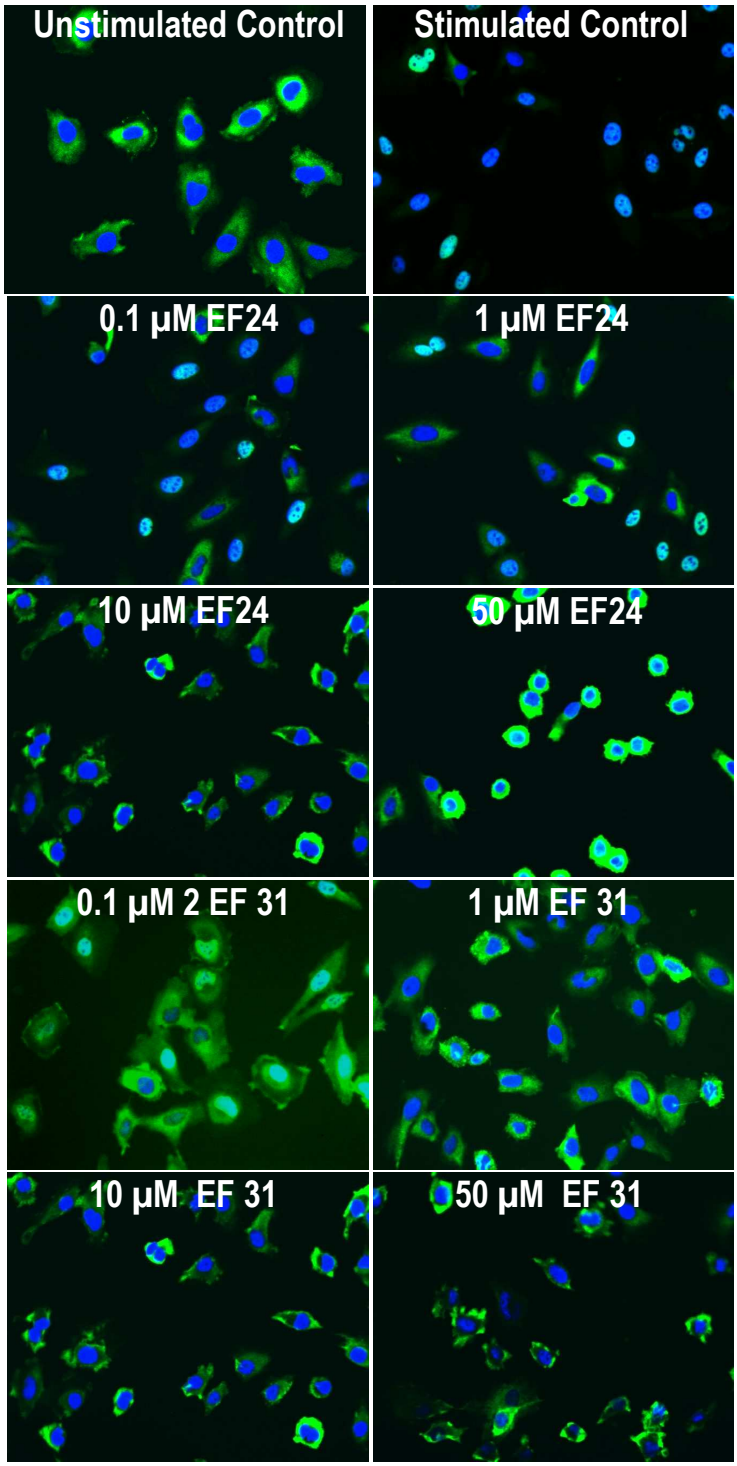
Unstimulated Control
Stimulated Control
0.1 µM EF24
1 µM EF24
10 µM EF24
50 µM EF24
0.1 µM 2 EF 31
1 µM EF 31
10 µM EF 31
50 µM EF 31

Figure III-17. Cell toxicity studies.

Cell toxicity study was carried out using Promega CellTiter 96 Aqueous cell proliferation assay. U2OS and MDA-MB-231 cells were plated at 3000 cells/well, for 24 hours. Cells were treated with 0.1, 1.0, 10, and 50 μM of curcumin analogs with a final DMSO concentration of 0.1% for another 24 hours. As consistent with anti-kinase results, compound EF31 (**2.4**) was a better inhibitor of cell growth for MDA-MB-231 and U2OS cells than compound EF24 (**2.3**).

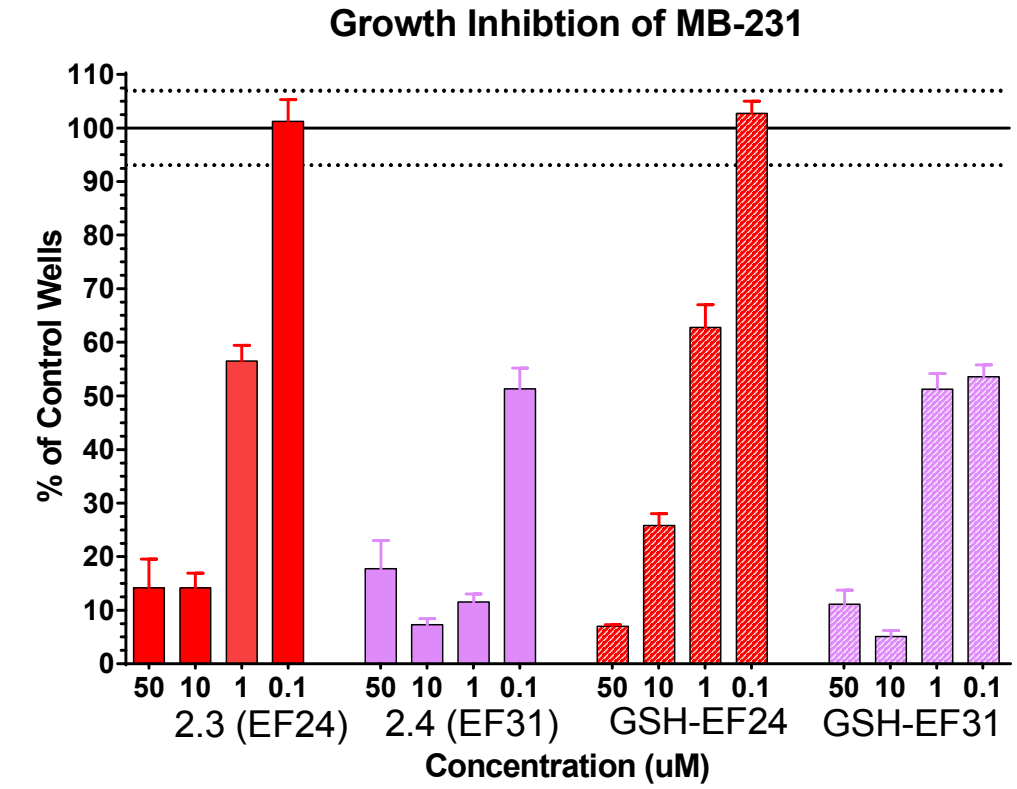
Growth Inhibtion of MB-231
% of Control Wells
110
100
90
80
70
60
50
40
30
20
10
0
50 10 1 0.1
50 10 1 0.1
50 10 1 0.1
50 10 1 0.1
2.3 (EF24)
2.4 (EF31)
GSH-EF24
GSH-EF31
Concentration (uM)

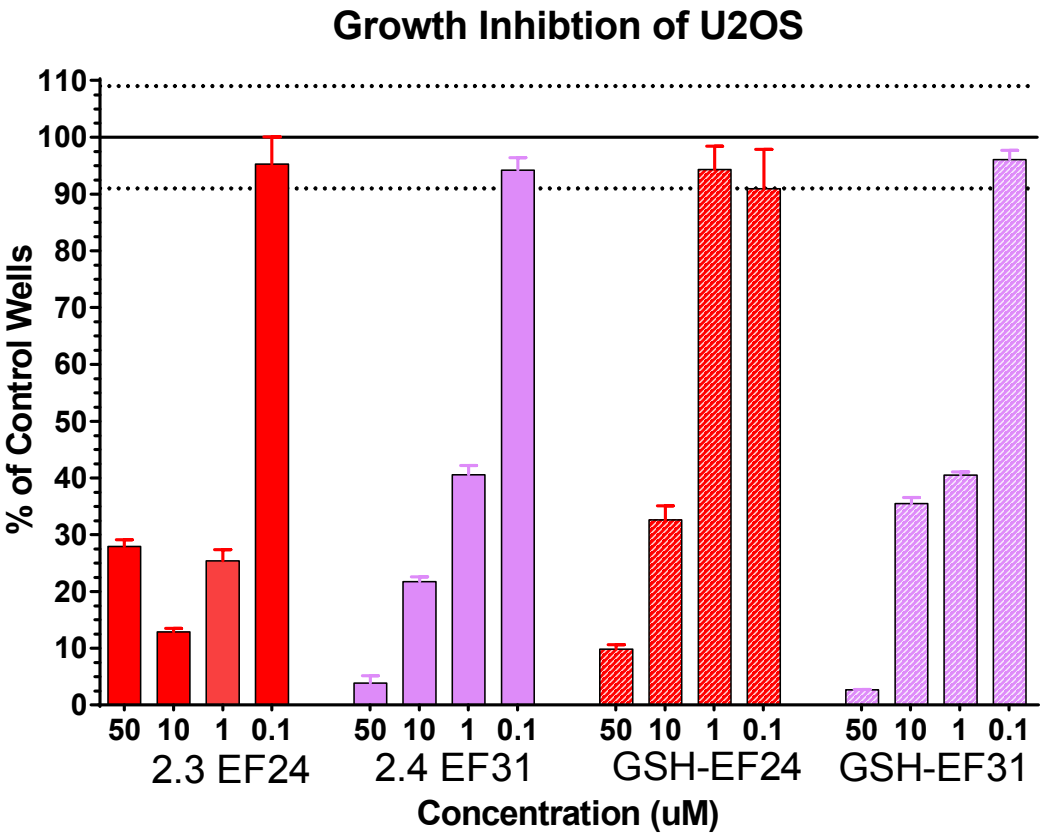
Growth Inhibtion of U2OS
% of Control Wells
110
100
90
80
70
60
50
40
30
20
10
0
50 10 1 0.1
50 10 1 0.1
50 10 1 0.1
50 10 1 0.1
2.3 EF24
2.4 EF31
GSH-EF24
GSH-EF31
Concentration (uM)

3.3.13 In vivo studies, inflammation and anti-tumor activity.

Figure III-18. Paw edema model.

Mice received drug treatments in a suspension of 90%: 0.1% Methyl Cellulose and 10%: PEG 200 everyday via oral gavage for 96 hrs. EF24 (**2.3**) and EF31 (**2.4**) were tested at 10 mg/kg and their glutathionated counterparts were tested at 30 mg/kg. Indomethacin a NSAID was used at a concentration of 5 mg/kg for a positive control.

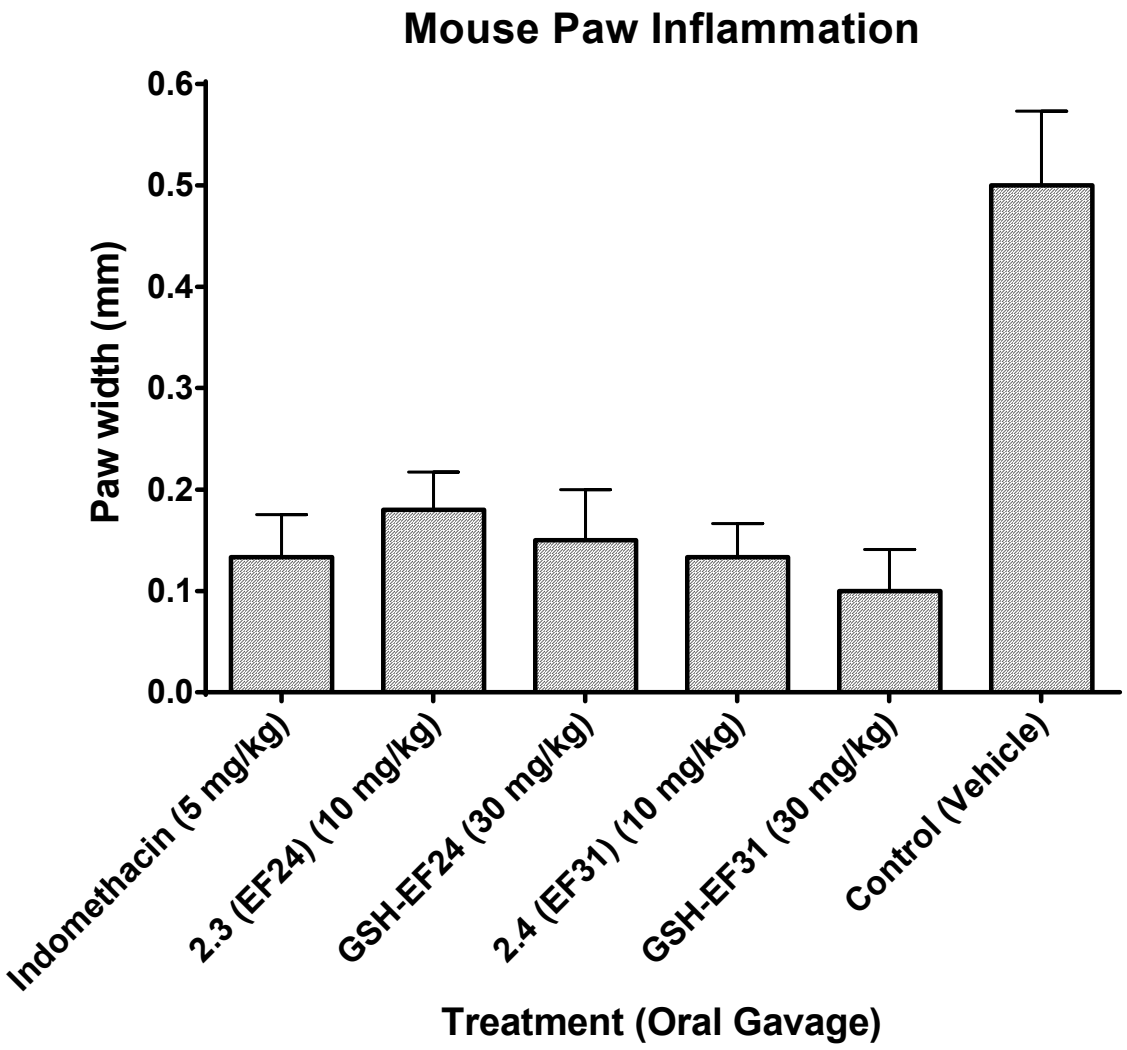
Mouse Paw Inflammation
Paw width (mm)
0.0
0.1
0.2
0.3
0.4
0.5
0.6
Indomethacin (5 mg/kg)
2.3 (EF24) (10 mg/kg)
GSH-EF24 (30 mg/kg)
2.4 (EF31) (10 mg/kg)
GSH-EF31 (30 mg/kg)
Control (Vehicle)
Treatment (Oral Gavage)

Figure III-19. MDA-MB-231 xenograft tumor model.

To test compound EF31's (**2.4**) bioavailability and efficacy in reducing the size of tumors in vivo, we used an animal model for tumor growth. In (A), 4 x 10^6 MDA-MB-231 cells were injected into the right and left flank of nude mice. The tumors were then allowed to grow for 1 week. After that, mice were dosed everyday via oral gavage for 5 weeks with 10, 75, and 200 mg/kg EF24 (**2.3**) suspended in 90%: 0.1% Methyl Cellulose and 10%: PEG 200. Each grouped contained 5 mice x 2 tumors for an n=10. The overall trend showed a nice dose response to drug treatment, there was too much variability within the groups to make any statistically significant claims.

We next conducted a similar experiment to make some comparisons between curcumin (**1.1**) and the analogs EF24 (**2.3**), EF31 (**2.4**), and the product of **2.3** reduction by glutathione. (B) In this experiment, 4 x10^6 MDA-MB-231 cells were injected into the right and left flank of nude mice. The tumors were then allowed to grow for 2 weeks, after which the mice were treated everyday for 3 weeks with 100 mg/kg of EF24 (**2.3**), glutathione congugatedEF24 (**2.3**), EF31 (**2.4**), and curcumin (**2.1**).

A

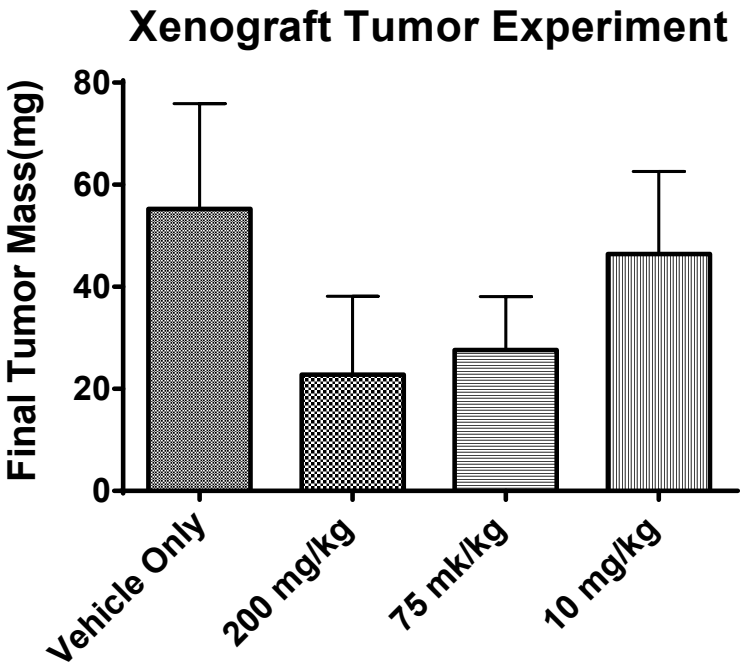
Xenograft Tumor Experiment
Final Tumor Mass(mg)
80
60
40
20
0
Vehicle Only
200 mg/kg
75 mk/kg
10 mg/kg

B

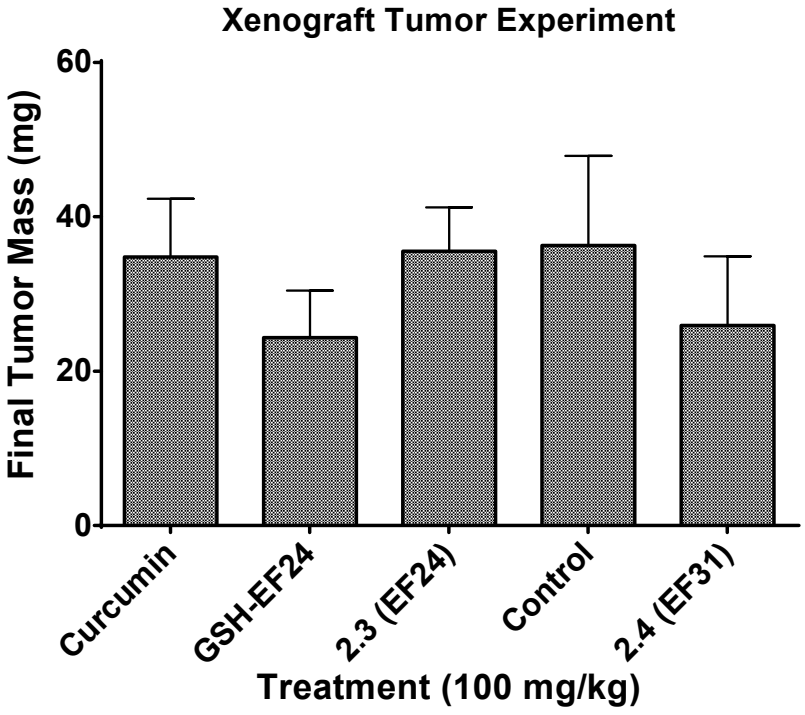
Xenograft Tumor Experiment
Final Tumor Mass (mg)
60
40
20
0
Curcumin
GSH-EF24
2.3 (EF24)
Control
2.4 (EF31)
Treatment (100 mg/kg)

Figure III-20. *In vivo* radiosensitization by EF31 (2.4) in a subcutaneous xenograft tumor model.

LN229/vIII cells were grown subcutaneously in the flank of nude mice (2 tumors/mouse) to a size of ~50 cubic mm prior to oral administration of UBS109 (50mg/kg) once/day x 7 days. 5 mice (10 tumors) were assessed for each group. 4 Gy x 3 fractions of radiation was administered (on days 2, 4 and 6 of drug dosing) locally to the flanks of the tumor-bearing mice. Mice was followed over time with caliper measurements made to estimate tumor size. UBS109 alone had no effect on tumor growth with the tumor growth curve showing similar results with the control (black line) and UBS alone (blue line) groups. While radiation alone (4Gy x 3) significantly delayed the growth of the flank tumors, UBS109 had apparent radiosensitizing effects with further inhibition of flank tumor growth when comparing the UBS109 + radiation group (green line) to the radiation alone group (red line).

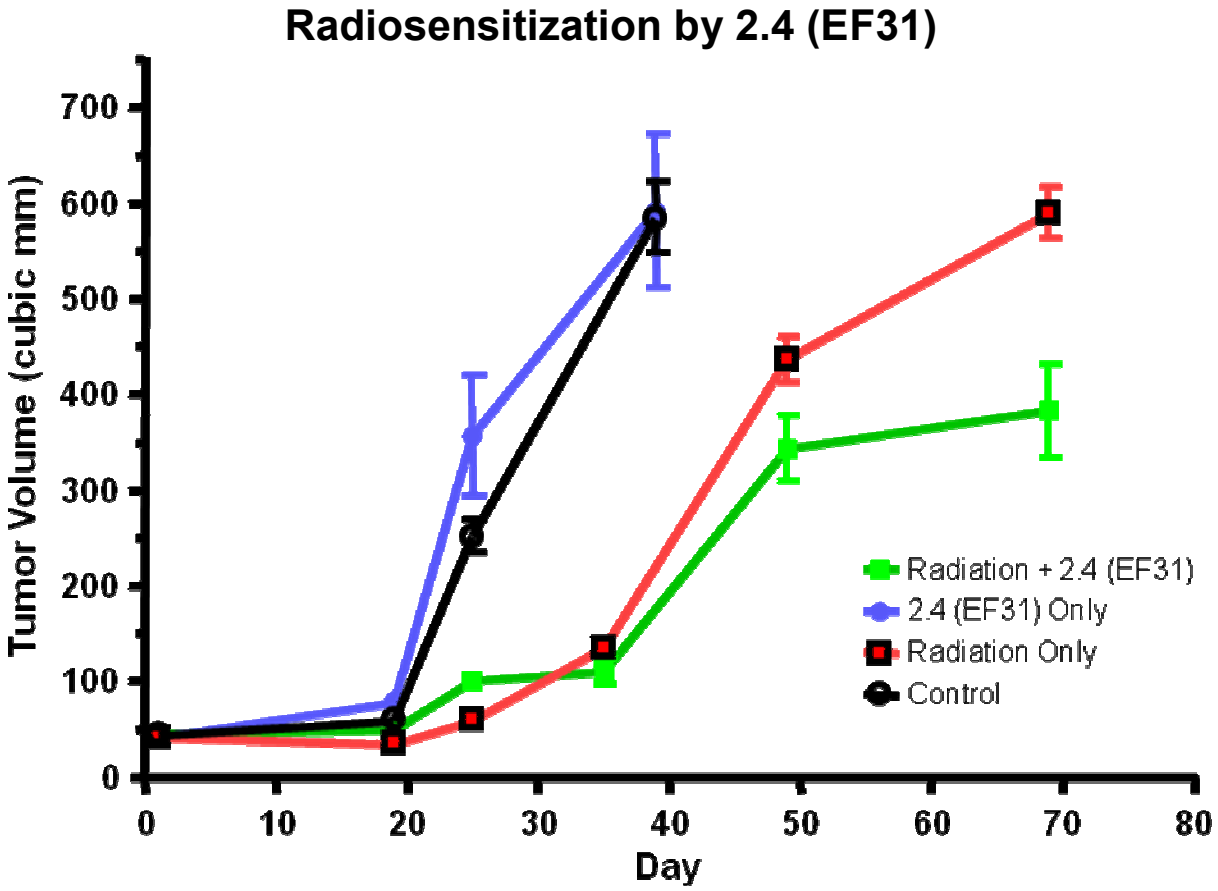
Radiosensitization by 2.4 (EF31)
Tumor Volume (cubic mm)
700
600
500
400
300
200
100
0
0
10
20
30
40
50
60
70
80
Day
Radiation + 2.4 (EF31)
2.4 (EF31) Only
Radiation Only
Control

3.4 Discussion

By examination of 50 kinases, we have identified many that are inhibited by a small panel of curcumin mimics, nearly a dozen of which are blocked at micromolar or submicromolar concentrations. The kinases are associated with cellular pathways important for inflammation cell growth, and angiogenesis, processes that are critical for tumor development. Furthermore, two MAP kinase cascade pathways have been identified from the present kinase inhibition data (p38α-MAPKAPK2 and RAF1-MEK1-ERK2). They illustrate that the pleiotropic nature of these analogs leads to dampening of pathways without dependence on a single kinase for inhibition (Figures III-5 (A), III-7, III-8). In a cancer context, one might expect drug resistance to be significantly diminished in cells following treatment with such inhibitors. With the rising importance of the –omes (genome, proteome, kinome, transcriptome, etc.) and our ability to understand and map the complexities of intracellular signaling, we can now target multiple enzymes with a "magic shotgun". (Roth, Sheffler et al. 2004) This is especially true for diseases like cancer that are complex and often involve mutations in multiple genes. In fact, this represents a new philosophy in drug discovery, where "dirty" or "promiscuous" drugs that target multiple enzymes or pathways may be superior to mono therapies that are selective for only one target. (Fojo 2008; Hopkins 2009; von Eichborn, Murgueitio et al. 2011)

Enzyme kinetics studies reveal that kinase inhibition by compounds within series **2** operates by multiple mechanisms, with ATP competition appearing to dominate. Complementary molecular modeling at the ATP binding sites of AKT-2 and KDR provides a qualitative explanation for ligand activity for certain kinases. Michael addition to curcumin mimetics by cysteine residues in the kinases is compatible with the observed mixed mechanism kinetics and the flat IC_{50} values for the KDR kinase.

CHAPTER IV: Conclusions and Future Studies

4.1 Triptolide

The NF-κB based screen of the triptolide analogs, was a good screening process and seemed to be able to select compounds that performed well in later assays. With most of the analogs performing as well or better than triptolide, we could have had a more stringent screening process that looked at results independent of triptolide. The use of eletorphoric mobility shift assay (EMSA) could have been a great secondary assay to confirm the screening results.

Once we started looking at the behavior of cells in response to triptolide analog treatment, a biologically relevant picture started to emerge. Looking at various cytokines regulated by NF-κB as a readout for NF-κB activation proved to be successful. Further testing looking at Luciferase expression using NF-κB binding sequence for activation would have summarized and built upon the results that we got testing mRNA levels.

Our studies where meant to work toward pushing these or similar compounds towards the clinic. That being said, the second reason most drugs fail are due to safety issues. While we touched upon this subject with the triptolide analogs, our studies were vastly insufficient. With the toxicity being a major issue with the parent compound, then impetus for synthesizing new compounds, a more focused study of toxicity should be conducted. By examining which pathways are affected by triptolide and leading to toxicity issues, we could have developed better tests, to further differentiate our compounds from triptolide. As it stands, looking at only one cell line, does not deem a series of compounds safe. The work done at Charles Rivers Laboratories was excellent, but the inclusion of triptolide would have made a good comparison.

The in vivo studies really had some of the most promising data for this class of compounds. The paw edma experiment, while not showing a great reduction in paw swelling (compared to the curcumin analogs anyway), did have some promising results when we started looking at the cytokine mRNA levels in the mouse livers. If anything, these experiments at least proved that the compounds were bioavailable in sufficient quantities to have a biological affect. The work that was done by Chris Yun and his model of IBD really showed an amazing biological effect, and an almost complete ablation of the disease state. Once again it was shown, that these compounds can have a significant effect on cytokine mRNA levels.

Our mechanistic studies, really only disproved some possible competing hypothesis about NF-κB inhibition. Looking at IKKB was very easy to do from our history working with kinase inhibition assays and the curcumin analogs. The specificity experiment looking at interference of HIF-1 binding to DNA, was also important from a toxicity standpoint as well. Epoxide ring structures are extremely strained and therefore more reactive. This assay helped to show that our compounds weren't just reacting with whatever DNA was available to them. The translocation assays were really what was necessary to show that the triptolide effects on NF-κB were happening within the nucleus. This experiment could have been expanded upon, by including more than one analog as well as triptolide itself. Lastly, all of our mechanistic studies were complicated by the fact that there is little evidence and varying opinions on what exactly triptolides MOA is.

4.2 Curcumin

The beginning of the curcumin project was mostly that of a screen to find more biologically relevant compounds. At first, whether or not the curcumin analogs inhibited kinases

was a question, but that hypothesis was quickly accepted with the multitude of kinases shown to be inhibited. With these results , and the research being done on the parent compound curcumin, an image of these compounds being pleiotrophic kinase inhibitors began to emerge. Nothing focused this image more than the kinase profile screen of fifty kinases.

With the discovery of an ever expanding list of kinases affected by the curcumin analogs, the idea that these analogs were affecting kinase cascades and kinase signaling networks within cells began to solidify. No longer were we concerned with just NF-κB, it now appears that the curcumin analogs are likely having effects on almost every cellular response. With the multitude of kinases inhibited, and the important cellular pathways (especially for cancerous cells), the real future of research for the curcumin analogs lies in further exploration of their effects on cell signaling .

The cell based studies, while supportive of our hypothesis didn't really shed that much new information on the body of research associated with the curcumin analogs. We knew that EF24 could was cytotoxic to cancers cells from the research done by Brian Adams. Furthermore, the work done by the Fu laboratory showed that EF24 did indeed inhibit NF-κB translocation. What this cell based studies did do for us, was allow us to make a comparison to EF31, which at the time was really flying under the radar of other groups studying the curcumin analogs. EF31 was and still seems to be the most potent of the curcumin analogs, at least when it comes to in vitro kinase inhibition.

We looked at a couple in vivo models, including the paw edema model and several mouse tumor xenografts. The paw inflammation data was quite promising, and showed that the curcumin analogs did indeed reduce inflammation. However the results, with the tumor

xenografts seem to be a little mixed. I think that this is due in large part to my inexperience with the model. In my opinion, experimentation in the vein should have been postponed until we had better pharmacokinetic data in which to judge dosages and dose schedules.

The mechanistic studies of the curcumin analogs were really important in tying the in vitro and in vivo work together with the modeling work done by Qi Shi. Our work shows a mixed model of inhibition for AKT-2 by the curcumin analog EF31 and similar results were published for EF24 and IKKB by other groups as well. The predominance of ATP competition in the inhibition of AKT-2 kinase helps us understand what is going on with this particular kinase. The Fu lab also got similar results with IKKB. What would be most interesting would be to see how different kinase and compound combinations affected enzyme kinetics. Would having a stronger/weaker Michael acceptor affect inhibition? Are there specific kinases that are more affected by the non-ATP competition inhibition, if so are there certain residues or traits that link them together? A more complete picture of the enzyme kinetics could be revealed with further experimentation. For instance, if the curcumin analogs do in fact bind to the cystienes in the substrate binding pocket of AKT-2, by varying the peptide substrate concentrations and keeping the ATP constant this question could be answered.

References

Adams, B. K., J. Cai, et al. (2005). "EF24, a novel synthetic curcumin analog, induces apoptosis in cancer cells via a redox-dependent mechanism." Anticancer Drugs**16**(3): 263-275.

Adams, B. K., E. M. Ferstl, et al. (2004). "Synthesis and biological evaluation of novel curcumin analogs as anti-cancer and anti-angiogenesis agents." Bioorg Med Chem**12**(14): 3871-3883.

Awasthi, S., U. Pandya, et al. (2000). "Curcumin-glutathione interactions and the role of human glutathione S-transferase P1-1." Chem Biol Interact**128**(1): 19-38.

Baeuerle, P. A. and D. Baltimore (1996). "NF-kappa B: ten years after." Cell**87**(1): 13-20.

Bayet-Robert, M., F. Kwiatkowski, et al. (2010). "Phase I dose escalation trial of docetaxel plus curcumin in patients with advanced and metastatic breast cancer." Cancer Biol Ther**9**(1): 8-14.

Berg, D. J., N. Davidson, et al. (1996). "Enterocolitis and colon cancer in interleukin-10-deficient mice are associated with aberrant cytokine production and CD4(+) TH1-like responses." J Clin Invest**98**(4): 1010-1020.

Chen, Y., W. J. Craigen, et al. (2009). "Nek1 regulates cell death and mitochondrial membrane permeability through phosphorylation of VDAC1." Cell Cycle**8**(2): 257-267.

Cohen, A. N., M. S. Veena, et al. (2009). "Suppression of interleukin 6 and 8 production in head and neck cancer cells with curcumin via inhibition of Ikappa beta kinase." Arch Otolaryngol Head Neck Surg**135**(2): 190-197.

D'Acquisto, F. and A. Ianaro (2006). "From willow bark to peptides: the ever widening spectrum of NF-kappaB inhibitors." Curr Opin Pharmacol**6**(4): 387-392.

Dai, Y. Q., D. Z. Jin, et al. (2006). "Triptolide inhibits COX-2 expression via NF-kappa B pathway in astrocytes." Neurosci Res**55**(2): 154-160.

Datta, S. R., A. Brunet, et al. (1999). "Cellular survival: a play in three Akts." Genes Dev**13**(22): 2905-2927.

Epelbaum, R., M. Schaffer, et al. (2010). "Curcumin and gemcitabine in patients with advanced pancreatic cancer." Nutr Cancer**62**(8): 1137-1141.

Fojo, T. (2008). "Commentary: Novel therapies for cancer: why dirty might be better." Oncologist**13**(3): 277-283.

Graves, A. P., D. M. Shivakumar, et al. (2008). "Rescoring docking hit lists for model cavity sites: predictions and experimental testing." J Mol Biol**377**(3): 914-934.

Gu, W. Z., S. R. Brandwein, et al. (1992). "Inhibition of type II collagen induced arthritis in mice by an immunosuppressive extract of Tripterygium wilfordii Hook f." J Rheumatol**19**(5): 682-688.

Hopkins, A. L. (2009). "Drug discovery: Predicting promiscuity." Nature**462**(7270): 167-168.

Ji, J. L., X. F. Huang, et al. (2011). "Curcumin and its formulations: potential anti-cancer agents." Anticancer Agents Med Chem**12**(3): 210-218.

Jurenka, J. S. (2009). "Anti-inflammatory properties of curcumin, a major constituent of Curcuma longa: a review of preclinical and clinical research." Altern Med Rev**14**(2): 141-153.

Karin, M. (2008). "The IkappaB kinase - a bridge between inflammation and cancer." Cell Res**18**(3): 334-342.

Kasinski, A. L., Y. Du, et al. (2008). "Inhibition of IkappaB kinase-nuclear factor-kappaB signaling pathway by 3,5-bis(2-flurobenzylidene)piperidin-4-one (EF24), a novel monoketone analog of curcumin." Mol Pharmacol**74**(3): 654-661.

Lee, K. Y., W. Chang, et al. (1999). "PG490 (triptolide) cooperates with tumor necrosis factor-alpha to induce apoptosis in tumor cells." J Biol Chem**274**(19): 13451-13455.

Lee, Y. K., S. Y. Park, et al. (2009). "Regulatory effect of the AMPK-COX-2 signaling pathway in curcumin-induced apoptosis in HT-29 colon cancer cells." Ann N Y Acad Sci**1171**: 489-494.

Lin, N., T. Sato, et al. (2001). "Triptolide, a novel diterpenoid triepoxide from Tripterygium wilfordii Hook. f., suppresses the production and gene expression of pro-matrix metalloproteinases 1 and 3 and augments those of tissue inhibitors of metalloproteinases 1 and 2 in human synovial fibroblasts." Arthritis Rheum**44**(9): 2193-2200.

Lipsky, P. E. and X. L. Tao (1997). "A potential new treatment for rheumatoid arthritis: thunder god vine." Semin Arthritis Rheum**26**(5): 713-723.

Liu, Q., T. Chen, et al. (2006). "Immunosuppressant triptolide inhibits dendritic cell-mediated chemoattraction of neutrophils and T cells through inhibiting Stat3 phosphorylation and NF-kappaB activation." Biochem Biophys Res Commun**345**(3): 1122-1130.

May, M. J., F. D'Acquisto, et al. (2000). "Selective inhibition of NF-kappaB activation by a peptide that blocks the interaction of NEMO with the IkappaB kinase complex." Science**289**(5484): 1550-1554.

Muller, J. M., H. W. Ziegler-Heitbrock, et al. (1993). "Nuclear factor kappa B, a mediator of lipopolysaccharide effects." Immunobiology**187**(3-5): 233-256.

Murthy, S. N., H. S. Cooper, et al. (1993). "Treatment of dextran sulfate sodium-induced murine colitis by intracolonic cyclosporin." Dig Dis Sci**38**(9): 1722-1734.

Nogueira, L., P. Ruiz-Ontanon, et al. (2011). "The NFkappaB pathway: a therapeutic target in glioblastoma." Oncotarget**2**(8): 646-653.

Ochiai, T., Y. Saito, et al. (2008). "Inhibition of IkappaB kinase beta restrains oncogenic proliferation of pancreatic cancer cells." J Med Dent Sci**55**(1): 49-59.

Olivera, A., T. W. Moore, et al. (2012). "Inhibition of the NF-kappaB signaling pathway by the curcumin analog, 3,5-Bis(2-pyridinylmethylidene)-4-piperidone (EF31): anti-inflammatory and anti-cancer properties." Int Immunopharmacol**12**(2): 368-377.

Ozaki, K. (2007). "[Targeted molecular strategies for cancer therapy based on the blockage of oncogenic pathways in human tumor cells]." Yakugaku Zasshi**127**(6): 983-991.

Perry, M. C., M. Demeule, et al. (2010). "Curcumin inhibits tumor growth and angiogenesis in glioblastoma xenografts." Mol Nutr Food Res**54**(8): 1192-1201.

Qiu, D. and P. N. Kao (2003). "Immunosuppressive and anti-inflammatory mechanisms of triptolide, the principal active diterpenoid from the Chinese medicinal herb Tripterygium wilfordii Hook. f." Drugs R D**4**(1): 1-18.

Qualls, J. E., A. M. Kaplan, et al. (2006). "Suppression of experimental colitis by intestinal mononuclear phagocytes." J Leukoc Biol**80**(4): 802-815.

Roth, B. L., D. J. Sheffler, et al. (2004). "Magic shotguns versus magic bullets: selectively non-selective drugs for mood disorders and schizophrenia." Nat Rev Drug Discov**3**(4): 353-359.

Sa, G. and T. Das (2008). "Anti cancer effects of curcumin: cycle of life and death." Cell Div**3**: 14.

Schmid, J. A. and A. Birbach (2008). "IkappaB kinase beta (IKKbeta/IKK2/IKBKB)--a key molecule in signaling to the transcription factor NF-kappaB." Cytokine Growth Factor Rev**19**(2): 157-165.

Schrödinger (2009). Glide. New York, NY, Schrödinger, LLC.

Schrödinger (2009). Prime. New York, NY, Schrödinger, LLC.

Sharma, R. A., W. P. Steward, et al. (2007). "Pharmacokinetics and pharmacodynamics of curcumin." Adv Exp Med Biol**595**: 453-470.

Siebenlist, U., G. Franzoso, et al. (1994). "Structure, regulation and function of NF-kappa B." Annu Rev Cell Biol**10**: 405-455.

Simmonds, R. E. and B. M. Foxwell (2008). "Signalling, inflammation and arthritis: NF-kappaB and its relevance to arthritis and inflammation." Rheumatology (Oxford)**47**(5): 584-590.

Sipos, W., P. Pietschmann, et al. (2008). "Strategies for novel therapeutic approaches targeting cytokines and signaling pathways of osteoclasto- and osteoblastogenesis in the fight against immune-mediated bone and joint diseases." Curr Med Chem**15**(2): 127-136.

Sun, A., Y. J. Lu, et al. (2009). "Curcumin analog cytotoxicity against breast cancer cells: exploitation of a redox-dependent mechanism." Bioorg Med Chem Lett**19**(23): 6627-6631.

Systems, I. (2012). IPA. 1700 Seaport Blvd, 3rd Floor

Redwood City, CA 94063, Ingenuity Systems, Inc. .

Tao, X., L. S. Davis, et al. (1991). "Effect of an extract of the Chinese herbal remedy Tripterygium wilfordii Hook F on human immune responsiveness." Arthritis Rheum**34**(10): 1274-1281.

Tao, X., H. Schulze-Koops, et al. (1998). "Effects of Tripterygium wilfordii hook F extracts on induction of cyclooxygenase 2 activity and prostaglandin E2 production." Arthritis Rheum**41**(1): 130-138.

Taylor, R. A. and M. C. Leonard (2011). "Curcumin for inflammatory bowel disease: a review of human studies." Altern Med Rev**16**(2): 152-156.

von Eichborn, J., M. S. Murgueitio, et al. (2011). "PROMISCUOUS: a database for network-based drug-repositioning." Nucleic Acids Res**39**(Database issue): D1060-1066.

Wachtel-Galor, S. and I. F. F. Benzie (2011). "Herbal Medicine: An Introduction to Its History, Usage, Regulation, Current Trends, and Research Needs."

Wadleigh, M., D. J. DeAngelo, et al. (2005). "After chronic myelogenous leukemia: tyrosine kinase inhibitors in other hematologic malignancies." Blood**105**(1): 22-30.

Yamaguchi, M., T. W. Moore, et al. (2012). "Novel curcumin analogue UBS109 potently stimulates osteoblastogenesis and suppresses osteoclastogenesis: involvement in Smad activation and NF-kappaB inhibition." Integr Biol (Camb).

Yang, C. L., Y. Y. Liu, et al. (2012). "Curcumin Blocks Small Cell Lung Cancer Cells Migration, Invasion, Angiogenesis, Cell Cycle and Neoplasia through Janus Kinase-STAT3 Signalling Pathway." PLoS One**7**(5): e37960.

Yang, Y., Z. Liu, et al. (1998). "Triptolide induces apoptotic death of T lymphocyte." Immunopharmacology**40**(2): 139-149.

Zhou, H., C. S. Beevers, et al. (2010). "The targets of curcumin." Curr Drug Targets**12**(3): 332-347.

Zhu, S., T. W. Moore, et al. (2012). "Synthetic curcumin analog EF31 inhibits the growth of head and neck squamous cell carcinoma xenografts." Integr Biol (Camb)**4**(6): 633-640.